UNIVERSITÀ
DEGLI STUDI
DI PADOVA

Sede Amministrativa: Università degli Studi di Padova

Dipartimento di Biologia

CORSO DI DOTTORATO DI RICERCA IN: BIOSCIENZE e BIOTECNOLOGIE

CURRICOLO: NEUROBIOLOGIA

CICLO XXIX

EXPLORING ORAI2 FUNCTION IN ALZHEIMER'S DISEASE MODELS BASED ON PRESENILIN 2 AND AMYLOID PRECURSOR PROTEIN MUTANTS

Coordinatore: Ch.mo Prof. Paolo Bernardi

Supervisore: Dott.ssa Cristina Fasolato

Dottorando: Mario Agostini

INDEX

SUMMARY

Alzheimer's disease (AD) is the most common form of dementia among elderly population. More than twenty years ago the so-called amyloid hypothesis was formulated based on the major histopathological hallmarks of AD, among which the amyloid plaques are the most known and studied. This hypothesis was prompted by the discovery of three genes that, whereas mutated, are associated with the familial forms of the disease (FAD). One of these genes encodes for the amyloid precursor protein (APP), a single-pass type I transmembrane protein that undergoes sequential cleavages operated by the secretase family of enzymes. The last and key secretase, called γ-secretase, is composed of four proteins, among which we found either presenilin 1 (PS1) or presenilin 2 (PS2), encoded by other two genes (*PSEN1/PSEN2*) that are responsible for FAD pathogenesis. Autosomic dominant mutations in either *APP*, *PSEN1* or *PSEN2* cause accelerated Aβ deposition due to an increased Aβ42/Aβ40 ratio. While the vast majority of AD cases are sporadic, FAD patients bearing PS2 mutations show a clinical course much similar to that of sporadic patients.

By many groups it was found that PSs are capable of perturbing cellular Ca^{2+} homeostasis, and, particularly, our group demonstrated that PS2, either bearing FAD-linked mutations or wild-type (WT), lowers endoplasmic reticulum (ER) and Golgi apparatus Ca^{2+} content, interacts with SERCA pump, dampening its function, and tethers ER and mitochondria; all of these pleiotropic effects are independent of its γ-secretase activity. Recently another group identified PS2 as a regulator of the ER Ca^{2+} content, together with Orai2, a plasma membrane channel implicated in the Store-Operated Ca^{2+} Entry (SOCE). This latter phenomenon is impaired in AD, and specifically it is down-tuned in mutant PS-bearing cells. Taken together this body of information offered an interesting background to study the interplay between ER Ca^{2+} levels, SOCE defects and APP processing/Aβ production. Taking advantage of the PS2-based AD mouse models available in our laboratory, namely the homozygous single transgenic (TG) line expressing the FAD-linked mutant PS2-N141I (line PS2.30H) and the homozygous double transgenic (2TG) line expressing PS2-N141I together with the *Swedish* double mutant APP-K670M/N671L (line B6.152H), we could investigate the expression pattern of Orai2 in the nervous tissue.

Western blot analyses on cortices and hippocampi revealed that Orai2 was overexpressed in cortices from TG and 2TG mice, when compared to C57BL/6 (WT) mice. This overexpression was mainly due to the neuronal contribution since it was even higher in cortical neuronal cultures and *in situ* Orai2 was found only in neurons, as assayed by immunohistochemical analysis of brain

slices. Orai2 up-regulation, that is the condition found in TG and 2TG neurons, is capable of perturbing cellular Ca^{2+} homeostasis. Particularly, when overexpressed it caused a significant decrease in IP3-induced ER Ca^{2+} release in both H4-APPswe and HEK29T cells; these results are consistent with a decreased ER Ca^{2+} level, as measured with the ER-targeted probe G-CEPIA1er. In addition to this, Orai2 revealed to be a less efficient mediator of SOCE than Orai1, since it dampened SOCE when overexpressed alone and it produced a much smaller SOCE when overexpressed with STIM1 as compared with Orai1 plus STIM1 overexpression. Conversely to our expectations, Orai2 downregulation had a noticeable effect neither on IP3-induced ER Ca^{2+} release nor on total store Ca^{2+} content; it however improved Ca^{2+} entry upon store depletion. As far as subcellular localization goes, Orai2 overexpression did not increase the fraction of protein present in the ER and it appeared that most of the protein was found at the early endosomal level, as revealed by immunofluorescence staining of various subcellular compartments. This holds true moving to cortical neurons, where Orai2 was preferentially found in Rab5-EEA1 positive endosomes in primary cultures from WT mice, with a dramatic accumulation at this level in neurons from 2TG mice, possibly reflecting the increased early-endosome compartment that characterizes the AD phenotype. Orai2 localization is, however, dynamic, meaning that it moves in and out of endosomes when properly stimulating neurons with compounds able to induce neuronal activity or to stimulate SOCE. This behaviour is anyway different among the three genotypes, with TG neurons showing a greater tendency to retrieve Orai2 in endosomes upon cell stimulation, and 2TG neurons being unable to properly tune their endosome pool, possibly because of its higher accumulation level. Whether these changes involve also Orai1 has still to be evaluated and it will give us a better picture of this unknown phenomenon. Finally, evidence is provided that a down-tuning of SOCE is associated with increased levels of secreted Aβ42, as measured by ELISA performed on conditioned media from mutant APP-expressing cells such as CHO-7PA2 and H4-APPswe.

RIASSUNTO

La malattia di Alzheimer (AD) costituisce la forma di demenza più comune nella popolazione anziana. Ormai più di vent'anni fa è stata formulata la cosiddetta ipotesi della cascata amiloide, la quale si basa sulle placche amiloidi, uno dei principali marker di AD, tra i più conosciuti e studiati. La formulazione di quest'ipotesi fu permessa dalla scoperta di tre gene i quali, allorché mutati, sono associati con la forma familiare di AD (FAD). Uno di questi geni codifica per la proteina precursore dell'amiloide (APP), la quale è una proteina di tipo I a singolo dominio transmembrana che viene tagliata in maniera sequenziale dagli enzimi della famiglia delle secretasi. L'ultima secretasi a tagliare APP, nonché la più importante nell'AD, è chiamata γ-secretasi ed è composta da quattro proteine, che comprendono o la presenilina 1 (PS1) o la presenilina 2 (PS2), codificate dagli altri due geni (*PSEN1/PSEN2*) responsabili della patogenesi di FAD. Mutazioni autosomiche dominanti in *APP*, *PSEN1* o *PSEN2* causano una deposizione più veloce di Aβ, dovuta ad un aumentato rapporto Aβ42/Aβ40. La maggior parte dei casi di AD, tuttavia, è sporadica; i pazienti FAD con mutazioni in PS2 mostrano un decorso clinico della malattia molto più simile a quello dei pazienti sporadici.

Molti gruppi di ricerca hanno dimostrato la capacità delle PSs di perturbare l'omeostasi cellulare del Ca^{2+}, e in particolare il nostro gruppo ha dimostrato che PS2, sia nella forma mutata associata a FAD che nella forma wild-type (WT), abbassa il contenuto di Ca^{2+} del reticolo endoplasmatico (ER) e dell'apparato di Golgi. Inoltre essa interagisce con la pompa SERCA, diminuendone il funzionamento, e modula la vicinanza fra ER e mitocondri; tutte queste funzioni pleiotropiche sono indipendenti dalla sua attività γ-secretasica. Recentemente un altro gruppo ha identificato PS2 come un regolatore del contenuto di Ca^{2+} del ER, insieme ad Orai2, il quale è un canale della membrana plasmatica implicato nell'entrata di Ca^{2+} dipendente dallo svuotamento del ER (SOCE). Quest'ultimo fenomeno è alterato nell'AD, e in particolare è ridotto nelle cellule che esprimono PS mutate. Questa serie di informazioni rappresenta una base interessante per lo studio dell'interazione fra contenuto di Ca^{2+} del ER, diminuzione di SOCE e metabolismo di APP/produzione di Aβ. Grazie ai modelli murini di AD basati su PS2 presenti in laboratorio, specificatamente il modello singolo transgenico (TG), esprimente il mutante FAD PS2-N141I (linea PS2.30H) e il modello doppio transgenico (2TG), esprimente PS2-N141I insieme al mutante *Swedish* APP-K670M/N671L (linea B6.152H), abbiamo potuto investigare il pattern di espressione di Orai2 nel tessuto nervoso.

Nei Western blot di cortecce ed ippocampi abbiamo notato come Orai2 sia sovra-espressa nella corteccia dei topi TG e 2TG se confrontati con topi di controllo C57BL/6 (WT). Quest'aumento di espressione è dovuto principalmente ad un contributo neuronale, sia in quanto è maggiore in colture neuronali pure, sia perché Orai2 è presente solamente nei neuroni *in situ*, come rivelato dall'analisi immunoistochimica di fettine di cervello. L'aumentata espressione di Orai2, così come si ritrova nei neuroni TG e 2TG, è in grado di alterare l'omeostasi cellulare del Ca^{2+}. In particolare, quando sovra-espressa, Orai2 causa una riduzione significativa del rilascio di Ca^{2+} indotto da IP3, sia in cellule H4-APPswe che HEK293T; questi risultati sono in accordo con una riduzione del contenuto di Ca^{2+} del ER, condizione osservata utilizzando la sonda G-CEPIA1er, direzionata al ER. Inoltre, Orai2 si è rivelato essere un mediatore di SOCE meno efficiente di Orai1, infatti diminuisce SOCE quando espresso da solo e, se co-espresso con STIM1, dà vita ad un SOCE meno ampio di quello prodotto da Orai1 co-espresso con STIM1. Contrariamente a quanto atteso la riduzione di Orai2 non produce alcuna diminuzione né del rilascio di Ca^{2+} indotto da IP3, né del contenuto totale di Ca^{2+} dei depositi intracellulari; essa tuttavia produce un lieve aumento dell'ingresso di Ca^{2+} causato dalla deplezione dei depositi. Per quanto riguarda la localizzazione subcellulare, la sovra-espressione di Orai2 non aumenta la frazione di questa proteina presente nel ER, la maggior parte di Orai2 è infatti presente a livello degli "early endosomes", come dimostrato marcando numerosi compartimenti subcellulari in immunofluorescenza. Ciò resta vero anche nei neuroni corticali in coltura. Nei neuroni WT, Orai2 si trova preferenzialmente negli endosomi positivi per Rab5 ed EEA1, a questo livello la localizzazione aumenta nei neuroni 2TG, un accumulo causato probabilmente dall'aumento degli "early endosomes" tipico del fenotipo AD. Nonostante sia presente a livello endosomiale, la localizzazione di Orai2 è dinamica, e cioè cambia fra dentro e fuori dagli endosomi a seconda dello stimolo usato per aumentare l'attività neuronale o per indurre SOCE. Questo dinamismo appare diverso fra i tre genotipi, dove i neuroni TG mostrano una maggior tendenza ad accumulare Orai2 negli endosomi dopo stimolazione della cellula, mentre i neuroni 2TG risultano incapaci di modulare questo aspetto, probabilmente perché in queste cellule l'accumulo di endosomi è prossimo alla saturazione. Resta da valutare se questi cambi di localizzazione interessano anche Orai1, un'informazione che ci permetterà di avere un'idea più precisa di questo fenomeno sconosciuto. Infine vi è evidenza che la diminuzione di SOCE è associata ad un aumento dei livelli di Aβ42 secreta, così come misurato tramite saggio ELISA sui terreni condizionati provenienti da cellule che esprimono una forma mutata di APP, quali le CHO-7PA2 e le H4-APPswe.

ABBREVIATIONS

$[Ca^{2+}]$	calcium concentration
$[Ca^{2+}]_i$	intracellular calcium concentration
a.u.	arbitrary units
AD	Alzheimer's disease
ADAM	A disintegrin and metalloproteinase
AEQ	aequorin
AICD	APP intracellular domain
AM	acetoxymethyl ester
Aph-1	anterior pharynx defective-1
ApoE	apolipoprotein E
APP	amyloid-β precursor protein
ATP	adenosine triphosphate
Aβ	amyloid-β
Aβo	amyloid-β oligomers
B2M	beta-2-microglobulin
BACE-1	β-site APP cleaving enzyme
BAPTA-AM	(1,2-bis(*o*-aminophenoxy)ethane-*N*, *N*, *N'*, *N'*-tetraacetic acid – acetoxymethyl ester
BSA	bovine serum albumin
BTP-2	[N-4-[3,5-bis (trifluoromethyl)-1H-pyrazol-1-il] phenyl-4-methyl-1,2,3-thiodiazol-5-carboxamide
Ca^{2+}	calcium ion
CaM	calmodulin
CCE	capacitative Ca^{2+} entry
cDNA	complementary DNA
CHO	Chinese hamster ovary cells
CICR	Ca^{2+}-induced Ca^{2+} release
CNS	central nervous system
CPA	cyclopiazonic acid
CTF	C-terminal fragment
cypA	cyclophillin A
cytAEQ	cytosolic aequorin

DAG	diacylglycerol
DAPT	N-[N-(3,5-difluorophenylacetyl)-L-alanyl]-S-phenylglycine t-butylester
DMEM	Dulbecco modified Eagle's medium
EGTA	ethylene-glycol-bis(2-aminoethyl)-*N, N, N', N'*-tetraacetic acid
ELISA	enzyme-linked immunosorbent assay
ER	endoplasmic reticulum
FAD	familial Alzheimer's disease
FCS	foetal calf serum
FL	full-length
FRET	Foerster resonance energy transfer
GAPDH	glyceraldehyde-3-phosphate dehydrogenase
GFP	green fluorescent protein
HEK	human embryonic kidney cells
HEPES	4-(2-hydroxymethyl)-piperazin-1-ethansulphonic acid
HRP	horse-radish peroxidase
I_{CRAC}	Ca^{2+} release activated Ca^{2+} current
IP3	inositol-1,4,5-trisphosphate
IP3R	IP3 receptor
kDa	kiloDalton
LTD	long-term depression
LTP	long-term potentiation
MAMs	mitochondria-associated (ER) membranes
MAPs	microtubules-associated proteins
MCU	mitochondrial Ca^{2+} uniporter
NCT	nicastrin
NFT	neurofibrillary tangles
NICD	notch intracellular domain
NP-40	nonidet P-40
NTF	N-terminal fragment
PAGE	polyacrylamide gel electrophoresis
PBS	phosphate buffered saline
Pen-2	presenilin enhancer-2

PLC	phospholipase C
PM	plasma membrane
PMCA	plasma membrane Ca^{2+} ATPase
PS	presenilin
PS1	presenilin 1
PS2	presenilin 2
RIPA	radio-immunoprecipitation assay buffer
ROCCs	receptor-operated Ca^{2+} channels
RT	room temperature
RyR	ryanodine receptor
SAD	sporadic Alzheimer's disease
SDS	sodium dodecyl sulphate
SERCA	sarco-endoplasmic reticulum Ca^{2+} ATPase
SMOCCs	second messenger-operated Ca^{2+} channels
SOCCs	store-operated Ca^{2+} channels
SOCE	store-operated Ca^{2+} Entry
STIM	stromal interaction molecule
TEMED	tetramethylethylendiamine
TMB	tetramethylbenzidine
VOCCs	voltage-operated Ca^{2+} channels
WB	Western blot

INTRODUCTION

While writing these lines I'm getting acquainted with the press release regarding the promising monoclonal antibody *aducanumab* (Sevigny, et al. 2016), the first of many attempts to finally be successful in reducing the so-called amyloid burden in Alzheimer's disease (AD) patients' brains. Will it be enough?

Some light has to be shed on the pathogenesis of AD and the recent extensive list of unsuccessful clinical trials aimed at removing the amyloid plaques surely puts a question mark on what we thought so far being the milestone in AD aetiology (Marciani 2016; Selkoe and Hardy 2016).

To do this we have to retrace the history of the hypotheses that were made since the discovery of AD in the early XX century.

Alois Alzheimer, a German neurologist, first discovered the disease in 1906, publishing the results of his analysis of the brain of Frau Deter, that suffered of a familial form of AD (FAD), as it was recently recognized. During the following years we came to know that AD is an irreversible neurodegenerative disorder of the central nervous system (CNS) characterized by the arising of dementia. In the early stage a mild loss of memory and cognitive function appears, a phenomenon that gets worse bringing together personality disorders, severe memory and learning impairments, decline in lexical abilities and spatio-temporal disorientation. Usually, depending on the "strength" of the disease, within 5-10 years from the diagnosis, the clinical picture worsens toward hallucinations, loss of face recognition, aphasia, aggressive behaviour and self-sufficiency is usually lost (Forstl and Kurz 1999).

As for 2016 we count more than 44 million people with AD or related dementia, and the number is growing, especially in the developing countries, to reach 75 million in 2030 and 130 million in 2050. These are dreadful numbers, especially because only 20 to 50% of AD cases are diagnosed in high-income countries (https://www.alz.co.uk/research/statistics), hindering a thorough estimate of the costs on society. Ageing is, trivially, the strongest risk factor for developing the pathology, however environmental factors, diet and metabolic dysfunctions are day by day becoming more central in the field. Another prominent peculiarity of AD is that out of three patients, two are women, and this is probably related with the longer life expectation typical of women. AD is usually divided according to the age of onset, giving the most common "late onset AD", that affects people > 65 years old, and the "early onset AD", for people younger than 65, representing 1 – 5 % of the total cases. Of interest for the biomedical research is another distinction, between the sporadic form, and the FAD, indeed ensuing from a mutation in one of

the following genes: *PSEN1*, coding for Presenilin 1 (PS1), 80% of FAD cases, showing the most aggressive phenotypes, *APP*, coding for Amyloid Precursor Protein (APP), 14% of FAD cases, and *PSEN2*, coding for Presenilin 2 (PS2), 6% of FAD cases (Ertekin-Taner 2007; Goedert and Spillantini 2006). We will soon get into details for what concerns these mutations, but something has to be said and kept in mind along the discussion: FAD cases, that are, for the large majority, "early onset", represent around 15% of this sub-category, and this makes less than 1% of the total cases (Karran, et al. 2011). Despite these small numbers and the fact that these mutations often give rise to very aggressive forms of AD, FAD offers us the only way to model the disease, expressing the mutated proteins in cell lines or in transgenic animals. Interestingly, compared to PS1 mutations, those in PS2 are associated with milder phenotypes, more easily referable to the sporadic forms of AD (Jayadev, et al. 2010). Strictly speaking, AD is a human disease and mice do not live long enough to develop AD. In addition, none of the afore-mentioned mutant genes, whether expressed alone or even together in a transgenic or knock-in mouse, are going to recapitulate the full disease. The expression of APP mutants, linked to FAD, is only partially mimicking the disease. The combination of two of those genes, usually *PSEN1* together with *APP,* accelerates the disease but still does not recapitulate the full AD phenotype. This is due to the fact that the endogenous murine APP does not behave as the human counterpart and has therefore to be replaced with the human orthologue. Even the combined expression of human PS (either 1 or 2) and APP mutants are however still unable to closely mimic the disease (see below), but at least some features are recapped and can be assessed, such as the deposition of amyloid-β (Aβ), the so-called senile plaques, one of the two major AD markers, the appearance of gliosis and some behavioural tasks that relate to cognitive impairment. Lack of neurofibrillary tangles (NFTs), the other major AD marker (see below), and minimal or variable neuronal loss make these mouse lines incomplete AD models (Zahs and Ashe 2010).

Back in 1907 Alois Alzheimer pointed out the histological hallmarks of the disease, that were later identified in the two categories of NFT and senile plaques (Parihar and Hemnani 2004; Perl 2010). Post-mortem analysis of brain specimen coming from AD patients revealed how the cortex is interested by a modest degree of atrophy, mainly in the fronto-temporal and parietal lobe, met by a more severe atrophy of the hippocampus. This shrinking causes a general rearrangement of the ventricles as well, that become bigger. This phenomenon is evident in young subjects, slowly overlapping with the general ageing of the brain for older patients. Being post-mortem diagnosis of AD useless for the patient by definition, it is of tremendous importance to find early biomarkers and neuroimaging tests to promptly identify the disease, given the fact that the few medications

available nowadays have an appreciable effect only in the early stage of the disease. PET neuroimaging, utilizing radioactive fluoro-deoxiglucose as a tracer, is currently employed; by this way regional hypometabolism, that correlates with the disease's progression, is revealed. Brain deposition of senile plaques is associated, in the cerebrospinal fluid (CSF), with decreased levels of soluble Aβ together with increased amounts of the microtubule-associated protein tau and its phosphorylated form, p-tau, one of the major components of NFTs, the most common index of neurodegeneration. There is a clear correlation between the levels of these markers in the CSF and the progression of the disease, however a large consensus on their diagnostic use is yet to be achieved (**Figure 1**) (Edmonds, et al. 2015; Perrin, et al. 2009). Going back to the histological hallmarks, as mentioned above, the NFTs are abnormal fibrous inclusions within the perikaryal cytoplasm of some neurons, but most commonly they're found along dystrophic axons that surround the senile plaques. Ultrastructural analysis revealed their composition: they are made of abnormal 10 nm thick fibrils, occurring in pairs and wound in a helical fashion with a regular periodicity of 80 nm. The main constituent of these fibrils is the microtubule-associated protein tau, that in AD is hyperphosphorilated, together with a number of other proteins such as ubiquitin, cholinesterases and Aβ (Perl 2010). The senile (amyloid) plaques are instead extracellular large aggregations

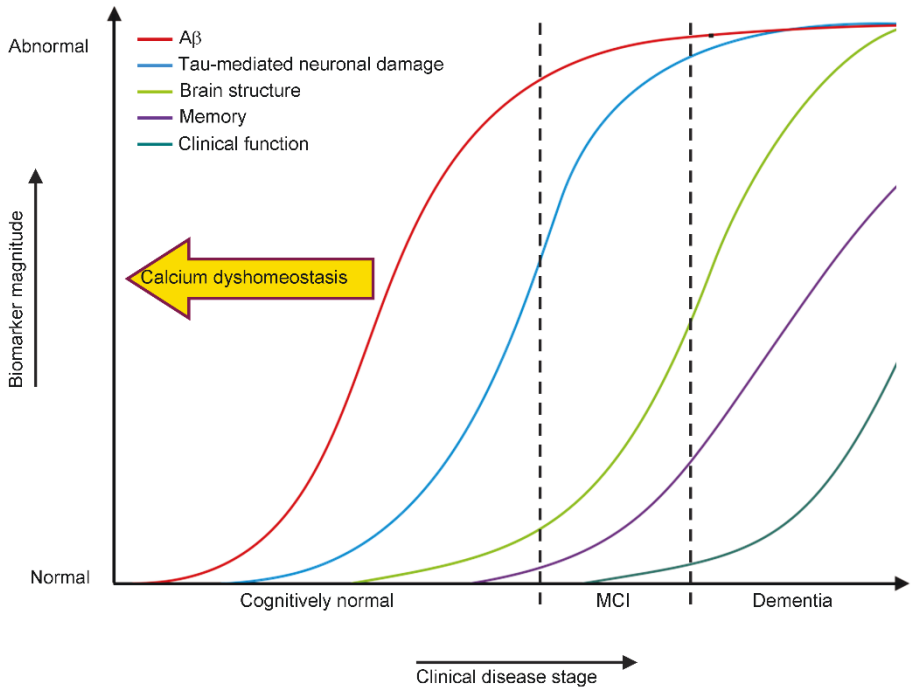

Figure 1: *differential appearance of AD markers.*

built by insoluble fibrils of Aβ. This term includes a mix of different peptides, in the range of 4 kDa, all derived from the proteolytic processing of the aforementioned APP. They assume a typical β-

sheet configuration that enable them to form large aggregates (fibrils) detected, through binding, by the unspecific dyes Congo Red and thioflavin-S. Immunohistochemical techniques are now preferred to identify them because of specificity and capability to detect also diffuse plaques made of large oligomers and proto-fibrils. They are not indeed the only amyloid-like structures that can be found in the brain, notably α-synuclein and huntingtin, two proteins respectively involved in parkinsonism and Huntington's Chorea, are reported to form insoluble plaques as well. The central cores of senile plaques are known to contain several other proteins, such as heparin sulphate glycoproteins, apolipoprotein E and complement proteins (Perl 2010). Not only neurons are hit by the presence of senile plaques: microglia and reactive astrocytes are involved as well and can be found in the surroundings of the plaques. Whether these players are actively involved in the pathogenesis of the disease is still a matter of intense debate. Nowadays a consensus has formed around the idea that the inflammatory processes, mediated by glial cells, can exacerbate the intrinsic amyloid toxicity (Verkhratsky, et al. 2016).

γ-SECRETASE

γ-secretase is a large enzymatic complex whose role is pivotal in AD: it is both the enzyme that contains PS1 or PS2 and that, through them, cleaves APP. It belongs to a particular class of enzymes called i-CLiPs (intramembrane-cleaving proteases) and together with APP it cleaves different substrates such as Notch, Delta1, E- and N- cadherins, CD44, ErbB4 and the β2 subunit of the voltage dependent Na^+ channel (McCarthy, et al. 2009). Substrates must be type I transmembrane (TM) protein probably bearing a brief "consensus" sequence (Tolia and De Strooper 2009); these requirements dim the light on a very recent discovery that enriches the list of substrate with STIM1, yet inverting the sequence, making it a type II TM protein; it is therefore unclear if it can be considered a proper substrate (Tong, et al. 2016).

The γ-secretase is composed of four subunits, shown to be necessary and sufficient for the enzymatic activity, namely: PS (either PS1 or PS2), nicastrin (NCT), anterior pharynx-defective 1 (Aph-1) and PS enhancer-2 (Pen-2). The stoichiometry appears to be 1:1:1:1 (De Strooper, et al. 2012). In the following chapter, we will better deal with PSs, that are indeed the catalytic core of the enzyme, and the only components for which a direct involvement on Ca^{2+} homeostasis was proved; here, a brief overview of the roles of the other components is presented.

Nicastrin is a 709 amino-acid (AA) long, type I glycoprotein (80-130 kDa, depending on the glycosylation state) with a transmembrane domain that serves as the main site for interaction with Aph-1 and PS. The large extracellular/luminal glycosylated domain undergoes a range of post-

translational modifications that allow it to be critical for the initial binding of the substrate to the enzymatic complex.

Aph-1 is a 7 transmembrane domain protein, weighing 30 kDa, with the N-terminus protruding in the extracellular/luminal space and a cytosolic C-terminus. The TM4 domain contains a GxxxG motif that was shown to be necessary for the interaction with Pen-2 and PS, but not NCT. The role of this component is not yet clear and it appears to be a structural/scaffold protein necessary for proper assembly of the complex.

Pen-2 is a small protein weighing around 10 kDa with three TM domains with the N-terminus facing the cytosolic side, while forming a hairpin, and the C-terminus facing the extracellular/luminal side (Sun, et al. 2015; Zhang, et al. 2015b). The N-terminus is important for the interaction with PS while the C-terminus and the TM1 are necessary for activating the endo-proteolysis of PS, although with an unknown mechanism (Tolia and De Strooper 2009). In the ER, NCT and Aph-1 firstly form a sub-complex (De Strooper, et al. 2012) that interacts with PS to form an intermediate trimeric complex; the incorporation of Pen-2 in the hetero-tetramer results in the endoproteolysis of PS that reaches its mature, active structure. The tetrameric state has been reported to assemble immediately before or within COPII vesicles, the ER exit carriers (Kim, et al. 2007). An intense cycling back and forth between Golgi apparatus and ER has been reported, with only a small fraction of complexes that reaches the trans-Golgi network for further glycosylation of NCT. The small portion of active γ-secretase is mainly found in plasma membrane and endosomes, presumably after having completed the cycle ER → Golgi apparatus → plasma membrane → endosomes (Chyung, et al. 2005; Kaether, et al. 2006). A precise structure of this enzymatic complex has yet to be made available, mainly because of the difficulties in crystallizing a complex harbouring 20 TM domains, deeply buried in the intermembrane space, an extremely hydrophobic compartment where the cleavage is executed. Notwithstanding, very recently the human complex was purified and analysed by electron cryo-EM, which freezes the protein in its native conformation. By three-dimensional (3D) electron density maps reconstruction at 4.32 Å resolution was thus obtained (Sun, et al. 2015). Knowing the structure of γ-secretase is still a primary goal in AD research because it allows the scientist to design effective and selective inhibitors or modulators that can rescue to normality the abnormal APP cleavage.

PRESENILINS

PS1 and PS2 are homologous membrane proteins respectively encoded by the genes *PSEN1* on chromosome 14 and *PSEN2* on chromosome 1. They weigh around 50 kDa and are 467 and 448

AA long, respectively. Their homology is confirmed by a 65% identity between the two sequences and both are thought to be the catalytic core of γ-secretase, since the enzymatic activity of the latter is abolished in cells knock-out for PS1 and PS2 (Herreman, et al. 2000). Either PS1 or PS2 can be incorporated in the enzymatic complex, never the two together, thus allowing two (at least, isoforms of Aph-1 are reported) different γ-secretase complexes with possibly different recognizing/cleaving specificity (De Strooper, et al. 2012; Meckler and Checler 2016; Sannerud, et al. 2016). Some general considerations can be made for both proteins, since morphologically, topologically and biochemically they apparently do not differ much. They possess 10 hydrophobic regions, of which 9 are spanning the membrane and one is comprised in a long cytosolic loop, the N-terminus is cytosolic and the C-terminus is extracellular/luminal (**Figure 2**). Upon Pen-2 recruitment within the γ-secretase complex, the immature PS holoprotein undergoes an endo-proteolytic cleavage at the level of the cytosolic loop between the 6th and the 7th hydrophobic domain, giving two fragments called N- and C-terminal fragments (NTF and CTF, around 30 and 20 kDa, respectively). It is the dimer NTF/CTF to be considered catalytically active, with the two critical aspartate residues facing each other on the 6th and 7th TM domain; mutation of either one or both of these residues to alanine causes a loss of function (Kimberly, et al. 2000). As for the other components of γ-secretase they are enriched in the ER and Golgi apparatus, with only a minor part in the plasma membrane. Whether the PS, which is found in large amount at the ER level, is inactive (in the full-length form) or catalytically active (as a dimer) is still a matter of debate; recent evidence suggests their presence as well as their activity as APP cleaving protein in the ER mitochondria-associated membranes (MAMs) (Leal, et al. 2016). At the tissue level, both PSs are highly expressed in the brain and still detectable in any adult human tissue (Brunkan and Goate 2005). I already anticipated the importance of these homologous proteins in AD and indeed their mutant forms are responsible for almost the majority of FAD cases. Almost 200 autosomal dominant mutations in PS1 and around 14 in PS2 are associated with FAD aetiology; interestingly, especially in the case of PS1, mutations appear to be randomly distributed along the structure, hampering the attempts at individuating a peculiar cause-effect nexus. I am going to deepen soon the catalytic process that involves APP, however I can shortly say that γ-secretases, and therefore PSs, are involved in the last of its cleavages, the one that generates the infamous Aβ. It was initially thought that FAD-linked PS mutants were associated with an increased activity, generating more Aβ. This however, despite holding true for some mutations (Citron, et al. 1997; Scheuner, et al. 1996), was recently challenged by other studies reporting instead a reduced enzymatic activity with a shift in the ratio of the two major Aβ species, Aβ42 and Aβ40 (Florean, et al. 2008; Shimojo, et al. 2007; Walker, et al. 2005). Currently the leading hypothesis posits a general tendency to the

loss of function, met by a less precise cleavage that favours the production of Aβ42, thus altering the ratio. Being Aβ42 more prone to aggregation, the increased production of oligomers and proto-fibrils, followed by Aβ deposition, is reflected, in AD patients, by lower CSF Aβ42 levels (De Strooper 2007). In addition to their well-defined catalytic role, PSs are known to have pleiotropic, γ-secretase-independent functions, primarily in regulating Ca^{2+} homeostasis, but also in protein trafficking, cell adhesion and autophagy (De Strooper and Annaert 2010; De Strooper, et al. 2012). PS functions regarding Ca^{2+} handling will be extensively discussed below and serve as the main ground of this study.

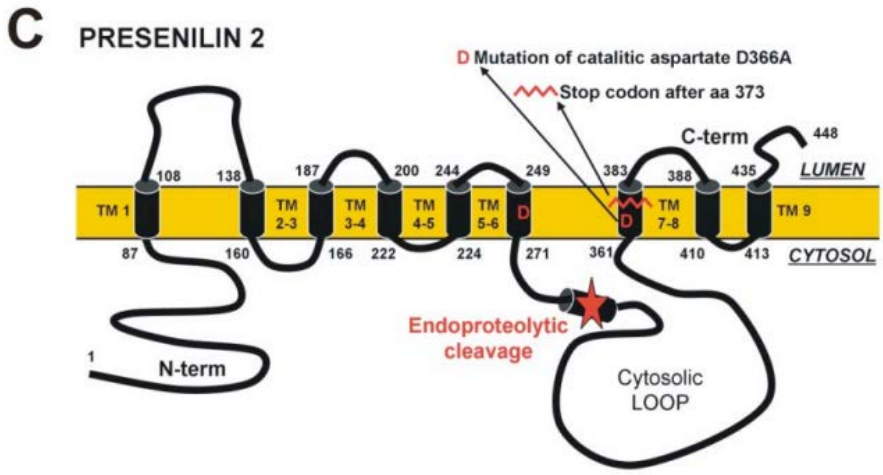

Figure 2: *Presenilin-2 (modified from Filadi et al, 2016)*

APP

APP stands for amyloid precursor protein and, as previously shown, it is one of the three proteins that whether mutated cause FAD. It is a single transmembrane domain protein of the type I family, that is saying extracellular/luminal N-terminus and cytosolic C-terminus. Mammals possess other members of this family that are called APP like protein 1 and 2 (APLP1/2); these proteins have diverse well conserved domains, especially in the extracellular portion. The Aβ domain that spans the membrane is not conserved, making the homologues APLP1/2 redundant for the signalling functions, but not for amyloidogenesis (Wolfe 2007). The APP gene is located on chromosome 21, and this fact is instrumental in understanding the Down Syndrome-related dementia; consisting of 18 exons it undergoes tissue-specific splicing, generating various isoforms. The most represented three splicing variants are those 695, 700 and 751 amino acids long, the first being peculiar of the nervous system. By Western-blotting APP, several immune-bands can be identified,

and those ranging from 90 to 130 kDa represent the maturation state of the protein: during the journey through the secretory pathway APP is O- and N- glycosylated, sent to the plasma membrane and then retrieved to endosomes; in doing this it resembles its cleaving enzyme γ-secretase (Thinakaran and Koo 2008). AD research filed is interested in the pathological aspects of APP, although a more thorough investigation on its physiological meaning could only be beneficial. Thus far it is accepted its involvement as a trophic factor in cellular adhesion and signalling (Thinakaran and Koo 2008; Zheng and Koo 2006). A by-product of its cleavage, soluble APPα, promotes neurite growth and synaptogenesis, in addition to promoting the growth of other cell types, such as fibroblasts. Based on the similarities with Notch (that is itself a substrate of γ-secretase), a well-known transmembrane receptor involved in a large variety of cellular signalling and neurogenesis, it was proposed that APP can function as a receptor as well; a specific ligand, TAG-1, has therefore been found (Ma, et al. 2008). APP also interacts with kinesin-1 and can hence be implicated in axonal transport; a role in transcriptional modulation cannot be excluded since the APP intracellular domain (AICD) was proven to bind to the adaptor protein Fe65. Of note, AICD exerts a direct homeostatic role in APP maturation by controlling, at the translational level, the expression of WAVE1, an APP-interacting protein in the trafficking to the plasma membrane (Ceglia, et al. 2015).

Being a substrate of various enzymes, APP can be cleaved in a sequential fashion, originating diverse by-products, with different roles; traditionally, its fate is divided into two different pathways, called non-amyloidogenic and amyloidogenic, respectively (**Figure 3**). The first is the predominant one and poses that APP is initially cleaved by α-secretase, a generic name that identifies ADAM family enzymes: this secretase hydrolyses APP within the Aβ containing sequence, thus preventing its formation. A soluble N-terminal fragment (sAPPα, with possible signalling functions, see above) is released in the extracellular /luminal space, whilst a C-terminal fragment called C83 remains membrane-bound. On the contrary in the amyloidogenic pathway APP is cleaved by β-secretase (encoded by *BACE1*), preserving the entire Aβ fragment and thus originating a shorter soluble portion (sAPPβ) with unknown functions, and a longer C-terminal peptide, called C99, that also stays membrane-bound. At this stage the two pathways converge on γ-secretase, further originating a so-called p3 fragment for the non-amyloidogenic and Aβ for the amyloidogenic one; AICD is generated as a result of both the pathways. However, the inter-membrane cleavage operated by γ-secretase is not very precise, this secretase appears to have multiple cleavage sites and proceeds by chopping away 3 amino acids at a time, thus giving an Aβ peptide that ranges from 49 to 38 AA (De Strooper and Annaert 2010; Fukumori, et al. 2010). The most abundant product is Aβ40 and about 10% is represented by Aβ42, that, thanks to those

two amino acids left, is more hydrophobic and more aggregation-prone, at least the human form. Unlike mutations in PSs, those of APP are located close to the cleaving sites of one of the three secretases, either reducing the α- cleavage, increasing the β- cleavage or altering the γ- one. These observations, together with comparisons of Aβ sequence among species immune to dementia, and the fact that simply overexpressing APP (see Trisomy 21, aka Down Syndrome) can lead to early onset dementia, give strong support to what have been called the amyloid cascade hypothesis for AD pathogenesis.

THE AMYLOID CASCADE HYPOTHESIS

When initially proposed in 1991 (Hardy and Allsop 1991), the amyloid hypothesis was aimed at giving thickness to a somewhat large body of evidence pointing toward the Aβ peptide. Many, if not all, mutations implicated in FAD have a prominent effect on the production of Aβ, at least when the mutant proteins (APP, PS1 or PS2) are expressed in a heterologous system such as a cell line (HeLa, MEF, SH-SY5Y etc.) or in a transgenic animal (Hardy and Selkoe 2002). In particular, the amount of Aβ42 produced is increased, or at least the ratio Aβ42/Aβ40 is altered in favour of the former (Haass and Selkoe 2007). This prompted toward the identification of Aβ42 as the pathogenic *noxa,* for much of the following studies aimed at establishing its aggregation/oligomerization-prone behaviour, that could serve as a seed for further Aβ40 deposition (Chen and Glabe 2006). Formulating this hypothesis has sure been an avid opportunity for the proponents, however some drawbacks are right behind the corner and eventually the multiple clinical trial failures are undermining this shining hypothesis. Without even going so far away as the clinical trials, scientists first discovered how the amyloid load, in form of senile plaques, very poorly correlates with the degree of dementia; they basically demonstrated how there can be an old brain, loaded with plaques but without AD, whereas there are no Aβ-free AD brains. The amyloid hypothesis was re-shaped right away (Haass and Selkoe 2007; Hardy and Selkoe 2002) to include the Aβ species, other than plaques and fibrils, that actually show correlation with the disease progression: the utterly famous Aβ oligomers. Research has produced a proper plethora of discoveries that posit Aβ oligomers in every field of neuroscience as a potent toxin, some examples: they inhibit the formation and maintenance of the long-term potentiation (LTP) in the hippocampus, thus hampering memory formation (Walsh, et al. 2002b); they alter cellular Ca^{2+} handling by creating pore channels in the plasma membrane (Arispe, et al. 2007); they impair mitochondrial metabolism and ROS production (LaFerla 2010; LaFerla, et al. 2007), they signal to, or inhibit the physiological signalling of, various plasma membrane receptors,

interacting with glutamate receptors and/or the prion protein (Lauren, et al. 2009; Um, et al. 2013b). Our lab proposed an activity-dependent internalisation that is blocked by inhibitors of neuronal activity and by tetanus toxin (Lazzari, et al. 2015), and tried to clarify many doubtful aspects of the aforementioned studies, three above all: i) Aβ42 oligomers were produced in F12 medium that itself evokes Ca^{2+} related abnormalities; ii) Aβ42 oligomers were administered to cells/slices in huge concentrations (well above 1 μM); iii) to produce channels a peculiar administration protocol should be followed (Arispe, et al. 2007). Not to mention the elusiveness of the definition "Aβ oligomers" on which Lesne and collaborators tried to shed some light (Lesne 2014; Lesne, et al. 2013; Lesne, et al. 2006), distinguishing between oligomers that you can find in the brain, versus those you can produce oligomerising synthetic Aβ42 or heterologously expressing mutant APP in a cell line. Extremely valuable also his contribution on the alterations brought by the extraction/blotting techniques. We also contributed to an attempt of harmonisation (Agostini and Fasolato 2016), bringing together the multiple evidence, that span from interaction with Ca^{2+} players to Ca^{2+} alteration of kinases/phosphatases (note that tau is hyper-phosphorylated in AD), putting this time Ca^{2+} on the centre stage.

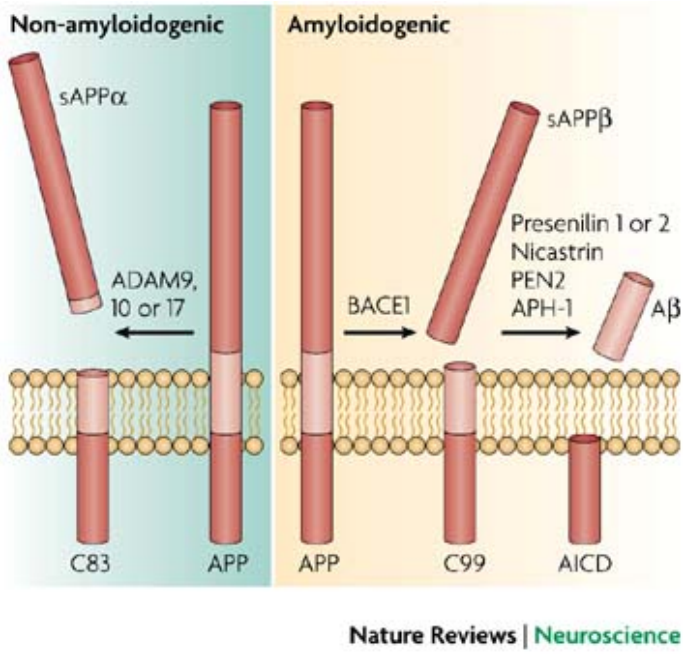

Figure 3*: APP proteolytic cleavage (modified from La Ferla et al., 2007)*

THE Ca^{2+} HYPOTHESIS

Ca^{2+} is one of the most important intracellular second messenger and has an essential role in different cellular processes, ranging from fertilization, active secretion, muscular contraction, cell

differentiation to cell death (Berridge, et al. 2000). Specificity of the Ca^{2+} signal is achieved through spatio-temporal regulation of its amplitude and frequency, with the deciphering task assigned to specific Ca^{2+} binding proteins and downstream signalling proteins, in order to activate proper cellular effectors. At the neuronal level, that is central to AD research, Ca^{2+} signal is tightly regulated and it is pivotal in excitability, neurotransmitter release, long-term synaptic plasticity and transcription of several genes (Berridge 1998).

As we already anticipated, Ca^{2+} and Aβ have been linked by several studies and, therefore, Ca^{2+} arises as an important player in AD pathogenesis; this is further corroborated by the fact that FAD-associated PS mutants display various degrees of Ca^{2+} homeostasis perturbation (Agostini and Fasolato 2016; Zampese and Pizzo 2012). A brief overview of cellular Ca^{2+} homeostasis, focused on neurons, is presented before addressing AD related alterations.

Ca^{2+} homeostasis

The majority of extracellular signals, such as hormones, neurotransmitters and growth factors, cannot freely cross the PM and therefore act by binding to PM receptors that in turn produce intracellular signals. Cells have developed a complex signalling machinery, made of "second messengers", whose role is to deliver, in a sort of relay race, the extracellular signal to the intracellular effectors. Some PM receptors possess an intrinsic enzymatic activity (*i.e.* tyrosine kinase growth factor receptors) to propagate the signal, other rely on the generation of a cascade of events; the inositol 1,4,5-trisphosphate cascade is paradigmatic of the latter case. The number of second messengers is relatively small and they can be classified in: (i) hydrophobic molecules, such as diacylglycerol and phosphoinositide; (ii) hydrophilic molecules, like cyclic adenosine monophosphate (cAMP), cyclic guanosine monophosphate (cGMP), inositol 1,4,5-trisphosphate (IP3), cyclic adenosine diphosphate-ribose (cADPR), nicotinic acid adenine dinucleotide phosphate (NAADP) and Ca^{2+}; (iii) gaseous molecules, such as nitric oxide (NO), carbon monoxide (CO), hydrogen sulphide (H_2S).

As far as Ca^{2+} is concerned, such a broad spectrum of functions is warranted, as mentioned above, by a fine spatial and temporal regulation of its concentration [Ca^{2+}]. Since Ca^{2+} is a small diffusible ion, it cannot be chemically altered, thus cells have developed specific compartments to store this ion and channels to release it in the cytosol when needed. Ensuring a tight control of [Ca^{2+}] requires a complex toolkit made of channels, antiporters, pumps and Ca^{2+}-binding proteins that are differentially expressed in the cell's sub-compartments.

Originally, cells began to exclude Ca^{2+} from the cytosol because of its ability to precipitate phosphates (Clapham 2007), indeed at resting conditions the cytosolic Ca^{2+} concentration $[Ca^{2+}]_{cyt}$

is maintained around 100 nM, compared to 1.8 mM of the extracellular space and up to 1 mM of the ER (Greotti, et al. 2016). Upon stimulation, such as neurotransmitter binding or depolarization, $[Ca^{2+}]_{cyt}$ rapidly increases up to 1-3 μM, triggering several intracellular events. Cytosolic Ca^{2+} increase occurs both in excitable and non-excitable cells, by mean of entry through PM channels or release from the internal stores, with the first being more common for excitable cells like neurons. ER Ca^{2+} release is usually achieved through the activation of phospholipase C (PLC) and generation of IP3. In skeletal muscle cells, cytosolic Ca^{2+} rises entirely rely on Ca^{2+} release through the type 1 ryanodine receptor (RyR1), whereas in cardiac muscle cells, Ca^{2+} entry, through voltage-gated Ca^{2+} channels, is pivotal to Ca^{2+} release through RyR2, via the so-called Ca^{2+} -induced Ca^{2+} release.

PLASMA MEMBRANE Ca^{2+} CHANNELS IN PHYSIOLOGY

The PM, being the boundary of the cell, is able to rapidly transmit signals across itself, in the form of ionic movements from the extracellular space to the intracellular one, or viceversa. These movements are electrochemical in nature, meaning that they give rise to both chemical and electrical gradients. In order to allow a proper control on these fluxes, an array of different ion channels is present on the PM and most of them are gated, meaning that their opening occurs only when specific conditions are met, for example membrane depolarization or binding of a specific ligand (Fasolato, et al. 1994; Pietrobon, et al. 1990). A distinction can be made based on their ionic selectivity and on the mechanism for their activation (Berridge, et al. 2003); we can divide PM Ca^{2+} channels in ligand-gated, voltage-operated and the peculiar case of store-operated. Specific pumps allow to maintain membrane ionic gradients that are invariably dissipated with time.

Ligand-gated channels

Ligand-gated Ca^{2+} channels display a lower selectivity for Ca^{2+} over monovalent cations if compared to the voltage-operated channels. This family is usually further divided into two subgroups:

1. Receptor-operated Ca^{2+} channels (ROCCs or ROCs). This first type of channels possesses a ligand binding site in the same polypeptide or in the same molecular complex forming the channel itself. The extracellular binding of the ligand, either hormones or neurotransmitters, triggers channel opening with the ensuing Ca^{2+} entry. NMDAR and

AMPAR belong to this category and they are activated by the neurotransmitter glutamate; of the two, only the first one shows a moderate Ca^{2+} permeability (the relative permeability of Ca^{2+} to Na^{+} estimated from permeability ratios is in the range of 10:1); their role in neurons is central for the cell functionality and at the basis of excitability, long-term potentiation and long-term depression (Wojda, et al. 2008). Another common type of ligand-gated receptor is the nicotinic acetylcholine ionotropic channel, that is expressed by the cholinergic neurons, which are affected in the early phase of the disease. In the CNS, their cell bodies are packed in dense nuclei in the basal forebrain whilst their axonal projections spread throughout the whole cortex, exerting a modulatory effect rather than pure excitation. Acetylcholine binds to two families of receptors, the ionotropic nicotinic receptor (nAChR) and the metabotropic muscarinic one (mAChR). The first one is a non-selective cation channel with a pentameric structure being formed by alpha or beta subunits, or a mix of the two. The subunit composition influences the pharmacological and kinetic properties of the channel, varying its permeability to K^{+}, Na^{+} and Ca^{2+}; with only the neuronal type being endowed of a discrete Ca^{2+} permeability (Albuquerque, et al. 2009).

2. Second messenger-operated Ca^{2+} channels (SMOCs). These channels are activated by second messengers produced or released after the activation of G-proteins or enzyme-coupled receptors. The most common second messengers are: cAMP, cGMP, IP3, DAG, arachidonic acid and Ca^{2+} itself (Clapham 2007). Some channels of the Transient Receptor Potential (TRP) family belong to this group, as well as the elusive ARC channels (Shuttleworth 2012). These channels are activated by various chemical and physical stimuli and are also implicated in osmoregulation; in particular, the TRPV4, which is highly expressed in astrocyte endfeet, shows a good Ca^{2+} permeability similar to that reported for NMDAR (Benfenati, et al. 2011).

Voltage-operated Ca^{2+} channels (VOCCs)

In excitable tissues, such as nervous system and heart, an important role is played by VOCCs, whose opening is regulated by membrane depolarization, a way of transforming electrical signal into a chemical one. VOCCs are multi-subunit complexes made up of primary subunits responsible for pore-forming and voltage-sensing as well as auxiliary subunits, implicated in channel modulation. They constitute a complex family of channels comprising a large number of different subtypes, whose common features are the steep voltage dependency of the opening probability and the high selectivity for Ca^{2+} over monovalent cations (Catterall 2000). Based on their

voltage/inhibitor sensitivity they have been classified into L-, N-, R- T- and P/Q- type. For example, the N- and P/Q- types are present in synapses and control the Ca^{2+} dependent release of neurotransmitters, while L-type are present in dendrites and soma and can mediate Ca^{2+}-dependent gene transcription (Berridge, et al. 2003). This Ca^{2+} signal causes the opening of a subtype of potassium channels that helps membrane repolarization.

Store-operated Ca^{2+} channels (SOCCs)

We already mentioned that cells, especially the non-excitable ones, store Ca^{2+} in intracellular organelles mainly at the ER level. ER is equipped with Ca^{2+} releasing channels and internalizing pumps in order to maintain the right internal concentration meanwhile allowing a proper signalling function. When the ER is partially or fully depleted of Ca^{2+}, a specific refilling mechanism is activated, bearing the name of Capacitative Ca^{2+} Entry (CCE) or, more commonly, Store-Operated Ca^{2+} Entry (SOCE). Its activation involves different steps (**Figure 4**):

1. A stimulus, usually a hormone or a neurotransmitter, triggers the release of Ca^{2+} from the ER, through IP3Rs and/or RyRs. Alternatively, the Sarco-Endoplasmic Reticulum Ca^{2+} ATPase (SERCA) can be blocked and Ca^{2+} can leak out of the ER through passive leakage. The net effect is a partial or full depletion of the ER Ca^{2+} content.
2. A sensor, called STIM (STromal Interaction Molecule), is able to sense the ER Ca^{2+} concentration thanks to its C-terminal EF-hand domains. STIM is structured in a way that allows a prompt oligomerization after the detachment of Ca^{2+} from the EF-hands.
3. STIM, by oligomerizing and moving along microtubules, reaches the ER-PM junction, where it forms the so-called *punctae*, specialized structures where STIM1 interacts with a protein located in the PM that is able to form a Ca^{2+} selective channel named Orai, a CRAC channel subunit, where CRAC means Ca^{2+} release-activated Ca^{2+}. In particular, four Orai molecules are the pore-forming subunits of the channel (Lewis 2007). The crystal structure from *Drosophila* Orai (dOrai), that shares 73% sequence identity with Orai1, suggests a hexameric assembly of Orai subunits, arranged as a trimer of dimers around the central pore (Amcheslavsky, et al. 2015; Hou, et al. 2012).
4. Ca^{2+} enters the cell and is promptly pumped into the ER by Sarco-Endoplasmic Reticulum Ca^{2+} ATPases (SERCAs) present at the ER-PM junction (Clapham 2007).

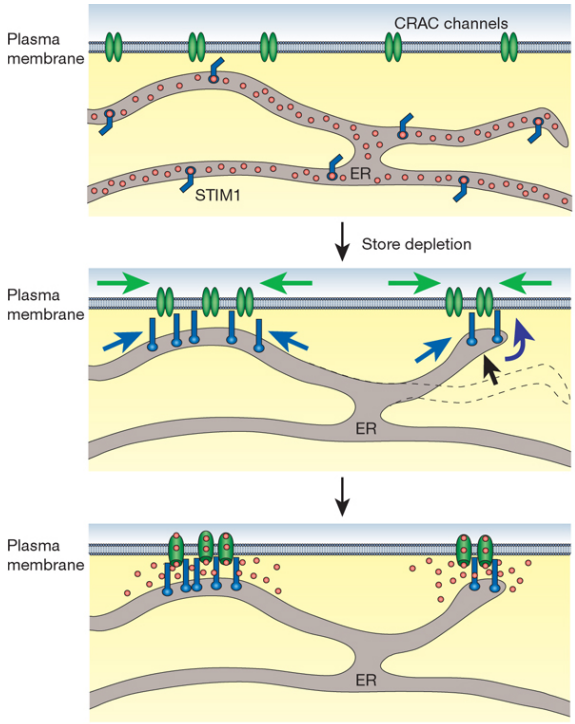

Figure 4: *SOCE activation steps (modified from Lewis, 2007)*

Mutations in the main actors of CCE, STIM and Orai, are associated with severe phenotypes in both animals and humans, for example the Severe Combined ImmunoDeficiency (SCID) syndrome and nonsyndromic tubular aggregate myopathy (Feske, et al. 2006; Lacruz and Feske 2015). Many regulators (scaffolds, Ca^{2+} binding proteins and chaperones) have been reported to interact with STIM and Orai, to finely tune their activities (Shim, et al. 2015). STIM has also been found to interact with and regulate VOCCs in addition to CRAC channels, extending the intricate relationships between these two Ca^{2+} entry pathways in neurons (Harraz and Altier 2014; Nguyen, et al. 2013; Park, et al. 2010; Wang, et al. 2010a). These discoveries underline the possibility that, upon ER depletion, STIM and Orai play different roles in excitable and non-excitable cells, inhibiting VOCCs in the former, while activating CCE in the latter. Moreover, CCE is inhibited by an intrinsic negative feedback called Ca^{2+}-dependent inactivation (CDI), whose molecular mechanism is still poorly understood (Muik, et al. 2012).

SOCE component: STIM

STIM1 was firstly identified as a regulator of CCE in 2005 (Liou, et al. 2005; Roos, et al. 2005), despite being already known for other minor functions (Sabbioni, et al. 1997). Two forms of STIM are present in mammals, called STIM1 and STIM2, located in humans on chromosome 11 and 4,

respectively. As far as we know, the two forms are different in sequence, tissue expression and possibly role, with STIM1 being ubiquitous and necessary for CCE activation, and STIM2 highly expressed in the central nervous system with modulating tasks (Hooper, et al. 2014; Kar, et al. 2012).

STIM1 is a type I single-pass TM domain phosphoprotein of 75-85 kDa (depending on the glycosylation state), mainly located in the ER, with around 10% of it expressed at the PM level, hence the acronym. Structurally (see **Figure 5**) it can be divided in:

1. An N-terminal portion, located in the ER lumen, that hosts the EF-hand Ca^{2+}-binding domain, constituting the actual Ca^{2+} sensor (Liou, et al. 2005). This same region contains also the Sterile Alpha Motif (SAM) that regulates oligomerization occurring after ER Ca^{2+} depletion (Baba, et al. 2006). The EF-hand Ca^{2+} affinity is around 200 μM for STIM1 and 400 μM for STIM2, making the latter more sensitive to changes in the steady-state ER Ca^{2+} level (Brandman, et al. 2007). Moreover, STIM2 EF-hand has slower unfolding and aggregation kinetics, making this protein less efficient in triggering CCE (Stathopulos, et al. 2009; Zheng, et al. 2008).
2. A single-pass TM motif, the most conserved part between the two STIMs (Williams, et al. 2001).
3. The C-terminal portion, organized in different modules:
    a. A domain called CRAC activation domain (CAD), located in the cytosolic loop, responsible for Orai binding and activation (Stathopulos, et al. 2008).
    b. Another domain, located close to CAD, called coiled-coil domain1 (CC1), reported to play an inhibitory role in STIM1 activation: the model proposes that ER Ca^{2+} depletion causes the dimerization of CC1, thus freeing CAD to interact with Orai (Zhou, et al. 2013).The C-terminus of the protein is crucial for CCE activation, since it mediates the interaction with Orai channel on the PM; this part of the molecule is highly divergent between STIM1 and STIM2, making the latter less prone to Orai binding, underlying the functional difference between the two (Shim, et al. 2015). In resting cells STIM1 is a dimer evenly distributed within the ER membrane, bound to EB1, a microtubule-plus-end-tracking protein (Grigoriev, et al. 2008). The decrease in ER Ca^{2+} content causes a conformational change in STIM1, thus initiating the oligomerization and the movement toward the ER-PM junction (Liou, et al. 2007).

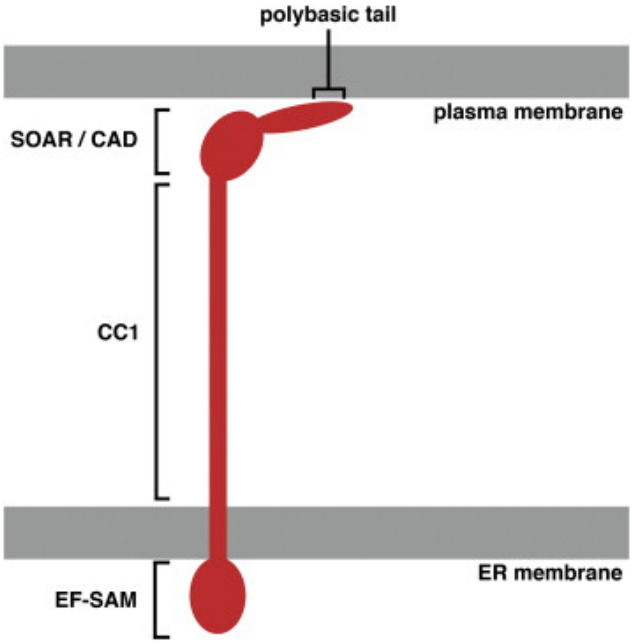

Figure 5: *STIM1 in an extended conformation (modified from Hogan et al, 2015)*

SOCE component: Orai

In 2006, another molecular player of CCE was discovered and it has been called Orai, like the gate-keepers of heaven in the ancient Greek mythology (Feske, et al. 2006; Vig, et al. 2006; Zhang, et al. 2006). Later it was confirmed that it is indeed the direct molecular interactor of STIM (Cahalan 2009). Orai is the pore-forming subunit of the CRAC channel and consists of 4 TM domains, with both N- and C- termini facing the cytosol, thus being able to interact with STIM and to control itself oligomerization (Zhou, et al. 2010) (**Figure 6**). It was thought that the functional channel is made up by a tetramer of Orai, but lately this view has been challenged and the Drosophila orthologue has been crystallized, showing a hexameric structure (Amcheslavsky, et al. 2015; Hou, et al. 2012). The C-terminus of Orai has been reported to interact with STIM via coiled-coil packing (Stathopulos and Ikura 2010), while less is known about STIM-Orai interaction at the N-terminus of the latter, which seems to be involved in the channel gating (Li, et al. 2007). What has been said untill now applies to Orai1, that is the main represented form, but Orai2 and Orai3 exist as well. For example, while STIM1 and Orai1 co-expression always leads to a massive CCE, STIM1 with Orai2 or Orai3 does not display such feature: as far as CCE goes, the efficiency of the three Orai follows the Orai1>Orai2/Orai3 paradigm (Mercer, et al. 2006). In addition, Orai1 is inhibited by low micromolar concentrations of 2-APB (2-aminoethyl-diphenyl borate), while Orai2 and Orai3 show different sensitivity to this compound. As far as CDI goes, Orai3 is rapidly inactivated, whilst

Orai2 and Orai1 are less sensitive to this mechanism (Muik, et al. 2012). The formation of hetero-tetramers (or hetero-hexamers) has been postulated to explain the differences in conductance, inactivation and responsiveness to inhibitors, found, for instance, in cells coming from different tissues. To this day and to the best of my knowledge CCE represents one of the most intriguing cellular mechanism, displaying a huge heterogeneity of the players and an intricate activation; its almost unknown roles, excluding the refilling of the ER, add mystery to the picture.

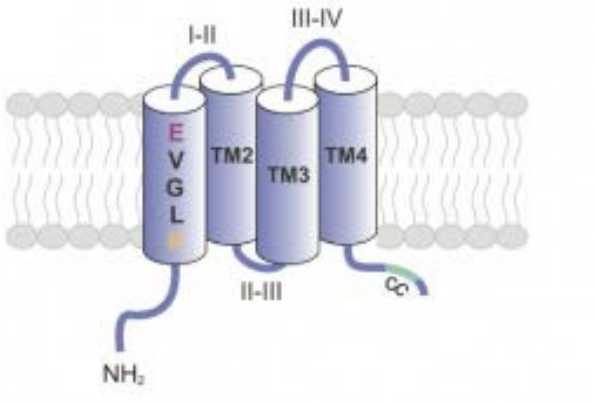

Figure 6: *Orai monomer (modified from Shaw et al. 2012)*

PLASMA MEMBRANE Ca^{2+} CHANNELS IN AD

It was initially suggested that Aβ peptides are capable of forming plasma membrane channels (Arispe, et al. 2007); indeed, remarkable increases in the cytosolic Ca^{2+} concentration ($[Ca^{2+}]_{cyt}$) were reported upon challenging cultured cells with either Aβ40 or Aβ42 (Alberdi, et al. 2010; Demuro, et al. 2005; Resende, et al. 2008). The "ion channel hypothesis" for Aβ toxicity, as proposed by Arispe's group, was mainly supported by *in vitro* studies demonstrating the formation of cation selective channels, whose permeation is inhibited by metals such as Zn^{2+} and Cu^{2+} and by particular peptides designed to line the pore-forming region (Arispe, et al. 2010; Simakova and Arispe 2006). The ion channel hypothesis got further support from Demuro's studies showing that, in oocytes, Aβ injection causes cytosolic Ca^{2+} rises due to Ca^{2+} entry across Aβ channels formed in the PM as well as Ca^{2+} release via stimulation of the Gq/PLC pathway (Demuro and Parker 2013). This hypothesis contrasts with *in vivo* data showing that exogenously applied Aβ enhance the overall PM permeability to anions and cations rather than forming a Ca^{2+}-selective pathway (Sokolov, et al. 2006). Since the first observations describing the increase in the $[Ca^{2+}]_{cyt}$ of cells directly harvested from AD patients (Adunsky, et al. 1991), many groups had focused their attention on this phenomenon changing the paradigm from the channel-forming to the channel-modulating hypothesis. This intense effort led to a plethora of hypothetical

candidates capable of mediating cellular Ca^{2+} overload by Aβ since neuronal cells have a vast array of Ca^{2+}-permeable PM channels at their disposal. As suggested players implicated in the pathogenesis of AD, and possibly mediating Aβ toxicity, I will here consider the voltage-operated Ca^{2+} channels (VOCCs), the nicotinic acetylcholine receptors (nAChRs), the ionotropic glutamate receptors [*N*-Methyl-D-aspartate receptors (NMDARs) and α-amino-3-hydroxy-5-methyl-4-isoxazolepropionic acid receptors (AMPARs)] as well as the store-operated Ca^{2+} channels (SOCCs). For a thorough investigation on this issue, also including the plethora of Aβ binding receptors, the readers should refer to excellent more extensive reviews of which only a few are cited here.

VOCCs

VOCCs, especially those of the L-type subfamily, have long been implicated in aging and AD. Several studies have reported an elevated activity of these channels, with a subsequently larger Ca^{2+}-dependent hyperpolarization, as a possible explanation for the deterioration of synaptic efficiency (Gant, et al. 2006; Landfield 1994; Stutzmann, et al. 2006; Thibault, et al. 2001). Given that the Ca^{2+} signal is spatially and temporally well defined, it is conceivable that even a little delay in its clearance from the cytosol after depolarization can have dramatic effects; for instance, the differential activation of the Ca^{2+}-Calmodulin-dependent kinase II (CaMKII) and the phosphatase calcineurin (CN) is based on their different reaction times to cytosolic Ca^{2+}elevations (Berridge 2010; Reese and Taglialatela 2011).

An impaired intracellular Ca^{2+} handling, that derives either from an increased and sustained entry through the membrane channels or from an inefficient clearance, can lead to an imbalance between long-term potentiation (LTP) and long-term depression (LTD), the electrophysiological correlates that support learning and memory, thus eventually resulting in disbanded memory storage. L-type ion channels are required for LTP at synapses between mossy fibres and CA3 pyramidal neurons. This type of LTP does not depend on NMDARs and involves postsynaptic Ca^{2+} influx carried by L-type VOCCs (Kapur, et al. 1998). Patients with AD show higher L-type VOCC expression in the hippocampus compared with healthy individuals (Coon, et al. 1999). Forette and co-workers found that the blockage of L-type VOCCs with dihydropiridines, a class of drugs mainly used to treat systolic hypertension, was able to prevent dementia in some AD patients (Forette, et al. 2002). Consistently, in CA1 neurons of the hippocampus, Ca^{2+} currents through L-type VOCCs increase during aging in rats, together with a marked decline in learning and memory faculties. Chronic nimodipine treatment ameliorates memory loss, suggesting that excessive Ca^{2+} influx, through L-type Ca^{2+} channels, impairs learning and memory (Veng, et al. 2003). However, it has

been demonstrated that in cultured neurons from $APP_{sw,Lon}$ mice, Aβ suppress gene transcription that is mediated by Ca^{2+} influx (and cAMP surge) and agonists of L-type VOCCs efficiently reverse these transcriptional deficits, implicating a defect in Ca^{2+} influx rather than an augmentation (Espana, et al. 2010). Furthermore, in cell lines and primary cerebellar granules from the Tg2576 mice, dihydropyridines, and especially the most used nimodipine, increase Aβ42 secretion through a mechanism that is independent of Ca^{2+}entry-blockage thus raising doubts to the possible therapeutic use of these compounds (Facchinetti, et al. 2006). The effect of Aβ on L-type VOCCs, whenever present, is likely dose- and time-dependent, since a 1-h exposure of mouse cortical wild-type neurons to Aβ42 oligomers (Aβ42o), at submicromolar concentrations, does not affect Ca^{2+} peaks and long-lasting Ca^{2+} plateaus due to membrane depolarization (Lazzari, et al. 2015).

Interestingly, Aβ globulomers (the 48-kDa component of Aβo) suppress spontaneous synaptic activity of both GABAergic and glutamatergic synapses by acting selectively on presynaptic P/Q type Ca^{2+} currents (Nimmrich, et al. 2008). At the presynaptic level, Aβo also affect Ca^{2+}influx through VOCCs, possibly explaining fast axonal transport defects (Gan and Silverman 2015).

nAChRs

Aβ were reported to affect cholinergic neurons precociously. Ionotropic nAChR exist in various forms, among which the homomeric (α7) and the heteromeric α4β2-nAChR were the first to be investigated in AD and they still represent the most promising targets (Puzzo, et al. 2015; Shen and Wu 2015). Recently a heteromeric α7β2 nAChR has been added to the list of Aβ-binding nAChRs (Wu, et al. 2016). They differ in their Ca^{2+} permeability and sensitivity to α−bungarotoxin, and, functionally speaking, they are thought to take part in memory formation and attention and they have been long known to interact with Aβ. In particular, several studies demonstrated the different affinities and exerted effects upon binding to Aβ40 or Aβ42 by the α7-nAChR and the α4β2-nAChR (Wang, et al. 2000). Summarizing, we can say that both receptor subtypes bind Aβ, preferentially the 42 amino-acid long peptides, which activate α7-nAChR in the picomolar range and inhibit it in the nanomolar one, whilst α4β2-nAChR binds Aβ only in the nanomolar range with an inhibitory effect. Given that amyloid deposition is a spatially defined phenomenon, with certain brain areas exposed to premature deposition, it is conceivable that widely different interstitial Aβ concentrations can be achieved, causing diverse effects on nAChRs. Albeit contrasting with regard of the Aβ concentrations, species (oligomers *vs* monomers) and models used, almost all the evidence points towards a disruption of the physiologically nAChRs-driven LTP, which predicts an

impairment in memory formation (Lombardo and Maskos 2015). This was tested further by generating *in vivo* models bearing AD-related APP mutations in a α7-nAChR knock-out (KO) context. However, depending on the APP mutations employed, different results were obtained. The KO of α7-nAChR in a $APP_{swe,Indiana}$ mouse model was protected against synaptic loss and memory deficits, when tested at 13 and 16 months of age (Dziewczapolski, et al. 2009), while the same KO in a APP_{swe} mouse model worsened both memory and Aβ pathology, with increased amount of soluble high molecular weight (HMW) oligomers when tested at 5 months of age (Hernandez, et al. 2010). To our knowledge, no studies were conducted to shed light on the intracellular pathway involved in these effects and, therefore, Ca^{2+}contribution is inferred only on the basis of the high Ca^{2+} permeability of neuronal nAChRs. Indeed, a likely recruitment by Aβ of astrocytic α7-nAChR, altering both Ca^{2+}homeostasis and gliotrasmission, further complicates the picture (Lee, et al. 2014; Pirttimaki, et al. 2013).

Ionotropic glutamate receptors

A vast majority of excitatory neurons rely on glutamate as neurotransmitter and are therefore defined glutamatergic. Glutamate exerts its excitatory effect interacting with a diverse array of ionotropic receptors (NMDARs, AMPARs, KainateRs) and metabotropic receptors (mGluRs). In the AD/aging field, the best characterized is the NMDAR since it is pivotal in LTP. It has been proposed that the interaction of Aβo with NMDARs is an initiating/propagating event in the pathogenesis of AD. A high percentage of the reports concerning the physical and functional interactions between Aβo and NMDARs relies on synthetically prepared, poorly characterized oligomers, thus leading to contrasting and misleading results. Co-immunoprecipitation with the NMDAR subunit NR1, together with genetic knockdown of the latter and pharmacological blockade of the whole channel, had proven that Aβo preferentially target the synapses due to the presence of NMDARs (De Felice, et al. 2007; Decker, et al. 2010). Recently, it was shown that soluble Aβo assemblies derived from the brains of individuals with AD interact with cellular prion protein (PrP^C) to activate Fyn (Lauren, et al. 2009; Um, et al. 2012). Aβo engagement of PrP^C-Fyn signalling requires mGluR5 as co-receptor, which leads to phosphorylation of the NR2B (also known as GluN2B) subunit, culminating in loss of surface NMDARs and dendritic spines (Um, et al. 2013a). Furthermore, PrP^C KO prevents the toxic effects on LTP ascribed to Aβo (Um, et al. 2013a). Nonetheless it was reported that PrP^C exerts a modulatory effect on the glutamatergic signalling, also in physiological conditions, with neurons from a PrP^C null mice exhibiting sustained and aberrant NMDAR mediated currents (Khosravani, et al. 2008); a competition between PrP^C and Aβo for the

modulation of the NMDAR activity could be present since they exert opposite effects on glycine binding at the co-agonist site, with PrP^C negatively modulating it (You, et al. 2012).

It has recently been suggested that Aβo, by triggering astrocytic release of glutamate to the extrasynaptic space, preferentially affect extra-synaptic GluN2B-NMDARs that, at variance with synaptic GluN2A-NMDARs, further promote the amyloidogenic pathway and Aβo production (Rush and Buisson 2014). The increased amyloid burden can eventually lead to neuronal toxicity by inhibition of excitatory amino acid transporters (EAATs). The subsequent increase in the extracellular concentration of glutamate in turn activates its receptors in an aberrant way; albeit never demonstrated, the interaction between Aβo and EAATs is extremely likely and there are studies reporting an altered expression pattern of EAATs in the AD brain (Scott, et al. 2002). Taken together, these findings suggest a neurotoxic action mediated by Aβo through the disbandment of the excitatory glutamatergic transmission. However, the only strong evidence at the *in vivo* level is the positive effect of the weak NMDAR antagonist memantine, which has long been used in AD treatment, and its successor nitro-memantine. Both are efficient at blocking or reversing the deleterious actions of Aβo largely because of their selectivity for extrasynaptic NMDARs (Paula-Lima, et al. 2013; Rush and Buisson 2014). The hypothesis of Aβ toxicity involving extra-synaptic NMDARs got only partial validation given that the GluN2B-NMDAR antagonist Ro 25-6981 is protective against excitotoxic neuronal death and Aβ-induced synapse loss in some AD mouse models (Liu, et al. 2007; Ronicke, et al. 2011), however it was not confirmed in others (Hanson, et al. 2015).

Among other intracellular events prompted by Aβo, the activation of calcineurin and the dephosphorylation of NMDARs and AMPARs are primary mechanisms prompting receptor internalization (Jurgensen, et al. 2011; Kurup, et al. 2010; Minano-Molina, et al. 2011). Of note, the synaptic loss induced by Aβo through NMDAR activation seems independent of Ca^{2+} influx, relying mainly on p38-MAPK activation (Birnbaum, et al. 2015).

An issue of extreme importance, that has unfortunately gone almost unseen, is the fact that a substantial amount of data on the interaction between Aβo and glutamate receptors come from studies employing synthetic Aβo that have been prepared by dissolving and aging the monomers in DMEM/F12 medium (Lambert, et al. 1998). The latter type of medium specifically causes cytosolic Ca^{2+} increases on its own, likely because of its high content in glutamate and, especially of glutamine, that undergo degradation during the aging procedure. It has been estimated that a 100 µM stock solution of Aβo aged in DMEM-F12 medium might contain up to 100 µM glutamate (Zempel, et al. 2010). Using Aβo at concentrations equal or above 1 µM thus means

stimulating cells with glutamate at concentrations sufficient to elicit Ca^{2+} rises through NMDA- and mGluRs (Zempel, et al. 2010). With this caveat, data interpretation is extremely complicated. Moreover, Aβo were often administered to neuronal cultures or slices, at concentrations considerably higher than those found in the AD brain (5–10 μM). Neuronal Ca^{2+} rises, due to addition of different culture media used for preparing Aβo, were recently described also by Caballero et al. (Caballero, et al. 2016). The same authors show that culture media devoid of glutamate and glutamine but containing sub-micromolar amounts of Zn^{2+}, Cu^{2+}, Fe^{2+} allow production of low molecular weight (LMW) oligomers that are responsible for cytosolic and mitochondria Ca^{2+} overload (Caballero, et al. 2016). I have recently contributed to demonstrate that neither synthetic Aβ monomers nor oligomers (ranging from low to high MW), when aged in distilled water, can elicit neuronal Ca^{2+} increases when acutely applied to neuronal cultures and PC12 cells at concentrations ranging from 0.5 to 5 μM (**Figure 7**) (Lazzari, et al. 2015). Conversely, a 1-h exposure of cortical neurons to Aβ42o profoundly disturbs neuronal Ca^{2+} stores through a pathway that involves mGluR5 but not NMDARs (Lazzari, et al. 2015). Our findings point to a subtler but insidious effect of Aβo, rather than to a massive Ca^{2+} load. Indeed, the idea that a long-lasting disease, such as AD, might act simply through the disruption of a neurotransmission as ubiquitous as the glutamatergic one, shed shadows on a generalized, massive involvement of neuronal glutamate receptors, and forces to investigate AD dysfunctions also at different levels such as the glia and the neurovascular unit (De Strooper and Karran 2016; Lim, et al. 2016).

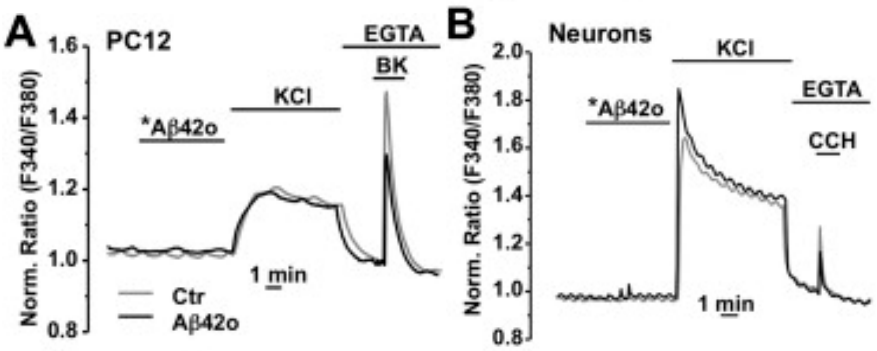

Figure 7: *Aβ42 oligomers (*) do not elicit any Ca^{2+} rise when acutely applied to cells (modified from Lazzari et al, 2015)*

SOCCs

All the major components (Orai and STIM proteins) of the SOCCs have been described at the neuronal level and a significant amount of studies have underlined the relevance of Capacitative

Ca^{2+} Entry (CCE) on the pathophysiology of the CNS (Hooper, et al. 2014; Kraft 2015; Moccia, et al. 2015) and AD (Berridge 2014; Putney and Ribeiro 2000). Notwithstanding, very little is known on the effects of Aβo at this level. As originally reported by Verkhratsky and coll. (Shmigol, et al. 1994), in central but not peripheral rat neurons, caffeine-sensitive Ca^{2+} stores are almost empty at rest, likely because of a highly dynamic ER Ca^{2+} efflux, caused by the ongoing neuronal spiking activity and neurotransmitter release. Despite the fact that these neurons can efficiently refill their store Ca^{2+} content during KCl-evoked depolarization, they lose the releasable Ca^{2+} very quickly (Shmigol, et al. 1994). Similarly, in mouse cortical neurons IP_3-sensitive Ca^{2+} stores are very labile, and can be maximally refilled by prolonged depolarization (Zatti, et al. 2006). On these premises it is expected that CCE, to name all the Ca^{2+} entry pathways linked to store depletion, is constitutively active at rest (Lalonde, et al. 2014). We have recently shown that acute treatment of mouse cortical neurons with Aβo before the refilling process does not significantly modify the store Ca^{2+} content, suggesting that neuronal CCE is not acutely blocked by soluble Aβo (Lazzari, et al. 2015). We can also exclude that a 1-h exposure to Aβo exerts an indirect effect on CCE given that the total store Ca^{2+} content is not affected, as assayed by ionomycin treatment (Lazzari, et al. 2015). Taken together, we do not envisage a direct effect of Aβo on CCE. Indeed, the opposite is likely true, with CCE having a direct effect on Aβ secretion: a high Ca^{2+} influx through CCE reduces Aβ secretion, while a low influx increases it (Zeiger, et al. 2013). Given the fact that FAD-linked mutant PSs reduce CCE, their effect on Aβ accumulation is twofold: favouring Aβ production as well as secretion (Honarnejad and Herms 2012). Recently, it has been shown that the STIM2/neuronal SOC/CaMKII pathway is down-regulated in PS1KI mice, a condition that leads to loss of mushroom spines, the "stable memory spines" that are directly involved in long-term memory by making functionally stronger synapses (Sun, et al. 2014). The same group similarly demonstrated that, in hippocampal neurons of APPKI mice, mushroom spine loss is a consequence of the accumulation of extracellular Aβ42 (Zhang, et al. 2015a). The effect is due to overstimulation of mGluR5 by Aβ42, causing ER Ca^{2+} overload and consequently STIM2 down-regulation (Zhang, et al. 2015a). Unfortunately, the Aβo employed in that study were aged in F12 medium raising doubts about the effective toxic agent. Of note, the ER Ca^{2+} overload induced by Aβo, described in APPKI neurons (Zhang, et al. 2015a), is a chronic and indirect effect, since different FAD-linked APP mutations modify neither the cytosolic nor the store Ca^{2+} level (Stieren, et al. 2010). See, however (Oules, et al. 2012) for a reduced ER Ca^{2+}loading capacity in APP_{swe}-expressing cells.

It is worth noting that a major role for CCE is expected in astrocytes and microglia cells, whose signalling is largely based on ER stores. Interestingly, a reduction in Ca^{2+} release and sustained

Ca^{2+} influx upon agonist stimulation was reported in microglia of AD patients compared to non-demented individuals (McLarnon, et al. 2005) whereas chronic incubation of astrocytes with Aβo at nanomolar concentrations potentiates Ca^{2+} influx caused by activation of mGluRs (Alberdi, et al. 2013).

By using plasma membrane-targeted aequorin, it was recently shown that in mouse cerebellar granules, PrP^C exerts a tonic inhibition on SOCCs by reducing STIM1 phosphorylation, while treatment with Aβo rescues the level of SOCE (De Mario, et al. 2015). Indeed, it was suggested that Aβo target mGluRs through the interaction with PrP^C, one of the major Aβo binding sites (Haas, et al. 2016; Um, et al. 2013a) . Of interest, PrP^C-KO mice show higher levels of SOCE level and the effect of Aβo is lost (De Mario, et al. 2015).

CCE and Presenilins

The expression of FAD-linked PS mutants often causes defects in Ca^{2+} homeostasis, especially at the ER level, and, therefore CCE is impaired as well. To these days we know the phenomenology of Ca^{2+} dyshomeostasis and CCE impairment, without knowing how they are causally related. A brief overview of FAD-linked CCE defects is presented.

As for PS1 mutants:

1. M146L mutation decreases CCE in overexpressing MEF cells (Yoo, et al. 2000), HeLa cells and human fibroblasts heterozygous for the mutation (Zatti, et al. 2006).
2. M146V is associated to a CCE reduction in knock-in or transgenic mice (Leissring, et al. 2000{Herms, 2003 #7634).
3. A246E is ineffective in SH-SY5Y, but decreases CCE when overexpressed in HeLa cells (Zatti, et al. 2006).
4. L286V behaves in the same way when expressed in HeLa cells (Zatti, et al. 2006).
5. PS1dE9 is also associated with a diminished CCE in HeLa cells (Smith, et al. 2002).
6. P117L when present in human FAD fibroblasts causes no alteration, whereas the same mutation is effective in reducing CCE when overexpressed in HeLa cells (Zatti, et al. 2006).
7. The loss of function mutations D257A and D385A, that are not associated with FAD, display an increased CCE when expressed in MEF cells (Yoo, et al. 2000).

As for PS2 mutants:

1. T122R is reported to cause CCE reduction in HeLa (Zatti, et al. 2006), HEK293T cells and human FAD fibroblasts (Giacomello, et al. 2005), but not in SH-SY5Y cells (Zatti, et al. 2006).
2. N141I, the most common PS2 mutation, decreases CCE in HeLa cells (Zatti, et al. 2006), MEFs and primary neurons from transgenic mice (Yoo, et al. 2000).
3. M239I dampens CCE in HeLa but not human fibroblasts (Zatti, et al. 2006; Zatti, et al. 2004).
4. D366A, the loss of function mutation, decreases CCE in HeLa cells, contrary to the analogous PS1 mutation (Zatti, et al. 2004).

Recently Bojarski and co-workers found increased STIM1 and decreased STIM2 expression in PSs double knock-out MEFs and patient-derived B-lymphocytes (Bojarski, et al. 2009). Taken together, these results are consistent with the idea that PSs are negative regulators of CCE, a function that is potentiated by the FAD-linked mutations. Less is known about the mechanism as well as the relevance for AD aetiopathology of this phenomenon at the neuronal level.

INTRACELLULAR Ca^{2+} CHANNELS IN PHYSIOLOGY

Several subcellular compartments are endowed with the role of storing Ca^{2+}, releasing it, therefore shaping its transients; the main of them being the ER, together with Golgi apparatus, secretory granules and acidic pools (Pozzan, et al. 1994; Rizzuto and Pozzan 2006; Rutter, et al. 1998). Mitochondria cannot be classified as Ca^{2+} stores, in fact at rest their free Ca^{2+} concentration is similar to that found in the cytosol. Mitochondria however actively participate in temporarily buffering cytosolic Ca^{2+} rises and by sensing the intra and extra-cellular environment adapt their metabolic functions.

Endoplasmic Reticulum/Golgi apparatus

The ER is a complex and continuous membrane network that extends throughout the whole cytoplasm, with its luminal volume constituting up to 10% of the whole cell volume. It is generally divided into three different regions: the smooth ER, the rough ER (with ribosomes bound to its surface) and the nuclear envelope, albeit with no solution of continuity between them. Striated muscle cells, that are muscle fibres, possess a specialized version of ER, called Sarcoplasmic Reticulum (SR). ER is known as the place where many proteins are synthesized, folded, and eventually modified and transported, however it plays a major role, especially in the non-excitable cells, concerning intracellular Ca^{2+} handling (Csala, et al. 2006). Its Ca^{2+} handling ability is allowed by the presence of ATP-driven Ca^{2+} pumps (several isoforms of SERCA), Ca^{2+}-binding/buffering

proteins for luminal storage and two families of channels for Ca^{2+} release (IP3R and RyR). In addition to this we already saw the presence of Ca^{2+} sensors such as STIM. ER luminal Ca^{2+} concentration is several orders of magnitude higher than the cytosolic one and ranges from 200 μM up to 1 mM, depending on the techniques used to measure it (Meldolesi and Pozzan 1998), with a recent study reporting up to 2 mM (de la Fuente, et al. 2013).

In this last study an almost linear correlation between extracellular Ca^{2+} concentration and SERCA pump refilling rate is highlighted (de la Fuente, et al. 2013), underlying the presence of functional coupling between SOCCs and SERCAs. These latter belong to the super-family of P-type pumps that comprises also the PM-Ca^{2+}-ATPase (PMCA), sharing topology and mechanism of action: two Ca^{2+} ions are actively pumped in the ER lumen employing the energy of one molecule of ATP (Wuytack, et al. 2002). In mammals SERCAs are encoded by three different genes (ATP2A1, ATP2A2 and ATP2A3), which undergo splicing variations, giving several different SERCA pumps. The SERCA2b is considered the housekeeping isoform and is almost ubiquitously expressed (Brini and Carafoli 2009). SERCA pump is susceptible of inhibition and its blockage, achieved through the use of thapsigargin (TG) (Thastrup, et al. 1990) or cyclopiazonic acid (CPA) (Seidler, et al. 1989), alone causes a depletion of ER Ca^{2+} content, also possibly through an elusive leak channel. In the ER lumen there are several Ca^{2+}-binding proteins, acting as buffers or chaperones, such as calreticulin (CRT), that binds almost half the Ca^{2+}, calnexin (CNX), calsequestrin (CSQ) and proteins of the glucose-regulated protein (GRP) family. A common feature of these proteins is the low affinity of their Ca^{2+} binding sites, that is around 1 mM. With this characteristic they perfectly function as buffers, given the high concentration reached in the ER, however they can promptly release the ion upon opening of a Ca^{2+} releasing channel (Zampese and Pizzo 2012). The ER Ca^{2+} release is tightly controlled by several factors, including Ca^{2+} itself that can either favour or inhibit the release channels; second messengers such as IP3 are also pivotal in this precinct. When we talk about Ca^{2+} release channels we mean those who are gated (excluding therefore the leak channels) that are IP3R and RyR, with the latter found primarily in excitable cells. The IP3R is encoded by three different genes and exists indeed in three forms, differently expressed in various tissues, albeit with overlapping characteristics. IP3R is a ligand-gated Ca^{2+} channel, weighing 310 kDa, with 6 TM domains. Its opening is granted by the second messenger IP3, generated by the activation of PLC. However, Ca^{2+}, depending on its concentration at the "mouth" of the channel, exerts a strong modulatory effect, increasing or decreasing the channel conductance (Foskett, et al. 2007). The active form of IP3R is a homo- or hetero-tetramer (Joseph, et al. 1997; Patel, et al. 1999), in which the 5^{th} and the 6^{th} helices are critical for the pore-forming basic structure (Michikawa, et al. 1999). When IP3 binds to the N-terminus of the channels, it induces a

conformational change that allows the opening; the Ca^{2+} flux follows the huge chemical gradient between ER and cytosol, enabling the formations of microdomains of high Ca^{2+} concentration (Rizzuto, et al. 1993). The other main Ca^{2+}-releasing channel located on ER membrane is the RyR, owing its name to the plant alkaloid *ryanodine*, a highly specific antagonist of the channel. RyR, similarly to IP3R, exist in three isoforms, with again different expression at the tissue level. The main subunit is constituted by a large protein, weighing 550 kDa, that assembles into a giant homo-tetramer, that, reaching 2 MDa, represents the biggest known channel (Zampese and Pizzo 2012). Most of the RyR protein folds into a large cytoplasmic assembly that is connected with 6 TM regions, the channel has been recently crystallized, opening new windows on its structure-activity relationships (Zalk, et al. 2015). RyR shares some similarities with IP3R, as for instance the biphasic Ca^{2+} regulation, with low concentration facilitating its opening and high concentration prompting its closure (Roderick and Bootman 2003).

The Golgi apparatus (GA) is the main site for processing and sorting along the secretory pathway, ensuring that lipids and proteins synthesized in the ER are properly modified and eventually directed toward their final destination within or outside the cell. Morphologically, GA is a highly dynamic structure that consists of multiple membranous cisternae arranged in close apposition, forming polarized stacks. GA is composed of three regions: a cis-side associated with a tubular reticular network of membranes (cis-Golgi network, CGN), a medial area of disc-shaped flattened cisternae, and a trans-side associated with another tubular reticular membrane network (trans-Golgi network, TGN). GA plays a key role as intracellular Ca^{2+} store, containing up to 5% of whole cell Ca^{2+} (Chandra, et al. 1991). Indeed, the GA complex contains all the essential components of a Ca^{2+}-storage organelle: pumps for Ca^{2+} uptake, channels for Ca^{2+} release and Ca^{2+} binding proteins (Zampese and Pizzo 2012). The use of a specific Cameleon Ca^{2+} sensor targeted to the different GA compartments, allowed Pozzan's group to directly demonstrate the functional GA heterogeneity in Ca^{2+} homeostasis:

1. CGN. The cis-side of GA closely resembles the Ca^{2+} homeostatic properties of the ER, being endowed with IP3R, RyR and SERCA. The [Ca^{2+}] in this compartment is 250 μM (Pizzo, et al. 2011).
2. Medial Golgi. This compartment accumulates Ca^{2+} through SERCA pump and through the secretory pathway Ca^{2+} -ATPase 1 (SPCA1) and it releases Ca^{2+} through IP3R and RyR. The steady state [Ca^{2+}] is lower than in the ER, but higher than that found in TGN, being around 250-300 μM (Wong, et al. 2013).
3. TGN. Trans-Golgi is IP3-insensitive and utilizes solely SPCA1 to uptake Ca^{2+}, keeping [Ca^{2+}] around 130 μM (Lissandron, et al. 2010).

Mitochondria

Mitochondria are known as the “power supply” of eukaryotic cells: they metabolize organic molecules to produce ATP, through the pathway known as oxidative phosphorylation. When referring to mitochondria our mind usually goes to the “bacteria-like” shape depicted on our biology books, however, they are an extremely dynamic organelle, that fuses and fissions in a “worm-like” state. The mitochondrial network is organized together with the cytoskeleton and moves along the microtubule network aided by motor proteins dynein and kinesin. Mitochondria are constituted by:

1. The outer mitochondrial membrane (OMM), characterized by the presence of porins that allow molecules smaller than 5 kDa to freely diffuse.
2. The intermembrane space (IMS), whose milieu is similar to the cytosol.
3. The inner mitochondrial membrane (IMM), a highly impermeable membrane in which oxidative phosphorylation enzymes are embedded.
4. The cristae, generated by infolding and invaginations of the IMM, that expand its surface area, thus enhancing ATP synthesis.
5. The mitochondrial matrix, delimited by the IMM, contains the major part of mitochondrial proteins, among which those employed in fatty acids oxidation and Krebs cycle (Henze and Martin 2003).

Mitochondria have their own genome, albeit it encodes only 13 proteins, due to their endo-symbiotic origin; the vast majority of the mitochondrial proteome is however under nuclear control (Anderson, et al. 1981). Ca^{2+} concentration variations seem to be instrumental to the regulation of gene expression and efficiency of energetic processes. These latter exert as well an effect on Ca^{2+} accumulation inside the organelle, hence highlighting a mutual, bidirectional, influence. Ca^{2+} enters the mitochondria following indeed the electrochemical gradient established by the respiratory chain, boosting or dampening its activity in turn (Pizzo, et al. 2012).

The question now takes the form of how mitochondria can take up Ca^{2+}, which means Ca^{2+} crossing two membranes and an intermembrane space. A specific channel expressed on the OMM, called Voltage-Dependent Anion Channel (VDAC) allows passage of molecules up to approximately 5 kDa. Thus the OMM is believed to be freely permeable to Ca^{2+}. Nonetheless, VDAC was suggested to influence, through the variation of its permeability, the mitochondrial Ca^{2+} concentration (Bathori, et al. 2006; Rapizzi, et al. 2002). Ca^{2+} then diffuses along the intermembrane space and is taken up by the matrix, upon crossing the IMM under the huge driving force, imposed by the mitochondrial electrochemical gradient. In order to do this a recently discovered specific channel

exists and it is called Mitochondrial Ca^{2+} Uniporter (MCU) (De Stefani, et al. 2011). Well before its molecular identification, its properties as a channel were well known, defining it as highly selective, sensitive to ruthenium red and lanthanides, with low affinity for Ca^{2+} (Bernardi, et al. 1984; Bragadin, et al. 1979). MCU is part of a bigger molecular machine called MCU complex (MCUC), composed of several regulatory proteins (De Stefani, et al. 2015), among which MCUb, MICUs and EMRE. MCU weighs 35 kDa, has both C- and N-termini facing the matrix (Martell, et al. 2012) and is endowed with two EF-hand Ca^{2+} binding domains. Genetic ablation of MCU inhibits completely the mitochondrial Ca^{2+} uptake driven by IP3-induced ER Ca^{2+} release and its overexpression, conversely, enhances it. Recent data suggest that the monomeric 35 kDa subunit arranges into a tetramer (Raffaello, et al. 2013). MCUb is a MCU analogue, sharing 50% of the sequence however probably by forming hetero-complexes with MCU, it exerts an inhibitory effect on mitochondrial Ca^{2+} uptake (Raffaello, et al. 2013). MICU1, MICU2 and MICU3 are regulatory proteins endowed with Ca^{2+}-sensing EF-hand domains; they can influence the responsiveness of the channel to diverse Ca^{2+} concentration, as well as influencing its kinetics (Patron, et al. 2014). EMRE is the last discovered component of MCUC and its ablation completely blocks Ca^{2+} uptake, thus highlighting its importance (Vais, et al. 2016).

Acidic compartments

Acidic compartments comprehend endosomes, secretory granules and especially lysosomes, with the Ca^{2+} content being extremely heterogeneous, ranging from 10-40 μM in mast cells granules, to 100-200 μM in insulin granules. Endosomes and secretory vesicles can reach 1 mM and above and lysosomes usually lay around 500 μM (Zampese and Pizzo 2012). Recent results indicate that also peroxisomes are capable of taking up and storing Ca^{2+} within their lumen at concentrations much higher than those found in the cytosol (Drago, et al. 2008; Raychaudhury, et al. 2006). The mechanisms underlying Ca^{2+} uptake and release in acidic organelles is poorly understood, but evidence suggests that both SERCA-like and Secretory Pathway Ca^{2+}-ATPase (SPCA) -based system are present, at least in dense core secretory vesicles of neuroendocrine cells (Mitchell, et al. 2001). A different possible mechanism, other than ATP-dependent Ca^{2+} pumps, can be found in Ca^{2+}/H^{+} exchangers; acidic organelles, by definition, present a huge proton concentration that can be used to internalize Ca^{2+} exploiting the proton gradient and an exchanger (Patel and Docampo 2010). An indirect pathway is also possible, and has indeed been reported, based on the generation of a Na^{+} gradient thank to a Na^{+}/H^{+} exchanger that works in concert with a common Na^{+}/Ca^{2+} antiporter (Krieger-Brauer and Gratzl 1983; Mahapatra, et al. 2004). In general, acidic Ca^{2+} pools, are

considered slowly exchanging Ca^{2+} pools (Rutter, et al. 1998), nonetheless diverse channels and second messengers have been implied to release Ca^{2+} from these heterogeneous stores; among all IP3 and cADPR gained more attention (Zampese and Pizzo 2012). Recently, NAADP was shown to elicit Ca^{2+} release through the two-pore channel (TPC), with TPC2 mainly located to lysosomes and TPC1/3 to endosomes (Calcraft, et al. 2009; Zhu, et al. 2010a; Zhu, et al. 2010b) but the debate is still ongoing and convincing results identify a member of the transient-receptor potential family (TRPML) as the lysosomal Ca^{2+} channel (Feng, et al. 2014). Concerning secretory pools, luminal Ca^{2+} but not proton gradient is required to sustain optimal exocytosis of insulin granules (Scheenen, et al. 1998). Up to now, many obstacles have been encountered in measuring Ca^{2+} in acidic compartments, due to the peculiar luminal environment also rich in proteases. The expression of genetically-encoded, pH-resistant Ca^{2+} indicators, targeted to acidic pools, is at its dawn [see (Albrecht, et al. 2015)], and further studies could help in deciphering the signalling role of these organelles which are emerging as crucial in the cell life (Villasenor, et al. 2016).

INTRACELLULAR Ca^{2+} CHANNELS IN AD

Endoplasmic reticulum/Golgi apparatus

Amidst the complex scenario of ER Ca^{2+} dysregulation, another set of findings has shaken the scientific community over the past 15 years. At the beginning of the 21st century, several groups reported that PSs, the catalytic subunits of the γ-secretase, are able to modify the ER Ca^{2+} handling when overexpressed in cell lines [see for reviews (Honarnejad and Herms 2012; Shen 2014; Zampese, et al. 2009)]. Among the most successful set of studies was that produced by Bezprozvanny and co-workers, who defined the well-known paradigm of the "Ca^{2+} overload" hypothesis of AD (Tu, et al. 2006). According to this model, endogenous wild-type (wt) PSs work as the elusive ER Ca^{2+} leak channel that has puzzled scientists for decades, a function that is impaired when one PS allele bears a FAD-linked mutation. This situation leads to accumulation of Ca^{2+} inside the ER and consequently exaggerated, toxic release when the IP3Rs and RyRs open. This fascinating hypothesis has been questioned both by ourselves and other groups (Fedrizzi, et al. 2008; Shilling, et al. 2012). In fact, by using organelle-targeted Ca^{2+} probes, Pozzan's group first discovered that different types of PS2 mutants reduce the ER and Golgi apparatus Ca^{2+} content, with PS1 ones exerting no effect or even partially mimicking the PS2 mutants (Giacomello, et al. 2005; Zatti, et al. 2006; Zatti, et al. 2004). These latter exert their effects through a reduction of the SERCA pump activity with minor effects on ER Ca^{2+} leak (Brunello, et al. 2009). By using both cytosolic and ER Ca^{2+} probes, we provided evidence that not only cell lines but also neurons in

cultures and slices from PS2-N141I transgenic mice display a reduced store Ca^{2+} content and responsiveness to IP3-generating agonists, albeit in the presence of larger responses to RyR activation by caffeine (Kipanyula, et al. 2012a; Zampese, et al. 2011b). No clear differences in ER Ca^{2+} levels and dynamics were found between wt and PS double knockout (DKO) MEFs (Brunello, et al. 2009). Furthermore, Foskett and coworkers similarly found no clear evidence of ER Ca^{2+} overload due to the expression of PS1 or PS2 mutants (Shilling, et al. 2012), and partly solved the issue demonstrating that the "apparent" Ca^{2+} overload is due to exaggerated Ca^{2+} release following modulation of the IP3R's gating by PS mutants (Cheung, et al. 2010). Moreover, they demonstrated that in 3xTg AD mice, reduction of IP3R1 expression level attenuates Aβ accumulation and tau hyper-phosphorylation and rescues hippocampal LTP and memory deficits (Shilling, et al. 2014). In spite of the conflicting findings related to ER Ca^{2+} content and IP3R modulation, it might be possible to envisage a unifying hypothesis that sees the RyR over-expression/activation as a common pathway that brings together PS1 and PS2 mutants as well as Aβo (Chakroborty, et al. 2012; Del Prete, et al. 2014). Notably, dantrolene, a RyR1 blocker used to treat malignant hyperthermia, has been reported to soften the symptoms and to reduce the amyloid burden in AD mouse models (Ferreiro, et al. 2006; Oules, et al. 2012). Since RyR is present in three different isoforms, all of them represented at the brain level, and due to the lack of commercially available specific antibodies, it is difficult to prove which specific isoform is involved. In the previous work, using quantitative PCR (qPCR), the potentiated RyR response was attributed to up-regulation of RyR2, the isoform also linked to synaptic loss and neuronal death (Ferreiro, et al. 2006; Thibault, et al. 2007). Increased levels of RyR2 also characterize the mouse brain of transgenic mice based on mutant PS2 (Kipanyula, et al. 2012a). In contrast, the RyR3 isoform, which exerts a pro-survival effect, was not involved (Supnet, et al. 2010).

Mitochondria

Mitochondria are currently considered among the primary targets and players in neurodegenerative diseases, including AD, with mitochondrial dysfunctions being considered a hallmark of Aβ-induced neuronal toxicity. It has been shown that soluble Aβ accumulate precociously in neuronal mitochondria of Tg2576 mice (Manczak, et al. 2006). All the components of the γ-secretase complex were found at the mitochondrial level (Hansson, et al. 2004). Additionally, APP was suggested to enter the mitochondrial protein import machinery (TOM/TIM) with its N-terminal domain, containing a mitochondrial targeting sequence, while leaving the large part of the molecule with the Aβ-containing C-terminal domain outside (Hansson Petersen, et al.

2008). Insertion of the C-terminal with its TM region into OMM allows the APP cleavage by α/β and γ-secretases (Pavlov, et al. 2011). Dysfunctions might thus arise from AICD, P3 and Aβo generated inside the mitochondrial intermembrane space; how they cross the IMM is then a mystery. Altogether, in addition to the peculiar APP topology, in this model, also the γ-secretase appears upside-down if compared to its organisation in PM/endosomal vesicles. *In vitro* studies have shown that incubation of Aβo with cells or purified mitochondria leads to decreased mitochondrial function (Crouch, et al. 2005). Others have described deleterious effects of Aβo on OMM where, by activating the apoptotic BAK pore, they induce cytochrome *c* release and cell death (Kim, et al. 2014). Aβo interaction with BAK on the OMM is difficult to conceive giving that Aβo do not display a cytosolic localization, being both extracellular, following production at the PM (less than 10%) and active release, and intracellular, inside vesicles – endosomes and multivesicular bodies – where they are produced upon APP internalization and from which they cannot easily escape. Thus, under pathophysiological conditions, direct effects of Aβo on intracellular channels (MCU, PTP, VDAC, RyR, IP3R, ER leak channels, to mention a few) are not expected, unless they are translocated across membranes. Whereas Aβ mitochondrial localization and uptake were confirmed in brain human samples and *in vitro* studies (Hansson, et al. 2004; Manczak, et al. 2006), mitochondrial localization of both APP and γ-secretase components is still waiting, leaving the topology conundrum of Aβ production and transfer across membranes yet an open question. Furthermore, it remains to be explained what physiological role APP is playing at the mitochondrial level.

Among the dysfunctions through which mitochondria are likely responsible for neuronal death in AD are those occurring at the ER-mitochondria network level. Pozzan's group discovered that upon agonist stimulation, mitochondria from cell lines and neurons carrying FAD-linked human PS2 mutations experience much higher Ca^{2+} transients despite a lower ER Ca^{2+} content. The phenomenon is due to an increased number of ER-mitochondria close contact sites occurring at the level of mitochondria-associated ER membranes (MAMs), a finding reported with PS2 but not PS1 mutants (Filadi, et al. 2016; Hedskog, et al. 2013; Kipanyula, et al. 2012a; Zampese, et al. 2011a; Zampese, et al. 2011b). Knocking down mitofusin-2 increases ER-mitochondria contact sites (Filadi, et al. 2015). Notably, the latter effect results inn lower γ-secretase activity with reduced concentrations of intra- and extracellular Aβ (Leal, et al. 2016).

Indirect effects on the expression level of VDAC1 and IP3R3, the corresponding ER facing IP3R, have also been reported for Aβ at nanomolar concentrations (Hedskog, et al. 2013). Indeed, the effect is rapid since a 1-h incubation with Aβo is sufficient to significantly increase the IP3R3 mRNA level in cultured mouse cortical neurons (Agostini and Fasolato 2016) (Figure 8).

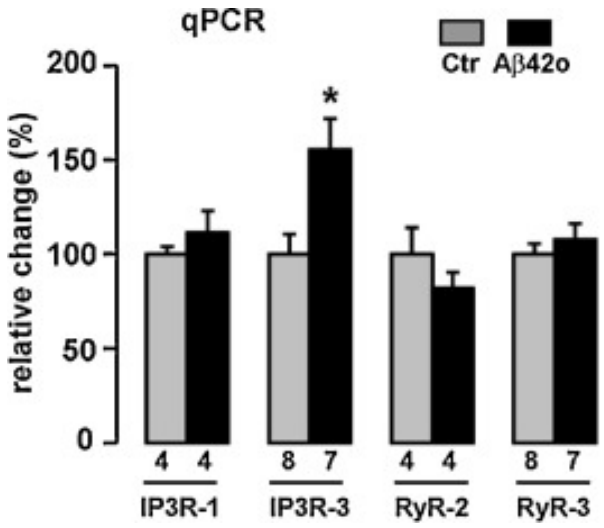

Figure 8: Quantitative reverse-transcription polymerase chain reaction (qPCR) after 1-hour treatment with Aβ42 oligomers (from Agostini et al, 2016)

How an increased ER-mitochondria coupling will ultimately cause pathological alterations at different levels such as energy metabolism, lipid synthesis, mitochondria remodelling and apoptotic signalling has yet to be fully investigated.

Lysosomes

A growing body of evidence has linked failure of the autophagic pathway to multiple outcomes in neurodegenerative disease. In AD, lysosomal Ca^{2+} storage/release defects accelerate amyloidogenesis, neuritic dystrophy and apoptosis. It is well known that vesicular Ca^{2+} is required for efficient vesicle fusion including lysosomal vesicles (Saftig and Klumperman 2009; Scheenen, et al. 1998). Lysosomal Ca^{2+} defects have been reported in $PSEN^{-/-}$ cells and neurons, thus suggesting an additional route through which PS dysfunctions impair cellular proteostasis and autophagic fluxes. Nixon and co-workers have shown that PS1 deficiency causes a primary defect in V-ATPase that determines lysosomal alkalinisation (Lee, et al. 2010). Furthermore, the same authors have suggested that anomalous alkalinisation causes hyperactivation of TRPML1 channels located in the lysosomal membrane, thus inducing both organelle Ca^{2+}depletion and cytosolic Ca^{2+} overload (Lee, et al. 2015). Whereas in PSEN-DKO MEFs and $PSEN1^{-/-}$ hippocampal neurons defects in lysosomal Ca^{2+} content and fusion were fully confirmed, defective V-ATPase and lysosomal alkalinisation were not reported (Coen, et al. 2012). How lysosomal Ca^{2+} depletion contributes to AD neuronal dysfunction and death is yet to be fully elucidated. Unfortunately, obtaining reliable measurements of Ca^{2+} dynamics inside acidic vesicles is still an unsolved challenge. Very recently, PS1- and PS2-based γ-secretases have been shown to be differently

located inside the cells, with PS2-complexes being selectively localized to late endosomes/lysosomes. FAD-linked PS2 mutations thus enhance accumulation of aggregation-prone Aβ42 in intracellular acidic pools (Sannerud, et al. 2016).

Ca^{2+} IMAGING

Ca^{2+} measurements in living cells

As we can foresee from the previously presented data, Ca^{2+} imaging is a serious matter. The perfect Ca^{2+} indicator does not probably exist, but if, it should be fast and sensitive, with low or null buffering capacity and minimal toxicity, it should have good spatio-temporal resolution, and finally be easy to use (Rudolf, et al. 2003). The right indicator should be capable of monitoring a free Ca^{2+} concentration that changes quickly, in different microdomains; for example, we are now aware that stimulation of HeLa cells with histamine results in a prompt cytosolic Ca^{2+} increase from around 100 nM up to 1-3 μM, met by a mitochondrial Ca^{2+} rise up to 30-100 μM. These numbers tell us that we need two indicators with different properties concerning the subcellular localization and the affinity for Ca^{2+}. Over the last decades, many classes of indicators, both chemical and genetically-encoded, have been developed to meet the demand of highly diverse Ca^{2+} signalling properties. We now have several probes at our disposal, differing in affinity, kinetics and spectral properties, with different excitation/emission wavelengths often used to image contemporarily different subcellular compartments. The biggest family is that of fluorescent probes, with single-wavelength indicators changing their fluorescence intensity upon Ca^{2+} binding, and ratiometric indicators changing their emission or excitation spectra. Single wavelength probes are usually brighter and facilitate Ca^{2+} detection when more than one fluorophore is used, for example imaging both cytosol and mitochondria. Ratiometric dyes, both synthetic and genetically encoded probes can in turn be calibrated in a precise manner, thus minimizing the common issues associated with fluorescent indicators, such as heterogeneous dye loading, photobleaching and changes in focal plane.

Synthetic Ca^{2+} indicators

The first family of Ca^{2+} probes that was developed is that of synthetic dyes. They derive, at the structural level, from Ca^{2+} chelators, fused with various fluorophores in order to obtain molecules

able to change their spectral properties upon Ca^{2+} binding. Usually, but not always, they are made in a way that increasing Ca^{2+} concentrations cause an increase in the emitted fluorescence. The initial problems encountered developing these indicators include modest Ca^{2+}/Mg^{2+} selectivity, high sensitivity to heavy metals, causing fluorescence quenching, significant Ca^{2+} buffering capacity, all issues that can influence the readout. The Nobel Prize winner Roger Y. Tsien designed the first Ca^{2+} indicator of the family, the UV excitable quin2 and its cell permeant form, quin2 acetoxymethyl-ester (quin2/AM) (Tsien 1980; Tsien, et al. 1982). In the latter, the carboxylic residues, responsible for Ca^{2+} chelation, are masked with the AM ester, thus neutralizing their polarity and allowing the molecule to freely pass the PM. Once in the cytosol, free esterases cleave the AM ester and regenerate the water-soluble indicator, both avoiding the reverse process and permitting dye accumulation (> 100x) inside the cells (Rudolf, et al. 2003). In the following years, Tsien and coworkers developed several other probes with better features (for spectral properties, dynamic range and quantum yield) such as the UV ratiometric dyes fura-2 and indo-1, (Grynkiewicz, et al. 1985), and the less toxic visible light dyes, rhod-1 and fluo-3 that are much brighter upon Ca^{2+} binding, albeit non-ratiometric (Minta, et al. 1989). Fura-2/AM is still widely used and represents the gold-standard of synthetic Ca^{2+} dyes; it possesses two excitation wavelengths, 340 and 380 nm, and it emits at 510 nm. Exciting the dye at 340 nm, the fluorescence at 510 nm increases upon Ca^{2+} binding, while that obtained exciting at 380 nm, decreases. In this way it is sufficient to alternatively excite the dye at 340 and 380 nm, always collecting the emission at 510 nm, and then divide the two emissions to obtain a Ratio that is virtually independent of focal drifts and different loading; photobleaching is reduced as well, for it affecting both wavelengths. Notably, this spectral behaviour implies the presence of an isosbestic wavelength (around 360 nm), that allows to reveal Ca^{2+} independent fluorescence changes. These indicators were perfect except for two restraints, the high Ca^{2+} affinity (the K_D ranges from 150 to 400 nM) and the lack of selective localization, thus allowing only cytosolic measurements. Of note, cytosolic localization is often hampered by unwanted organelle sequestration and/or extrusion, that false or prevent the proper cytosolic measurement. A definitive improvement was the introduction of sulphinpyrazone, an inhibitor of organic anion transporters, during the loading procedure, that partially prevents both phenomena (Di Virgilio, et al. 1988). The last, still unsolved problem, is that of targeting specific subcellular compartments with dyes endowed of the appropriate K_D. Mag-fura-2 (K_D = 53 μM) was used to target the ER, while rhod-2, a rhodamine-based indicator targets mitochondria, being accumulated, because of the negative IMM potential (Minta, et al. 1989). This dye, however, despite being mitochondriotropic, has poor performances and genetically encoded targeted indicators are now preferred.

Genetically-Encoded Ca^{2+} Indicators (GECIs)

The second big family of Ca^{2+} indicators came some 10 years later and is based on engineered proteins such as the chemiluminescent Aequorin or the Green Flurescent Protein (GFP), both derived from the jellyfish *Aequorea Victoria*. Incidentally, the use of aequorin as a Ca^{2+} sensor was known since the late '60, but the need to microinject it diverted the interest on the development of cell permeant synthetic dyes. The most important breakthrough in the field of Ca^{2+} imaging at the subcellular level stemmed directly from the discovery of those two proteins, and it is striking to note that Roger Tsien played a central role also in this field, merging is know-how in synthetic Ca^{2+} indicators with the new availability of these coloured proteins, thanks to the progress of molecular biology. We will highlight their functioning later, distinguishing between the bioluminescent aequorin and the fluorescent GFP-based probes. For now, is sufficient to say that with GECIs many of the drawbacks abovementioned were fixed, including targeting to different organelles. The array of advantages comprehends the possibility of easy modification by means of simple molecular biology techniques, allowing to change the localization or to put the construct under a tissue specific promoter. Being encoded by a plasmidic cDNA they can be easily transfected in cell lines using the traditional transfecting agents, but they can also be electroporated *in utero*, delivered via transgenesis or cloned into viral vectors, for *in vivo* imaging (Mank, et al. 2008). Different classes of GECIs have been created and specific parameters are taken into account to characterize each probe, in particular affinity and selectivity for Ca^{2+}, kinetics and dynamic range. Usually, the evaluation of these parameters is performed *in vitro*, however, an *in vivo* evaluation is necessary to obtain reliable measurements of absolute Ca^{2+} concentrations. These specifics are also instrumental to perfectly fit the designed experiment and must be carefully checked. GECIs can be divided into two branches, the aequorin-based probes, that are bioluminescent, and the GFP-based probes.

Bioluminescence-based GECIs: Aequorin

Aequorin (AEQ) was the first protein-based Ca^{2+} sensor used in biology, before the advent of modern molecular biology techniques, it was injected in the cells similarly to the synthetic dyes (Llinas, et al. 1972). Later it was cloned into a cDNA, hence avoiding the direct extraction from jellyfish, and spurring its use among researchers (Inouye, et al. 1985). AEQ is a naturally occurring, 22 kDa, Ca^{2+} sensitive photoprotein, endowed with a hydrophobic core that binds the prosthetic group coelenterazine, and three EF-hand motifs that sense Ca^{2+}. Upon Ca^{2+} binding, the covalent bond between coelenterazine and the apoprotein is broken, causing the oxidation of

coelenterazine to coelenteramide. This specific reaction is irreversible and accompanied by the emission of a photon that can be collected by a phototube. This means that AEQ cannot be regenerated inside the cell, and that the amount of collected photons correlates with the Ca^{2+} concentration. It is therefore possible to calibrate the probe in each experiment, using an algorithm that takes into account the speed of emitted light (photons/s) and the fractional rate of AEQ consumption L/Lmax, where L is the light intensity at a given time and Lmax is the total amount of light emitted after that point. Lmax decreases steadily as AEQ is consumed and represents the residual AEQ yet to be discharged[§]. This is the reason why at the end of the experiment the cells are permeabilized with a saturating Ca^{2+} solution, in order to make all the AEQ molecules react and emit, hence collecting Lmax (Allen, et al. 1977; Brini, et al. 1995). The "native" AEQ is a cytosolic protein whose role in the jellyfish is to excite the adjoining GFP, and therefore it lacks any targeting sequence. The first organelle-targeted AEQ was generated in this very lab (Rizzuto, et al. 1992) and was aimed at measuring mitochondrial Ca^{2+}; the localization sequence (the mitochondrial pre-sequence of subunit VIII of cytochrome c oxidase) was fused to an HA-tagged native AEQ. This solution was indeed very clever, since the targeting sequence is a pre-sequence, post-translationally removed from COX-VIII, and also from AEQ, making it a mitochondrial matrix probe. The higher mitochondrial Ca^{2+} concentrations pushed toward the modification of the EF-hand motifs in order to decrease Ca^{2+} affinity, thus sparing AEQ and allowing longer measurements (remember that AEQ is consumed during the experiment). Following these innovations several recombinant chimeric AEQs were generated, targeted to mitochondrial intermembrane space (mimsAEQ), nucleus (nuAEQ), ER (erAEQ), subplasmalemmal space (pmAEQ), Golgi apparatus (goAEQ), peroxisomes (peroxAEQ) and secretory vescicles (vampAEQ) [see (Bonora, et al. 2013) for review]. Among these, mimsAEQ allowed the discovery of microdomains of high Ca^{2+} concentration on mitochondrial surface, opening the road for the identification of ER-mitochondria functional coupling (Rizzuto, et al. 1998).

The noteworthy advantages of recombinant AEQ are:

1. The wide dynamic range obtained by mutation of the EF-hands and the usage of coelenterazine derivatives more suited to detect high Ca^{2+} concentrations.
2. The low interference with endogenous Ca^{2+} binding proteins.
3. The low pH sensitivity.
4. The high signal-to-noise ratio, especially in the low affinity mutated AEQs.

[§] Note that Lmax = Ltotal - Lcumulative, where this latter represents the AEQ that has already been discharged.

5. It can be co-transfected with other cDNAs, thus selecting the positive cells only, contrary to chemical dyes.
6. The instrumentation is relatively simple and cheap, a dark chamber with a phototube and a temperature controlled coverslip holder.

The main disadvantages are:

1. The need of transfection and longer planning time compared to the 30-60 minutes loading procedure of the AM chemical probes.
2. The need of reconstituting the apoprotein with coelenterazine at least one hour before (with store pre-emptying in the case of erAEQ and goAEQ.
3. The low quantum yield, actually hampering single cell analysis.
4. The consumption of the protein upon Ca^{2+} binding, hence shortening the experimental time (Bonora, et al. 2013; Brini 2008; Brini, et al. 1995).

The technological progress hasn't stopped and recently an innovative fusion protein has been created. It somehow brings back the natural architecture that sees aequorin coupled with GFP in the jellyfish, but does it in a different way. The two proteins are fused together but AEQ is not used to excite GFP, but to induce conformational changes, upon Ca^{2+} binding, that in turn influence the spectral properties of GFP (Rodriguez-Garcia, et al. 2014). The probe has been called GAP (GFP-Aequorin Protein) and conceptually resembles the single-fluorophore GFP-based indicators such as Pericams and GCamPs.

GFP-based fluorescent GECIs

We already briefly mentioned that a GFP-based GECI consists of a fluorescent protein (FP) whose spectral properties can be altered, in a controlled and finely tuned fashion, by Ca^{2+} binding. A fluorescent protein is a moiety able to emit light without the necessity of co-factors and with a usually high quantum yield. GFP, that is the first discovered, naturally occurring fluorescent protein, has a brilliant chromophore formed by amino acids 65 to 67, properly cyclized, dehydrated and oxidised. Moreover, and this is probably the reason of its success, the chromophore is deeply buried inside a cylindrical β-barrel, hence protected from environmental variations (Tsien 1998; Tsien and Prasher 1998). GFP can be easily modified by insertion of polypeptides and by circular permutation without affecting its spectral properties, a way treaded to design GECIs. Point mutations in the amino acids of the chromophore, or those in close proximity, allowed for the generation of multi-coloured, more brilliant FPs (Shaner, et al. 2005). GFP-based GECIs retain the same technological advantages of the other GECIs, such as the possibility of targeting to specific organelles or cell types, allowing in addition the generation of

transgenic animals for *in vivo* imaging. Recently developed GFP-based GECIs present a red-shift of the excitation wavelength in order to reduce phototoxicity, facilitate deep imaging and expand the colour palette for simultaneous imaging of different subcellular compartments. Two strategies have been pursued to obtain GFP-based GECIs: the first relies on a single FP, playing with the chromophore environment to achieve a Ca^{2+} sensitivity, the second takes advantage of the so-called Foester Resonance Energy Transfer (FRET), a physical phenomenon that allows for some smart probe constructions (see below) (Bajar, et al. 2016).

Single fluorophore GECIs

As we mentioned above, GFP tolerates insertions of relatively long polypeptides. This class of GECIs is therefore obtained introducing a Ca^{2+} binding peptide that can in turn induce a conformational change in the GFP (or derivatives) when Ca^{2+} is bound. The mechanistic foundation of this phenomenon lays on the protonation state of the chromophore, being buried inside the protein it can be better exposed to the surrounding environment by a conformational change, thus changing its fluorescence properties (Baird, et al. 1999). The most used Ca^{2+} binding peptide is calmodulin, endowed with four EF-hands, albeit other examples such as troponin are present.

This family of GECIs comprises several "variations on the theme", with GCaMP and Ca^{2+}-measuring organelle-entrapped protein indicators (CEPIA) being the most used.

1. Camgaroos. They are a family of GECIs deriving from the insertion of calmodulin in the yellow fluorescent protein (YFP). Ca^{2+} binding causes a shift in the absorbance peak of the FP from 400 nm to 490 nm, rather than an increase in the fluorescence intensity (Griesbeck, et al. 2001).
2. Pericam. Yet another YFP-based sensor, this time on the circularly-permuted YFP (cpYFP). Calmodulin here is accompanied by its binding peptide M13, upon Ca^{2+} binding calmodulin and M13 wrap around each other inducing a conformational change. Pericams were engineered in a way that allowed the generation of three different variants: flash Pericam, that becomes brighter upon Ca^{2+} binding, inverse Pericam that behaves in the opposite way, and ratiometric Pericam that undergoes a change in the emission spectrum (Nagai, et al. 2001).
3. GCaMP. This class resembles Pericams, because it was obtained by fusing calmodulin (CaM) and M13 at the circularly-permuted enhanced GFP (cpEGFP) (Nakai, et al. 2001). During the last years, various drawbacks were fixed, such as pH sensitivity and poor kinetics, giving now the GCaMP6 family. *In vivo* experiments in neurons proved the sensor

GCaMP6f (f stays for fast) and GCaMP7 to be the fastest GECIs available for monitoring cytosolic Ca^{2+} changes due to action potentials (Chen, et al. 2013; Podor, et al. 2015).

4. CEPIA and GEM-GECO. Based on the GCaMP they are intended to have lower affinity suitable for ER Ca^{2+} imaging (CEPIA) or different colour for simultaneous imaging in different compartments (GECO). They both exist in green and red variants or in the blue excitation ratiometric version called GEM (Suzuki, et al. 2014).

Single fluorophore GECIs have been widely used especially *in vivo*, albeit they suffer from pH sensitivity and "false positive" signals coming from shifts in the focal plane, rather than actual Ca^{2+} changes. Both issues can be fixed using FRET-based GECIs.

FRET-based GECIs

Not surprisingly, Tsien's group, and independently Romoser's group, generated in 1997 the first class of truly ratiometric FP-based Ca^{2+} sensors, named by the first "cameleons" (Miyawaki, et al. 1997; Persechini, et al. 1997). CaM and its binding peptide M13 are present also here, but their role is not that of inducing a conformational change, but indeed that of tethering two FP variants together upon Ca^{2+} binding. These two FPs must constitute a so-called FRET pair, meaning that the emission of one is able to excite the other one. Usually this is achieved using a blue FP as the donor and a yellow FP as the acceptor; when Ca^{2+} binds to CaM there is the usual wrapping with M13 that brings together the two FPs so that the energy transfer can occur. There are tight parameters that must be met, depending on the FP used, among which the Foerster radius, that determines the maximum distance at which the energy transfer occurs (usually 5-10 nm). From the technical point of view only the blue FP is excited, say at 430 nm, and its emission at 480 nm is collected; Ca^{2+} binding tethers the YFP, causing its excitation with the net result that blue FP 480 nm emission decreases and YFP 530 nm emission increases. The ratio between the emission intensity at these two wavelengths is what is used to monitor Ca^{2+} concentrations (Palmer and Tsien 2006). Nothing is perfect though, and recently many improvements have been done to fix the drawbacks of this design, like tendency to interfere with endogenous CaM targets, as well as the sensitivity to pH and chloride (Griesbeck, et al. 2001; Horikawa, et al. 2010; Miyawaki, et al. 1999; Nagai, et al. 2004; Palmer and Tsien 2006). Modifications have been made to improve brightness and expand the range of Ca^{2+} affinities, by mutating CaM or even substituting it with a different Ca^{2+} binding protein, such as troponin C (TnC) in the TN-series (Thestrup, et al. 2014).

RESULTS

Ca^{2+} stores, CCE and Aβ42 production: a close interplay

Ca^{2+} dysregulations in AD have long been reported and despite the lack of consensus as far as ER Ca^{2+} content goes, there is indeed a growing body of literature pointing toward SOCE defect, specifically claiming its down-tuning as a feature of AD (Sun, et al. 2014; Yoo, et al. 2000; Zhang, et al. 2015a) and a cause of the consequent failure of signalling cascade. The molecular link between Ca^{2+} dysregulation, particularly referred to ER content and SOCE functionality, is currently missing, but phenomenology tells us that messing up with SOCE can cause an imbalance in Aβ production. Yet contradictory data are available: initial studies carried out in CHO-APP cells demonstrated that the SOCE inhibitor SKF96365 increases Aβ42 release (Yoo, et al. 2000) whereas in neurons and SH-SY5Y cells an increased CCE also increases Aβ42 release (Al-Mousa and Michelangeli 2012; Pierrot, et al. 2004). Consistently with first data, Zeiger and colleagues reported decreased Aβ production following SOCE potentiation by means of overexpressing STIM1 and Orai1 in HEK-APPswe cells (Zeiger, et al. 2013).

We addressed this issue by using CHO-7PA2 cells as a model system, a cell line that constitutively expresses hAPP751 carrying the *London* mutation (V717F) (Walsh, et al. 2002a). Our approach was aimed at testing the role of both store Ca^{2+} content and Ca^{2+} influx on the accumulation of Aβ42 in the conditioned media (CM), when assayed by ELISA (see M&M). Cells expressing cyt-AEQ were incubated for 24 hours with a culture medium containing a reduced FCS (2% instead of 10%) and CPA at a low concentration. The rationale of this approach was that of causing a partial store depletion without any cytosolic Ca^{2+} changes. FCS was reduced to increase the effects of drugs, such as CPA and inhibitors. The effective dose of CPA was acutely tested in cyt-AEQ expressing cells; as shown in **Figure 9A**, CPA, at a concentration close to its IC50 (0.5 μM) caused neither Ca^{2+} release nor Ca^{2+} influx while the subsequent challenge with CPA at its maximal dose (20 μM) evoked both the phenomena. Upon a 24-hour-treatment with CPA (0.5 μM) as mentioned above, cyt-AEQ expressing cells were checked for their store Ca^{2+} content, by challenging the cells with ATP (100 μM) and CPA (20 μM) in the absence of extracellular Ca^{2+} (**Fig. 9B**). With respect to control, untreated cells, those pre-treated with low CPA showed a partial store depletion, around 40%, both in terms of peak height and area (**Fig. 9C**). Under these conditions, there was a significant increase (around 50%) in Aβ42 in the CM, as quantified by ELISA (**Fig. 10A**). The effect was not due to SOCE activation, since a 24-hour-incubation with low CPA in the presence of the

CRAC channel inhibitor BTP-2 (0.2 μM) (Zitt, et al. 2004), further increased the amount of Aβ42 released (+ 90% and + 26%, compared to control and CPA treatment, respectively) (**Fig. 10A**) while causing a further store depletion (-70% compared to control) (**Fig. 9C**).

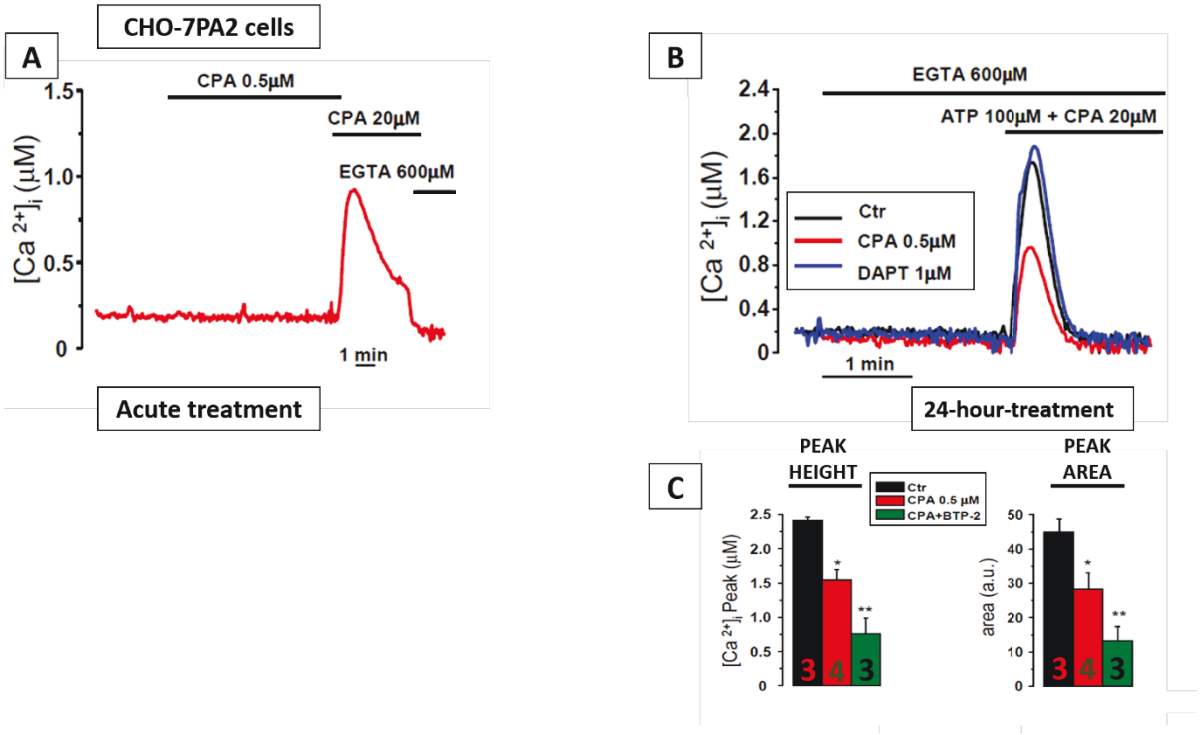

Figure 9: Sub-optimal prolonged SERCA inhibition maintain a lower store Ca2+ content. A) CHO-7PA2 cells, expressing cyt-AEQ, were bathed in mKRB and challenged with the SERCA pump inhibitor CPA at its IC50 (0.5 μM). No cytosolic Ca2+ increase, coming from either ER Ca^{2+} leak or SOCE, was observed. Perfusion with CPA, at higher concentration (20 μM), conversely yielded a noticeable cytosolic Ca^{2+} rise, abated by subsequent perfusion with a Ca^{2+}-free EGTA (600 μM) containing medium. **B)** CHO-7PA2 cells, expressing cyt-AEQ, were treated for 24-hour-treatment with CPA (0.5 μM) in culture medium containing low FCS (2%), during the transfection procedure. Cells were then challenged with CPA (20 μM) and ATP (100 μM), in a Ca^{2+}-free EGTA (600 μM) containing medium. With respect to control, untreated cells, or cells treated with the γ-secretase inhibitor DAPT (1 μM), only the prolonged treatment with CPA (0.5 μM) or CPA (0.5 μM) plus BTP-2 (0.2 μM), caused a noticeable reduction in the IP3/CPA-induced ER Ca^{2+} release. **C)** Bars quantify peak height and peak area under the curve (mean ± SEM, * p<0.05; ** p < 0.01, n=numbers of coverslips).

To go deeper on this issue (see below), I moved to cell lines of human or mouse origin because of the greater availability of antibodies suitable for molecular studies. I thus tested the role of SOCE alone in H4-APPswe cells, belonging to a human neuroglioma cell line, for its neural origin, stably transfected with human APP bearing the *Swedish* double mutation APP K595/M596L, the same present in our 2TG mouse line (and in most AD models, for instance). The cells were treated for 24 hours in a complete medium (10% FCS), therefore the concentration of BTP-2 was tested also at a higher concentration (0.2 and 1 μM). In spite of the high serum concentration and the lack of store depletion, the amount of Aβ42 released was significantly increased (about 16%) by BTP-2 (1

μM) (**Fig. 10B**). Of note, treatment with the selective γ-secretase inhibitor DAPT (1 μM) strongly abrogated the Aβ42 production, without affecting the store Ca^{2+} content (**Figs. 9B, 10B**).

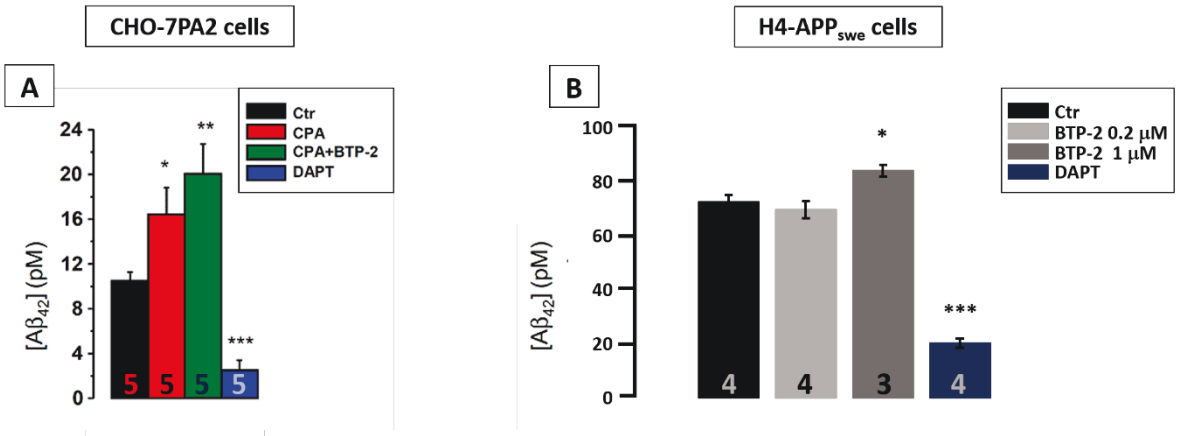

Figure 10: Altering ER Ca^{2+} homeostasis influences Aβ42 secretion. A) CHO-7PA2 cells, bathed in culture medium containing low FCS (2%), were treated for 24 hours with DMSO (0.1%) (Ctr), CPA (0.5 μM) (CPA), CPA (0.5 μM) plus BTP-2 (0.2 μM) (CPA+BTP-2) and DAPT (1 μM). Bars show the amount of Aβ42 detected in the conditioned media (CM) collected after 24 hours, in the presence of protease and phosphatase inhibitors, and quantified by Aβ42 ELISA kit (Anaspec). Treatment with CPA increased by 50% the detection of Aβ42 (* $p < 0.05$), while the addition of BTP-2 brought Aβ42 up by 90% (** $p < 0.01$). 24-hour-treament with the γ-secretase inhibitor DAPT (1 μM) drastically reduced the Aβ42 production, as expected (*** $p < 0.001$). Number of biological replicates is shown in the bars. **B)** H4-APPswe cells were treated for 24 hours with: DMSO (0.1%) (Ctr), BTP-2 (0.2 μM), BTP-2 (1 μM) and DAPT (1 μM) in complete culture medium (FCS 10%). CM were collected with protease and phosphatase inhibitors and quantified with Aβ42 ELISA kit (WAKO). Treatment with BTP-2 (1 μM) increased by 16 % the detection of Aβ42 (* $p < 0.05$), while DAPT (1 μM) drastically reduced it (*** $p < 0.001$). Number of biological replicates is shown in the bars.

The SOCE subunit Orai2 is overexpressed in mutant PS2-based AD mouse models

Meyer and co-workers highlighted how tweaking PS2 or Orai2 expression toward down-regulation increased the ER Ca^{2+} content, whereas the opposite was obtained by up-regulation (Bandara, et al. 2013). While the role of PS2, either wild-type or mutated, in regulating the ER Ca^{2+} content was firmly established by our group (Giacomello, et al. 2005; Kipanyula, et al. 2012a; Zampese, et al. 2011b; Zatti, et al. 2006; Zatti, et al. 2004), the role of Orai2 was unexpected and it drew our attention, possibly being the missing link between SOCE, ER Ca^{2+} content and Aβ. Before undergoing a thorough characterization of the Orai2 role in APP processing, we first checked its expression level in the AD mouse models based on PS2-N141I, i.e. the PS2.30H (TG) and the

B6.152H (2TG) with respect to the C57BL6/J (WT) control mice. Western blot (WB) analysis in TG mice revealed how Orai2 tends to be overexpressed in the cortex of 6-month-old mice, but not at the hippocampal level APP (**Fig. 11**, bars). In the same TG mice, Orai1 that is the main responsible of store-dependent Ca^{2+} entry in other tissues, did not show any difference at the expression level with respect to age and sex-matched WT mice (**Fig. 11**, left panel). In 2TG mice Orai2 showed a similar trend in the cortex whereas Orai1 was not tested (**Fig. 11**, right panel). Our mouse models, both the single and double transgenic, express the mutated PS2 under the mouse prion protein promoter, causing its overexpression also in astrocytes, that are the other major component of brain cells.

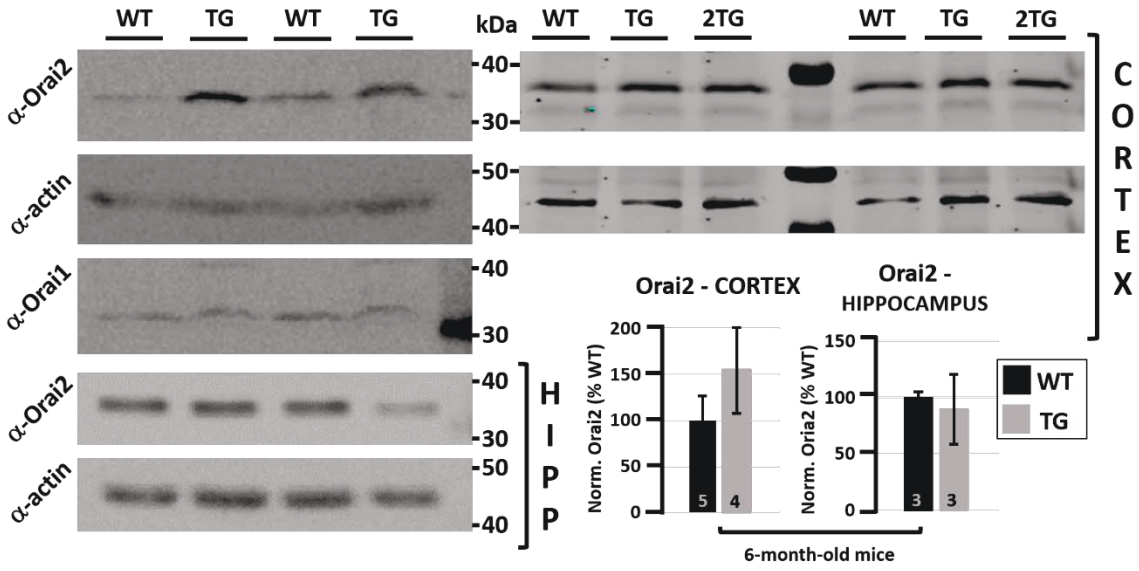

Figure 11: The CRAC channel Orai2 is overexpressed in the cerebral cortex of PS2-based AD mice. Immunoblot analysis of homogenates from 6-month-old mouse cortices and hippocampi were treated as described in M&M. Orai2 immuno-band shows increased intensity in cortices, but not hippocampi from TG and 2TG mice, compared to WT ones. Orai1 expression level was however unchanged. Densitometric analysis of the bands was performed with ImageJ and the Orai2/actin (Norm. Orai2) ratios are displayed as percentage of the WT. Number of mice per genotype is shown in the bars.

To properly quantify the Orai2 expression level in neurons, we prepared primary cultures of cortical neurons from new-born mice employing Neurobasal medium and Ara-C (3 μM) to increase the neuronal population over the glial one (see M&M). At 10-12 DIV, this type of culture shows about 20-25 % of non-neuronal cells [see (Lazzari, et al. 2015)]. In this model WB analysis of cortical neurons from TG mice yielded a significantly higher expression level of Orai2 when compared to neurons from WT mice, likely because of the enrichment in neuronal cells (**Fig. 12**).

It is worth pointing out that despite employing different extraction procedures (RIPA buffer with 2% SDS, 8 M Urea buffer) and denaturation techniques (mild to strong heating, increasing β-mercapto-ethanol and DTT), we were unable to obtain a reproducible band at around 28 kDa, which is the estimated molecular weight (MW) of Orai2 (Wissenbach, et al. 2007). Conversely we always saw a stronger band, slightly above 60 kDa, sensitive to the abovementioned extraction/denaturation solutions, probably representing an SDS-resistant dimer. As for cortices, the expression level of the better known Orai1 was found unchanged between TG and WT neurons (**Fig. 12**).

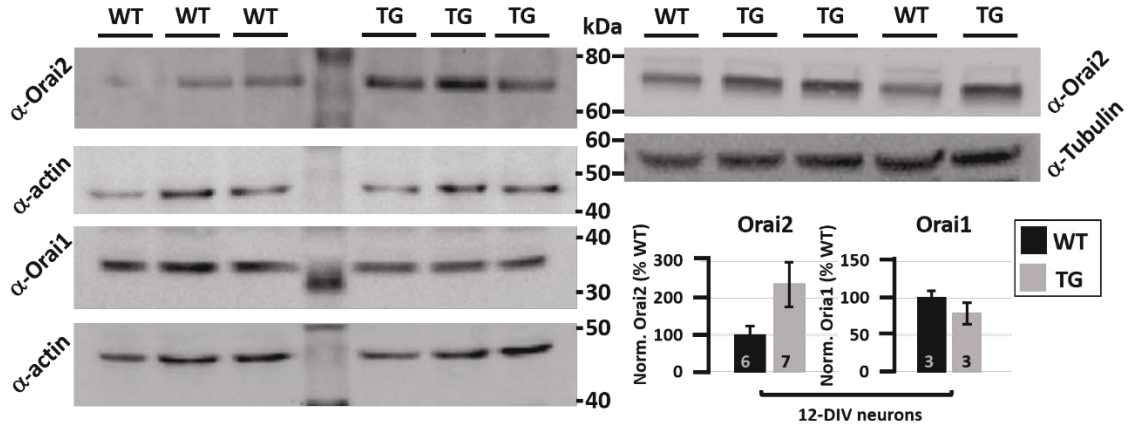

Figure 12: The CRAC channel Orai2 is overexpressed in cultured cortical neurons. Immunoblot analysis of 12-DIV cultured cortical neurons obtained from new-born WT and TG mice. The immune-band corresponding to dimeric Orai2 is increased in neurons form TG mice. Densitometric analysis of the bands was performed with ImageJ and the Orai2/ actin or tubulin (Norm. Orai2) and Orai1/actin (Norm. Orai1) ratios are shown as percentage of the WT. Number of neuronal coverslips per genotype is shown in the bars.

The SOCE subunit Orai2 is mainly expressed in cortical and hippocampal neurons *in situ*.

Given the fact that, between WT and TG neurons, differences in Orai2 expression levels were better found in a neuron-enriched environment, we went back to *in-situ* by staining endogenous Orai2 together with cell specific markers. Unfortunately, availability of Orai2 antibodies is very limited and restricted to the polyclonal ones raised in rabbit, and this holds true for astrocytic markers as well, hindering the possibility of a direct co-staining of Orai2 and astrocytes. We thus followed the indirect way by staining neuronal nuclei (NeuN), Orai2 and nuclear DNA (NucRed Dead 647) (**Fig. 13**). In this way, non-neuronal cells, only display the nuclear DNA staining, while neurons show a merged colour. In **Figure 13A**,**D**, the dentate gyrus (DG) of both WT and TG mice

showed densely packed neuronal nuclei, surrounded by a cytoplasmic Orai2 signal, which is clearly visible in the isolated neurons of the DG hilus. The same pattern could be seen in cortices, where neurons are less packed (**Fig. 13B**,**E**, and **C**,**F** at higher magnification).

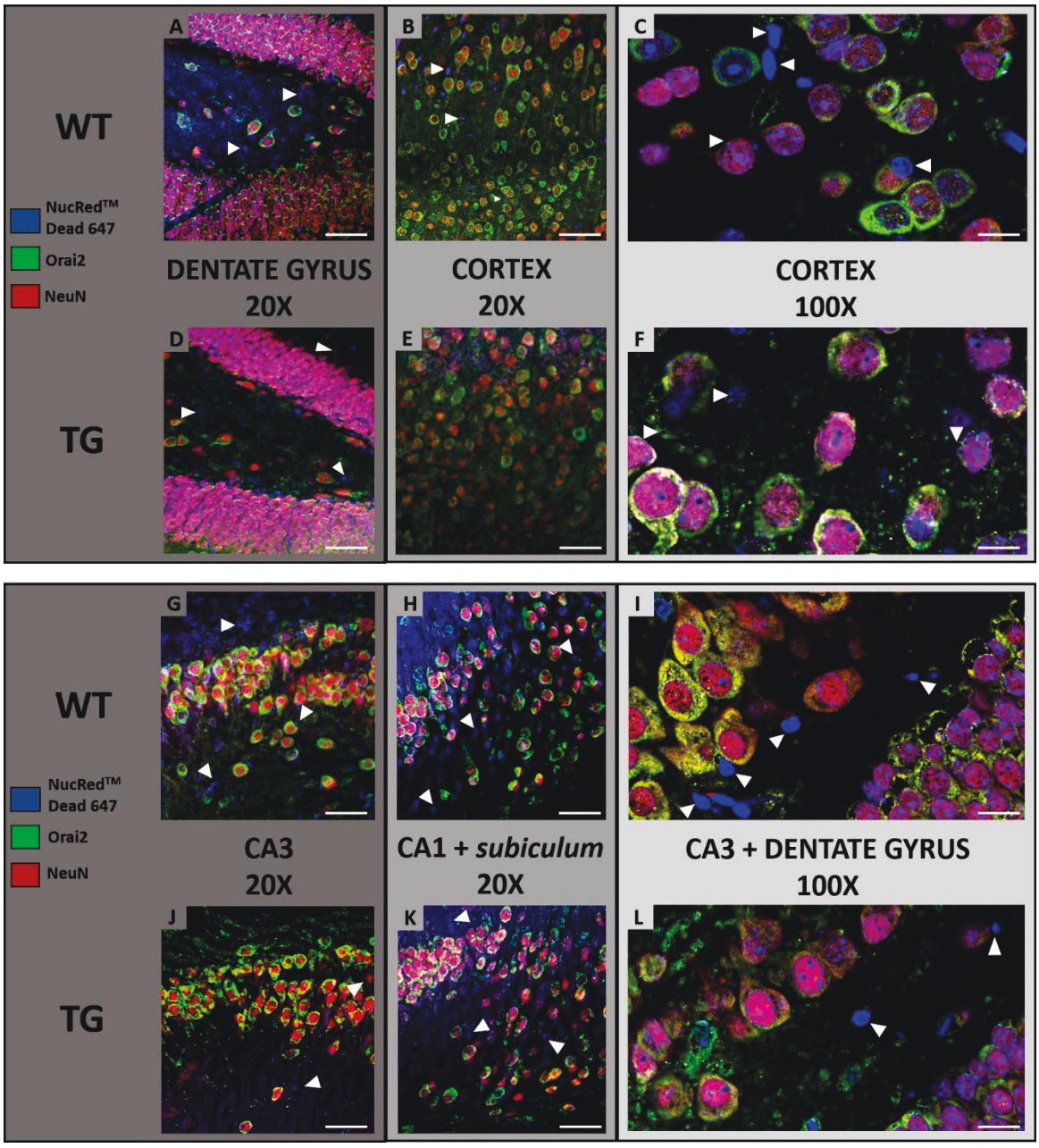

Figure 13: ***In situ*** **Orai2-expression mainly localizes to neurons.** Immunohistochemical staining of sagittal slices from 6-month-old WT and TG mice for nuclear DNA (NucRed Dead 647, blue) Orai2 (green) and neuronal nuclei (NeuN, red); the merged images are shown. **A, D)** 20X magnification of the dentate gyrus; bars, 50 μm. **B, E)** 20X magnification of the frontal cortex of WT and TG animals; bars, 50 μm. **C, F)** 100X magnification of the frontal cortex shows how Orai2 staining is mainly found surrounding NeuN stained nuclei. **G, J)** 20X magnification of the CA3 region of the hippocampus; bars, 50 μm. **H, K)** 20X magnification of the CA1 region plus the *subiculum*; bars, 50 μm. **I, L)** 100X magnification of the CA3 (*top left*) and dentate gyrus (*bottom right*) shows how Orai2 staining is mainly found surrounding NeuN stained nuclei; bars, 10 μm. White arrowheads point to blue and red-stained nuclei without any observable Orai2 staining. Images are representative of three slices per mouse and four mice per genotype.

In **Figure 13G**-**L**, we extended the analysis to other brain areas, such as the *subiculum*, which is among the first brain areas to be involved in AD pathogenesis [see (Fontana et al, 2017) for a thorough characterization]. White arrowheads highlight the nuclei that had been stained for DNA and/or neuronal marker but not for Orai2; at higher magnification (see **Fig. 13C**,**F**,**I**,**L**), the cytoplasmic staining appears punctuated to suggest a vesicular localization. Quantitative analysis was not carried out, however these images are representative of 4-6 slices coming from more than 3 animals per genotype, confirming, if not a pure neuronal Orai2 expression, a much better representation of Orai2 at the neuronal level. However, Orai2 signal can be seen surrounding some non-neuronal cells as well, although we cannot rule out that this staining is due to the neuropil entangling these cells. We are currently setting up pure astrocytic cultures for WB analysis and mixed cultures for microglial/oligodendrocytes staining, in order to better understand the cell specific expression pattern of Orai2.

Orai2 overexpression impairs IP3-induced ER Ca^{2+} release

As for October, 2016, the keyword "Orai2" yields 74 PubMed results on the NCBI search engine, compared to 1013 obtained typing "Orai1". Some of those 74 articles dealt with Orai2 function in cellular Ca^{2+} homeostasis (Inayama, et al. 2015; Kito, et al. 2015) and even with the role of Orai2 in the CNS (Moccia, et al. 2015), but none of them tackled the possible link between SOCE and AD. We therefore decided to perform Ca^{2+} imaging experiments in a H4-APPswe cells that would be later turn useful to measure Aβ secretion in the culture medium. When measuring Ca^{2+} changes with cytAEQ, we first induced a fast and complete store depletion by stimulating the cells with the IP3-generating agonist histamine (Hist, 100 μM) plus the SERCA pump inhibitor CPA (20 μM) in Ca^{2+}-free EGTA-containing medium. Under these conditions, the ER Ca^{2+} release was reduced by more than 50% by human Orai2 overexpression, when considering peak height and area under the curve (**Fig. 14A**,**B**). This holds true in HEK293T cells as well, where the same protocol was applied using carbachol (Cch, 500 μM) instead of histamine as IP3-elevating agent (**Fig. 15A**), with Orai2 over-expression leading to a 25% reduction of ER Ca^{2+} release. In HEK cells we checked human Orai1 overexpression, that also reduced the ER Ca^{2+} release, albeit to a lesser degree (**Fig. 15B**). These experiments confirm Meyer and co-workers' data (Bandara, et al. 2013), although challenging their interpretation: they posit Orai2 as an ER Ca^{2+} leak channel, but decreased ER Ca^{2+} release was also caused by Orai1 overexpression. Effectiveness of Orai2 and Orai1 overexpression was also checked, an example is shown below for H4-APPswe cells (see **Fig. 19**, left panels).

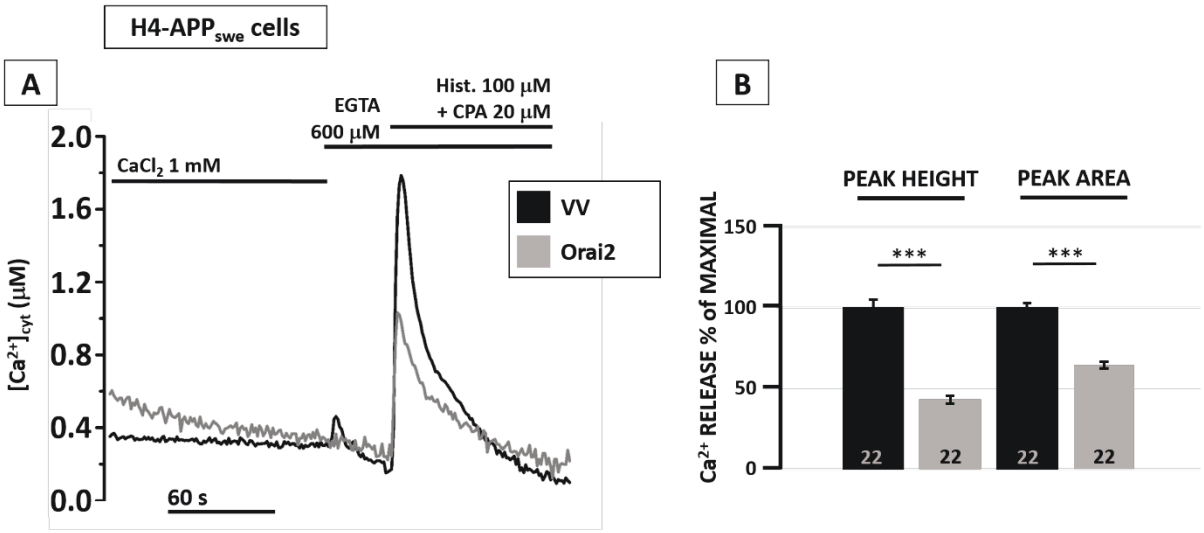

Figure 14: Orai2 overexpression decreases the IP3-induced ER Ca^{2+} release in H4-APPswe cells. H4-APPswe cells were co-transfected with the cDNAs coding for Orai2 (or void-vector) and cyt-AEQ in a 4:1 ratio. **A)** Cells were perfused for two minutes at 37°C with standard mKRB containing $CaCl_2$ (1 mM), then for 1 minute with a Ca^{2+} -free mKRB containing EGTA (600 µM) before being challenged with the IP3-generating agonist histamine (Hist. 100 µM) and CPA (20 µM) in the same medium. Representative traces are shown, black for the control (void-vector, VV) and grey for Orai2 overexpressing cells, respectively. **B)** Bars show the Ca^{2+} release peak height and area, upon baseline subtraction, expressed as percentage of the control. Orai2 overexpressing cells display a statistically significant reduction in both parameters (58.2 % and 36.7 % reduction, respectively, mean ± SEM *** $p < 0.001$). Number of coverslips is shown in the bars.

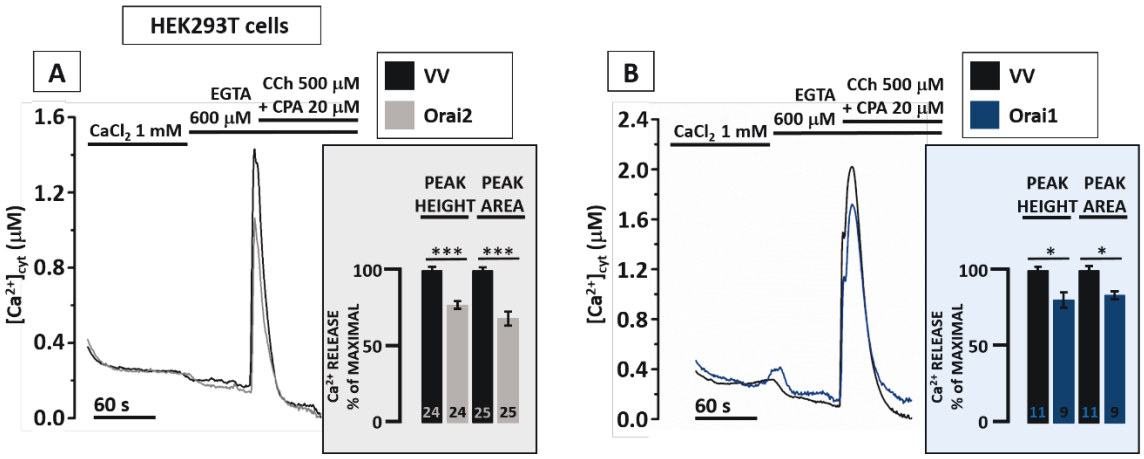

Figure 15: Orai2 or Orai1 overexpression decreases the IP3-induced ER Ca^{2+} release in HEK293T cells. HEK293T cells were co-transfected with the cDNAs coding for Orai2 (A) or Orai1 (B), or the void-vector and cyt-AEQ in a 4:1 ratio. **A)** Cells were initially perfused at 37°C with standard mKRB containing $CaCl_2$ (1 mM)**,** then for 1 minute with a Ca^{2+} -free mKRB containing EGTA (600 µM) before being challenged with the IP3-generating agonist carbachol (CCh, 500 µM) and CPA (20 µM). Representative traces are shown in black for control (void-vector, VV) and grey for Orai2 overexpressing cells, respectively. *Inset,* Bars show the average Ca^{2+} release peak height and area, upon baseline subtraction, expressed as percentage of the control. A statistically significant reduction in both peak height and peak area was found in Orai2 overexpressing cells (22.4 % 32.4 % reduction respectively, mean ± SEM, *** $p < 0.001$). Number of coverslips is shown in the bars. **B)** Cells were treated as described in panel A. Representative traces are shown in black for the control (void-vector, VV) and blue for Orai1 overexpressing cells, respectively. *Inset,* Bars show the average Ca^{2+} release peak height and area, upon baseline subtraction, expressed as percentage of the control. Orai1 overexpressing cells display a smaller but statistically significant reduction in both peak height and peak area under the curve (19.0 % and 16.0 % reduction respectively, mean ± SEM, * $p<0.05$). Number of coverslips is shown in the bars.

Orai2 overexpression decreases the ER Ca^{2+} content

A diminished ER Ca^{2+} release upon stimulation with an IP3-generating agonist can be due to multiple causes: a diminished ER Ca^{2+} content, of course, but also an impairment at the signal generation level, for example a defect in G-protein or PLC. To address this issue we transfected cells with an ER-targeted, low-affinity GECI of the last generation: we chose the G-CEPIA1er for its very low affinity and great dynamic range (K_d=672 μM, F_{max}/F_{min}=4.7) (Suzuki, et al. 2014). Although G-CEPIA1er should work in HEK cells we actually found high photo-bleaching occurring in the first minutes of cell imaging, thus forcing us to discard this cell model and employ another one such as HeLa cells, where a much higher probe stability was found (data not shown). I first confirmed that, also in HeLa cells, Orai2 overexpression reduced ER Ca^{2+} release when measured with cyt-AEQ (data not shown). In the same cell type expressing G-CEPIA1er, changes in ER Ca^{2+} level could be observed following different cell stimulation protocols. When compared to void-vector transfected HeLa cells, Orai2-overexpressing cells showed a reduced ER Ca^{2+} loss following full store depletion induced by the sequential addition of CPA (20 μM) and ionomycin (1 μM). Upon normalization to the fluorescence level reached upon ionomycin (F_{min}), it appears that in Orai2-overexpressing cells ER Ca^{2+} stores were already emptied and had a reduced steady-state ER Ca^{2+} level (**Fig. 16A,B**). As far as this cannot rule out a defect in the IP3 signalling cascade, it unearths a clear decrease in the ER Ca^{2+} content.

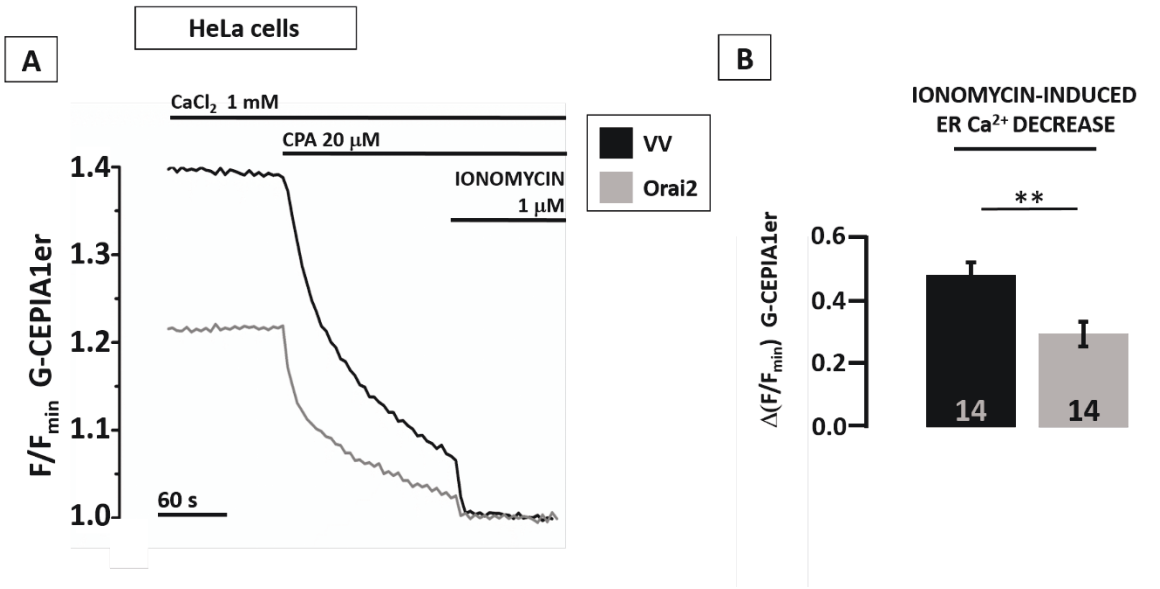

Figure 16: Orai2 overexpression decreases the ER Ca^{2+} content in HeLa cells. HeLa cells were co-transfected with the cDNAs coding for Orai2 or void-vector and the ER-targeted Ca^{2+} sensor G-CEPIA1er in a 4:1 ratio. **A)** Cells were bathed at RT in standard mKRB, containing $CaCl_2$ (1 mM)**,** and sequentially challenged, by quick mixing, with CPA (20 μM) and the Ca^{2+} ionophore, ionomycin (1 μM) to induce full store depletion. For presentation, the instantaneous G-CEPIA1er fluorescence (F) was normalized to the value measured after ionomycin addition (F_{min}). Representative traces are shown

in black for control (void-vector, VV) and grey for Orai2 overexpressing cells, respectively. **B)** Bars show $\Delta(F/F_{min})$ obtained upon ionomycin addition, an indication of the ER Ca^{2+} content (0.49 ± 0.04 for VV, 0.30 ± 0.04 for Orai2, mean ± SEM, ** $p < 0.01$). Number of coverslips, as shown in the bars, were derived from three independent cell batches.

Orai2 overexpression affects the Store-Operated Ca^{2+} Entry

There is another reason why Orai2 is unlikely to be an ER leak channel: its oligomerization with the subsequent pore formation is dependent on STIM1 clustering into specialized PM-ER structures called *punctae* (Stathopulos, et al. 2008). Despite being present at the ER level (see below), Orai2 is probably crossing the ER as a non-active precursor that needs further post-translational modifications and coupling with STIM1 to be effective. We therefore focused our attention on what was the most logical consequence of Orai2 overexpression, that is an impairment in SOCE that eventually dampens the ER Ca^{2+} content due to a defective refilling. To this end we used H4-APPswe cells transfected with Orai2 (or the void-vector) together with GFP (4:1 cDNA ratio) to identify Orai2-expressing cells; 24 hours upon transfection, cells were loaded with Fura-2 (see M&M) and challenged with histamine (100 μM), together with the SERCA pump inhibitor CPA (20 μM), in the presence of extracellular Ca^{2+}. This produces a peak in Fura-2 ratio that accounts for Ca^{2+} release through IP3Rs, followed by a plateau, and a further rise, due to Ca^{2+} entry through SOC channels (**Fig. 17A**,**B**). Note that, at variance with AEQ experiments, Fura-2 loaded cells were challenged with stimuli by quick mixing and no bath perfusion. Two minutes after the addition of the stimulus, which is a safe time-window to minimize the contribution of ER Ca^{2+} release to the cytosolic Ca^{2+} rise, we added EGTA (3 mM) to chelate extracellular Ca^{2+} and achieve a prompt decrease in Fura-2 ratio. Upon linear fitting of the Ca^{2+} trace, before and after EGTA addition, I could estimate the rate of Ca^{2+} efflux as a difference between the steepness of Ca^{2+} decrease (m2) and that of Ca^{2+} rise (m1). This value is a good estimation of the rate of Ca^{2+} influx that was occurring at the moment of Ca^{2+} removal. It is evident from the traces in panel **A** how Orai2 overexpression brings to a plateau that is already decreasing before the addition of EGTA, thus highlighting a defective store-operated influx. Experiments carried out also with CPA alone gave similar results, thus excluding the possible contribution of second messenger-operated channels, such as those of the TRP family (data not shown).

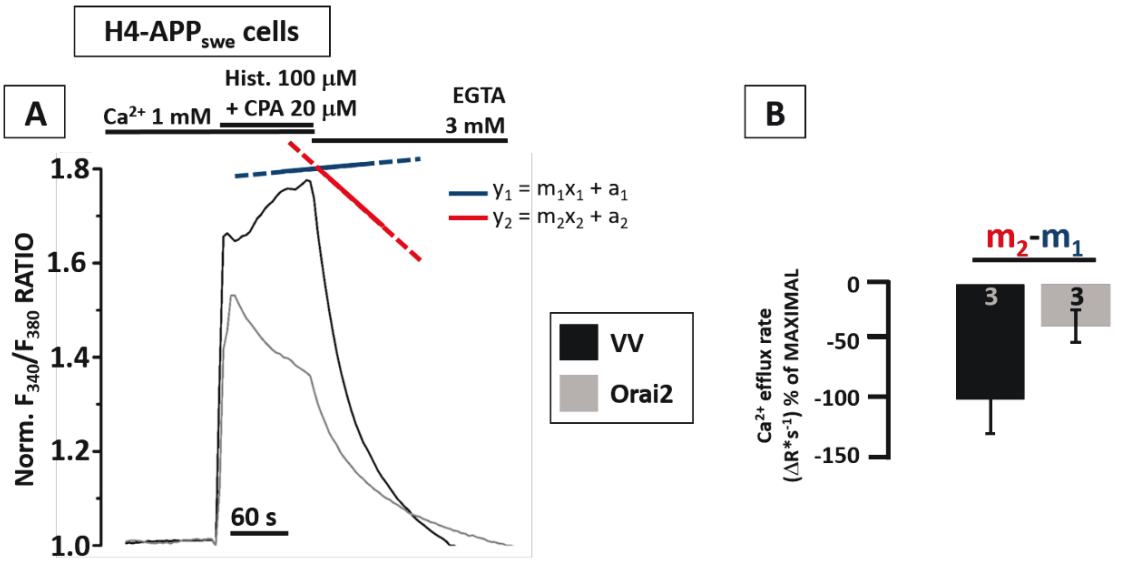

Figura 17: Orai2 overexpression reduces SOCE. H4-APPswe cells were co-transfected with the cDNAs coding for Orai2 or void-vector and cyt-GFP in a 4:1 ratio. Fura-2/AM (1 µM) was loaded as described in M&M. **A)** Cells were bathed in mKRB containing $CaCl_2$ (1 mM), and after 2 minutes they were challenged with the IP3-generating agonist histamine (Hist. 100 µM) and CPA (20 µM) to release Ca^{2+} from the ER while allowing it to entry through the CRAC channels. Representative Fura-2 Ratio traces, normalized to the last frame before stimulus addition, are shown in black for control (void-vector, VV) and grey for Orai2 overexpressing cells, respectively. Ca^{2+} influx rate was quantified, upon linear fitting, by subtracting to the slope (m_2) of the Ratio decay after EGTA (3 mM) addition, the slope (m_1) of the Ratio rising phase, before EGTA addition. The blue and red linear fits were obtained from the last 20 seconds and the first 10 seconds of the plateau and decay phase, respectively. **B)** The bars show the cytosolic Ca^{2+} efflux rate ($\Delta R*s^{-1}$), expressed as percentage of the control, its absolute value represents the Ca^{2+} influx rate before EGTA addition. Orai2 overexpressing cells display a reduction in the Ca^{2+} influx rate (63.8 % of VV, mean ± SEM). Number of coverslips, shown in the bars derives from a single transfection.

Orai2 is a less efficient SOCE mediator than Orai1

The standard protocol employed to assess SOCE calls for a complete store depletion by means of CPA application in the absence of extracellular Ca^{2+} and a following Ca^{2+} "add-back" to allow a Ca^{2+} inward current to be established (Pizzo, et al. 2001). We took advantage of this protocol to estimate SOCE activation upon down-regulation of either Orai1 or Orai2 by specific siRNAs in HEK293 cells expressing cyt-AEQ (**Fig. 18**). After 48 hours, cells were challenged for ten minutes with CPA (20 µM) in Ca^{2+}-free EGTA-containing solution, then $CaCl_2$ (2 mM) was added back and the level of SOCE activation was estimated by measuring both peak height and area at 2 minutes upon Ca^{2+} addition. Only Orai1 siRNA was effective in abating SOCE (**Fig. 18A,B**). Indeed, upon Western blotting of down-regulated cells, a dramatic decrease was seen only for Orai1, whereas Orai2 siRNA seemed much less effective (**Fig. 19A**,**B**). Multiple immunobands appear for Orai1 in Western blot, possibly because of various degree of post-translational modifications. At the mRNA level, however, siRNA-mediated silencing was effective for both Orai1 and Orai2 when assayed by qRT-PCR (**Fig. 19C**,**E**). Orai1 mRNA is deposited as a single

transcript variant, while 4 different variants exist for Orai2. We therefore designed two different primer-pairs for Orai2, “primer A” that bids to all the variants and “primer B” that binds to transcript variants 1,2 and 3. Of note, with three different housekeeping genes as internal controls (GAPDH, cypA and B2M), “primer B” always showed a greater degree of reduction compared to “primer A”. This could underlie a decreased efficacy of the siRNA on transcript variant 4. Nonetheless, a significant down-regulation (> 50%) was observed in all the conditions.

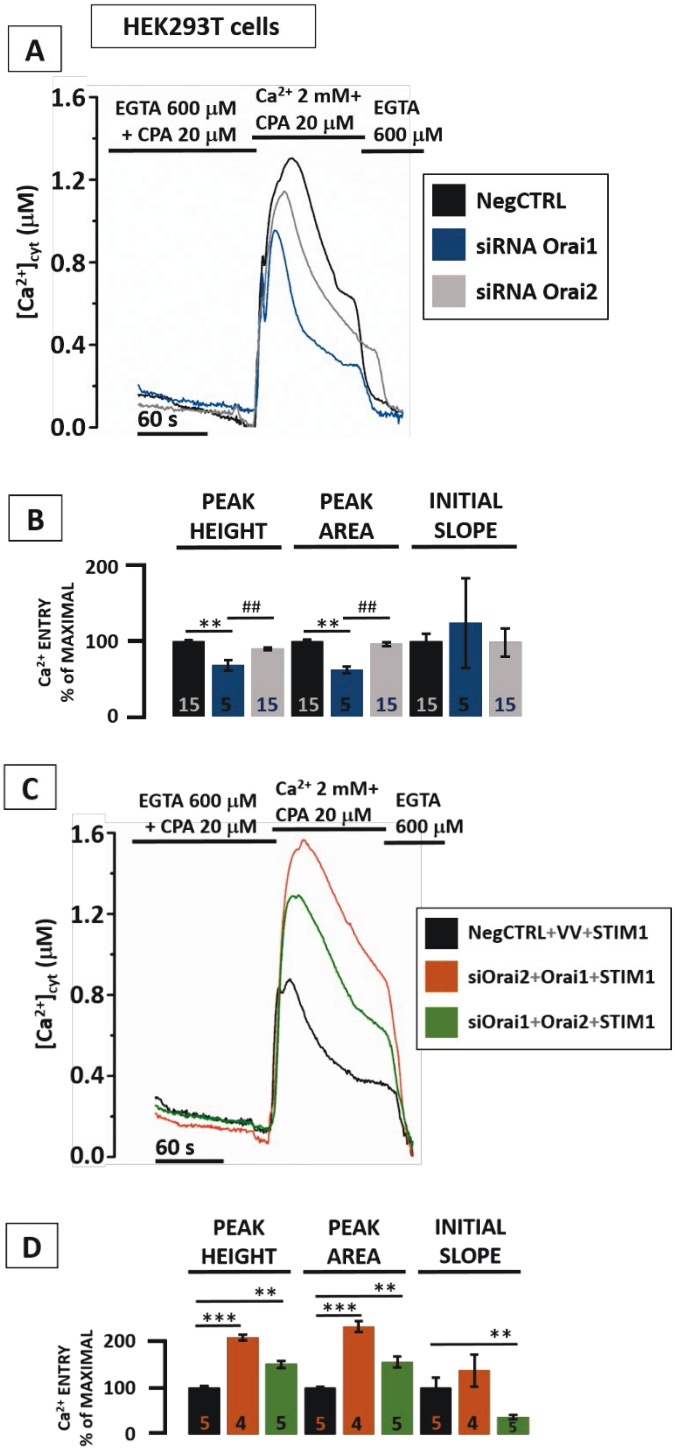

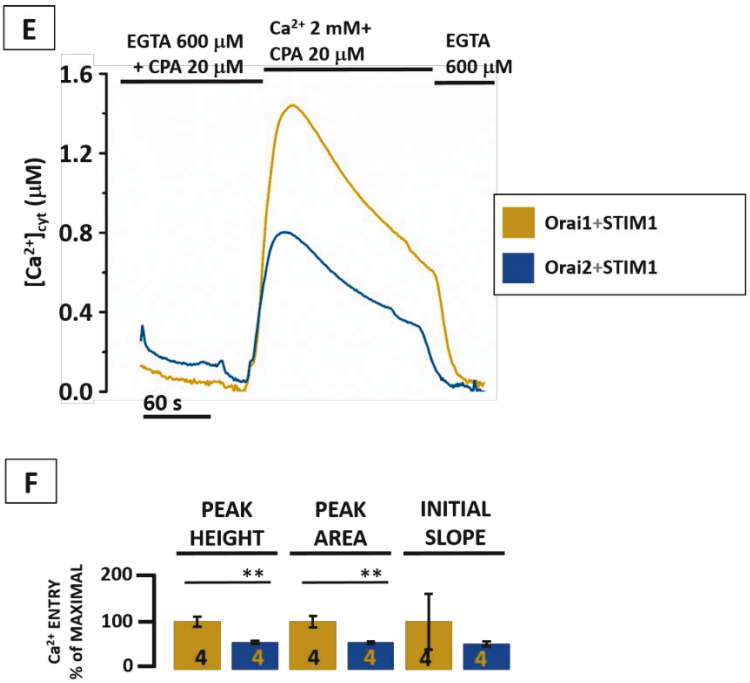

Figure 18: Orai2 is less efficient than Orai1 as SOCE mediator. A) HEK293T cells were co-transfected with siRNA-Orai2, or siRNA-Orai1, or negative siRNA control (negCTRL) plus the cDNA coding for cyt-AEQ in a 4:1 ratio. 48 hours later, upon cyt-AEQ reconstitution, cells were pre-treated at 37°C in Ca^{2+}-free mKRB containing EGTA (600 μM) and CPA (20 μM) for ten minutes. This protocol allows complete ER store depletion. Recordings started with 1 minute at 37°C in Ca^{2+}-free mKRB containing EGTA (600 μM); cells were then perfused with a mKRB containing $CaCl_2$ (2 mM) and CPA (20 μM) to detect the maximal SOCE amplitude. Representative traces are shown in black for negCTRL, grey for siRNA-Orai2 cells and blue for siRNA-Orai1 cells, respectively. **B)** Bars show the average SOCE peak height and area, measured within 2 minutes, upon baseline subtraction, and the initial slope of Ca^{2+} entry, expressed as percentage of control (mean ± SEM, Number of coverslips is shown in the bars). Orai2-KD cells display no significant alterations in either SOCE peak height/area or the initial slope. Conversely Orai1-KD cells show a statistically significant reduction in both SOCE peak height and area (31.6 % and 37.7 % reduction, ** $p < 0.01$, respectively), with no change in SOCE initial slope. The latter was obtained by fitting linearly the first 5-second-trace after $CaCl_2$ addition. **C)** HEK293T cells were co-transfected with siRNA-Orai2 plus the cDNAs coding for STIM1 and Orai1 (or with siRNA-Orai1 plus the cDNAs coding for STIM1 and Orai2) and cyt-AEQ. In the control, cells were transfected with negative siRNA control (negCTRL) plus the cDNAs coding for STIM1, the void vector (VV) and cyt-AEQ in a 3:3:3:1 ratio. Cell pre-treatment, recording conditions and analysis were as described in panel A. Representative traces are shown in black for negCTRL+STIM1+VV, orange for siOrai2+Orai1+STIM1 and green for siOrai1+Orai2+STIM1 cells, respectively. **D)** Bars show the average SOCE peak height and area and initial slope; siOrai2+STIM1+Orai1 cells display statistically significant increase in SOCE peak height and area (+108 %, and +114 % compared to NegCTRL+VV+STIM1, *** $p < 0.001$, respectively), but not in SOCE initial slope; siOrai1+STIM1+Orai2 cells show a statistically significant increase in both peak height and area and a significant decrease in SOCE initial slope (+50.4 % , +55.8 % and -63.5 % compared to NegCTRL+STIM1+VV respectively, ** $p < 0.01$). SOCE initial slope was obtained fitting linearly the first 5 seconds after Ca^{2+} addition. **E)** HEK293T cells were co-transfected with the cDNAs coding for STIM1 and Orai1 (or with the cDNAs coding for STIM1 and Orai2) and cyt-AEQ in a 2:2:1 ratio. Cell pre-treatment, recording conditions and analysis were as described in panel A. Representative traces are shown in yellow for Orai1+STIM1 and blue for Orai2+STIM1 cells, respectively. **F)** Bars show the average SOCE peak height and area and initial slope; Orai2+STIM1 cells display statistically significant decrease in SOCE peak height and area (-43.4 %, and -44.3 % compared to Orai1+STIM1, *** $p < 0.01$, respectively), but not in SOCE initial slope, despite showing a tendency towards it. SOCE initial slope was obtained fitting linearly the first 5 seconds after Ca^{2+} addition. Mean ± SEM, Number of coverslips is shown in the bars.

To overcome possible ineffectiveness of Orai2 down-regulation, we followed another route: in HEK293 cells, we overexpressed STIM1 in combination with Orai1, while simultaneously knocking-down Orai2. The parallel procedure was also exploited, i.e. the overexpression of

STIM1+Orai2 while knocking-down Orai1. The amplification of the signal brought about by STIM1+Orai1/Orai2 overexpression might better resolve the differences between Orai1 and Orai2 (**Fig. 18C**,**D**). The down-regulation of Orai2 when overexpressing Orai1, and viceversa, was aimed at reducing the interference of the endogenous CRAC channels. Upon 48 hours, we could observe that Orai1 overexpression produced an overall increase in SOCE activation, about twice the peak height and area with respect to Orai2 overexpression, when compared to cells expressing only control siRNA and STIM1 (see **Fig. 18D**). Interestingly, the initial slope of the Ca^{2+} rise (measured within the first 5 seconds), which reflects the speed of Ca^{2+} entry, was significantly reduced in cells overexpressing STIM1+Orai2 in Orai1 siRNA background, compared to cells over-expressing STIM1+Orai1 in Orai2 siRNA background. When overexpressing STIM1 together with Orai1 or Orai2, in the presence of endogenous CRAC channels, similar results were obtained (**Fig. 18E**,**F**). Of note the difference observed in the initial slope was lost, however a reduced trend was maintained. We can therefore conclude that Orai2 is a less efficient mediator of SOCE compared to Orai1.

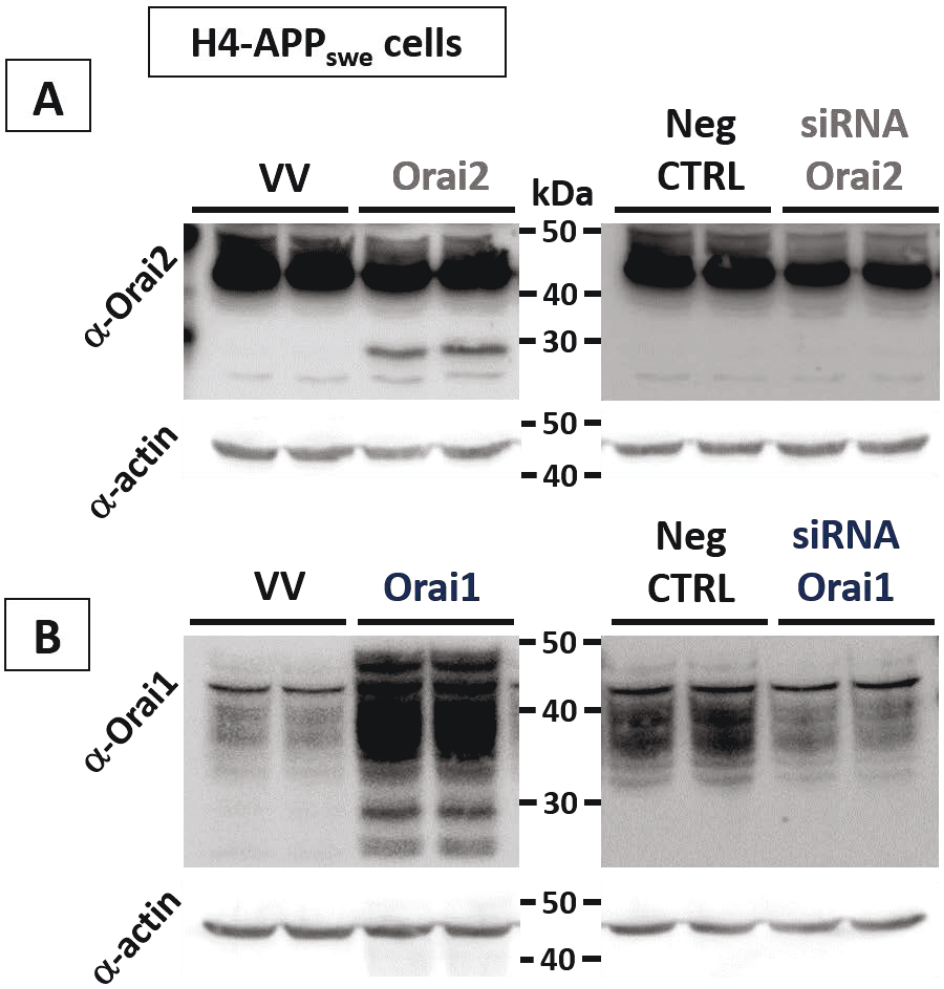

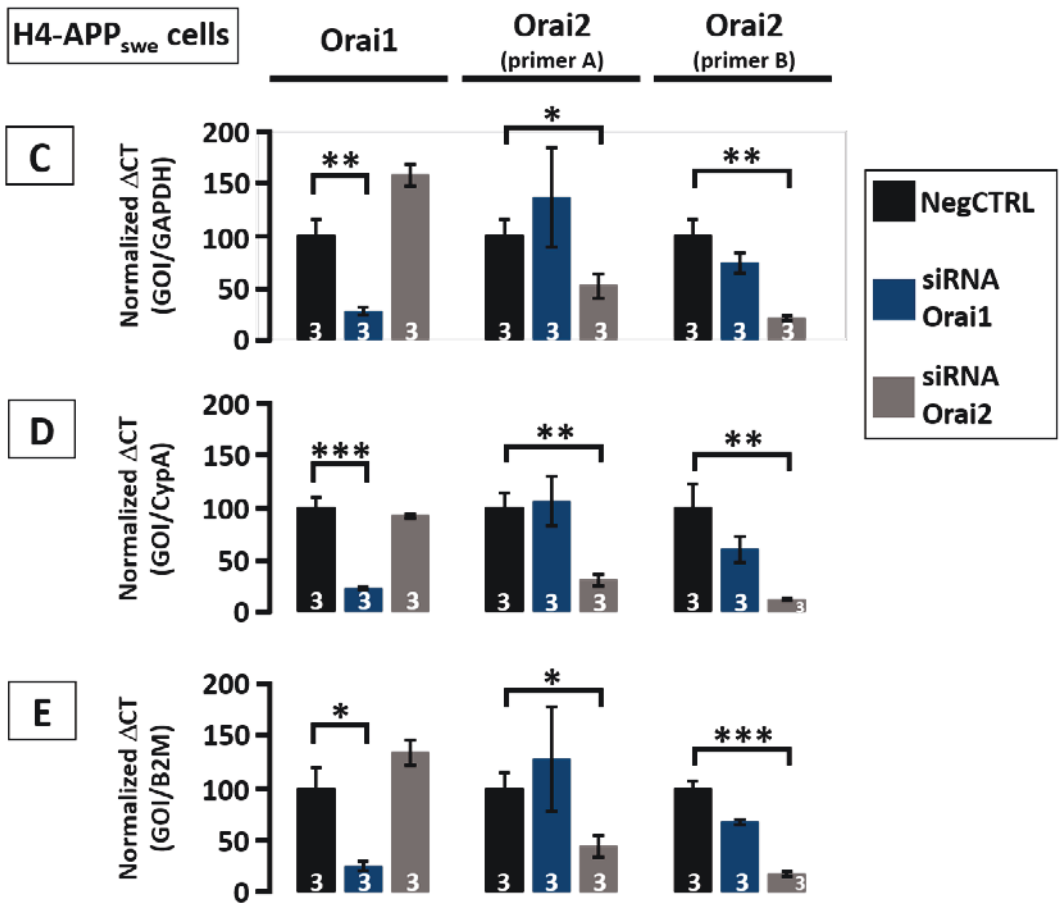

Figure 19: Expression analysis of SOCE-component transfection efficiency. A) H4-APPswe cells were transfected with either the void vector (VV, pcDNA3) or the cDNA coding for Orai2 (left), while Universal Negative control (NegCTRL) or siRNA-Orai2 (see M&M) was used for downregulation (right). After 48 hours, cells were collected and analysed by Western blotting as described in M&M. Note that the overexpressed Orai2 immuno-band falls at 28 kDa while in the VV, NegCTRL and siRNA-Orai2 transfected cells this band is not visible. The downregulation affects the dimeric Orai2 immuno-band. **B)** H4-APPswe cells were transfected with VV or the cDNA coding for Orai1 (left), while NegCTRL or siRNA-Orai1 (see M&M) was used for downregulation (right). Note that no discrete band is present for Orai1, in contrast, a set of bands ranging from 25 to 50 kDa is observable. **C, D, E)** H4-APPswe cells were transfected with Universal Negative control (NegCTRL), siRNA-Orai1 or siRNA-Orai2 for downregulation. After 48 hours, cells were collected and analysed by RT-PCR as described in M&M. Different housekeeping genes were employed such as GAPDH (**C**), cyclophillin A (**D**) and beta-2-microglobuline (**E**). The effectiveness of siRNA silencing was demonstrated for both Orai1 and Orai2 with all the housekeeping genes. (mean ± SEM, Number of biological replicates is shown in the bars, * $p < 0.05$, ** $p < 0.01$, *** $p < 0.001$).

Orai2 down-regulation does not alter the internal store Ca^{2+} handling

In a scenario in which a cell relies on both Orai1 and Orai2 as CRAC channels, the down-regulation of the latter should increase the efficiency of SOCE, by allowing Orai1 only to be contacted by STIM1 and preventing, or at least reducing, the formation of Orai1-Orai2 heterocomplexes that are less effective CRAC channels (Inayama, et al. 2015). Although in naïve HEK cells SOCE potentiation by Orai2 siRNA was not observed at the cytosolic level (see

Fig. 18A,**B**), Orai2 down-regulation might have had an impact on the ER Ca^{2+} content, by causing Ca^{2+} overload, given the 48 hours during which the cells can settle after the administration of siRNAs. In HEK cells expressing cyt-AEQ and knocked down for Orai2, we indirectly estimated the store Ca^{2+} content by measuring store depletion induced by Cch (500 μM) and CPA (20 μM), in the absence of extracellular Ca^{2+} (**Fig. 20A**). Under these conditions, no difference was found in peak height and area (**Fig. 20B**); similar results were also obtained in H4-APPswe cells upon Orai2 down-regulation (**Fig. 20C,D**). To understand whether Orai2 knock-down alters Ca^{2+} handling by different Ca^{2+} stores, we tested the Ca^{2+} release induced by ionomycin (1 μM) in Fura-2 loaded H4-APPswe cells. As it appears from **Figure 21**, neither the height nor the area under the ionomycin peak were significantly different between controls and down-regulated cells. The Fura-2 ratio traces do not show any noticeable difference in kinetics as well, reflecting similar, if not identical, Ca^{2+} content between the two conditions.

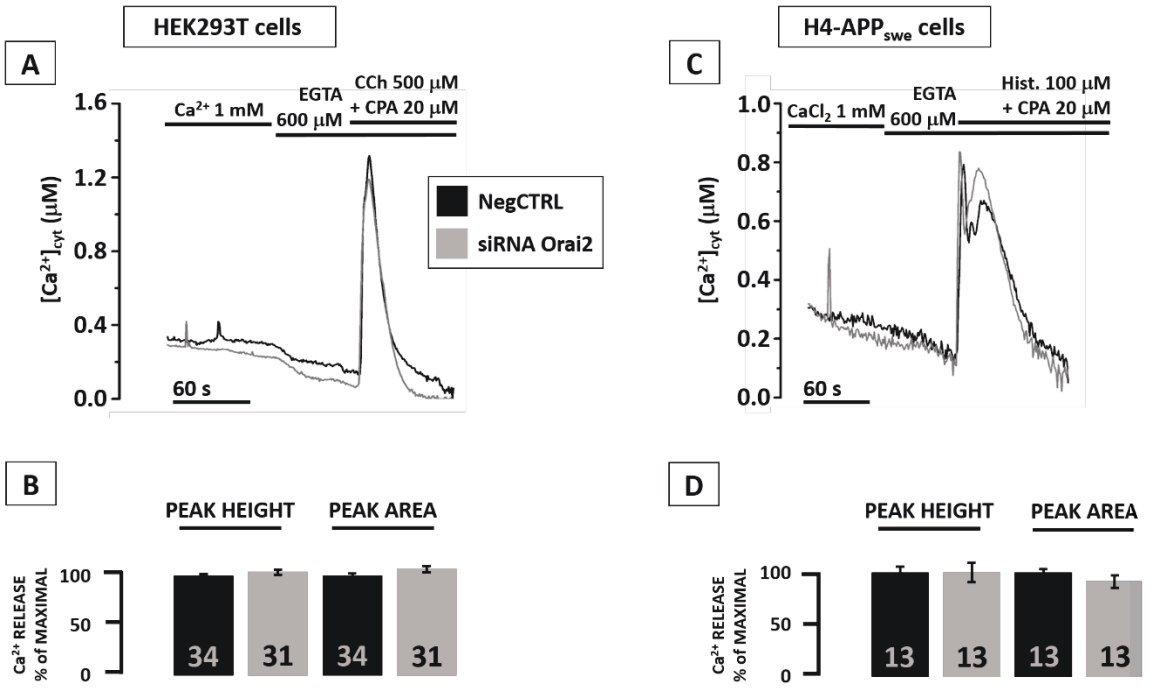

Figure 20: Orai2 downregulation does not alter the IP3-induced ER Ca^{2+} release. H4-APPswe and HEK293T cells were co-transfected with siRNA-Orai2 or negative control siRNA (negCTRL) and cyt-AEQ in a 4:1 ratio. **A, C)** HEK293T (A) and H4-APPswe (B) cells were perfused with mKRB containing $CaCl_2$ (1 mM), followed by 1 minute with a Ca^{2+} -free mKRB containing EGTA (600 μM). While in EGTA cells were challenged with CPA (20 μM) plus either carbachol (CCh, 500 μM) (A) or histamine (Hist, 100 μM) (B). Representative traces are shown in black for negCTRL and grey for Orai2 downregulated (KD) cells, respectively. **B, D)** Bars show the average Ca^{2+} release peak height and area, upon baseline subtraction, expressed as percentage of the control (mean ± SEM, Number of coverslips is shown in the bars); Orai2-KD HEK293 (C) and H4-APPswe (D) cells display no significant alterations in both parameters.

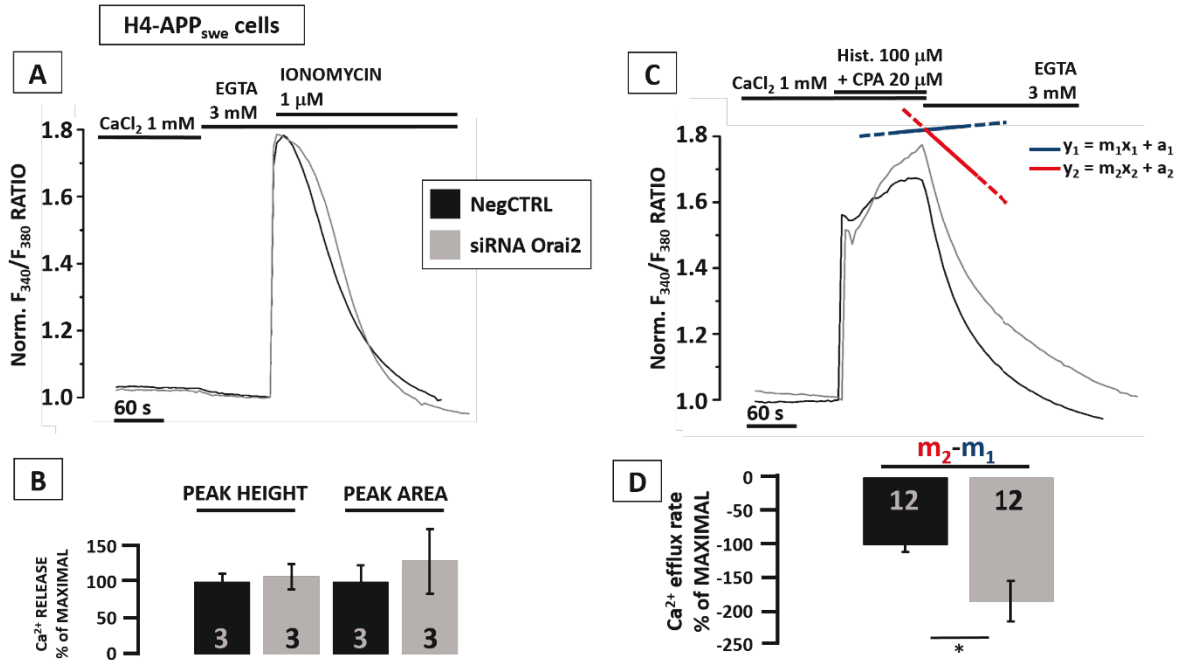

Figure 21: Orai2 downregulation does not alter the stores Ca^{2+} content, but enhances SOCE. H4-APPswe cells were co-transfected with siRNA-Orai2 or negative siRNA control (negCTRL) and cyt-GFP in a 4:1 ratio. Fura-2/AM was loaded as described in M&M. **A)** Cells were bathed at RT in mKRB containing $CaCl_2$ (1 mM), and after 2 minutes, EGTA (3 mM) was added. While in EGTA-containing medium, cells were challenged with ionomycin (1 μM) to discharge the Ca^{2+} stores at neutral pH. Representative Fura-2 Ratio traces, normalized to the last frame before ionomycin addition, are shown in black for negCTRL and grey for Orai2-KD cells, respectively. **B)** Bars show the average Ca^{2+} release peak height and area, upon baseline subtraction, expressed as percentage of the control (mean ± SEM, Number of coverslips is shown in the bars); Orai2-KD cells displayed no significant alterations in both parameters. **C)** Cells were bathed at RT in mKRB containing $CaCl_2$ (1 mM), and after 2 minutes they were challenged with histamine (Hist. 100 μM) plus CPA (20 μM) to release Ca^{2+} from the ER while allowing it to enter through SOCE. Representative Fura-2 Ratio traces, normalized to the last frame before stimulus addition, are shown in black for negCTRL and grey for Orai2-KD cells, respectively. **D)** Bar show the average Ca^{2+} efflux rate upon EGTA addition, an estimate of instantaneous Ca^{2+} influx rate as described in **Fig. 17** (mean ± SEM, Number of coverslips is shown in the bars); Orai2-KD cells display a significant increase in Ca^{2+} influx rate (+ 84.3 %).

Orai2 downregulation boosts the Store-Operated Calcium Entry

To further test the contribution of Orai2 on endogenous SOCE, Fura-2-loaded H4-APPswe cells were challenged with an IP3-generating stimulus (Hist, 100 μM) together with the SERCA blocker CPA (20 μM) in a Ca^{2+}-containing medium. Addition of EGTA (3 mM) during the prolonged Ca^{2+} plateau phase allows to estimate the instantaneous Ca^{2+} influx rate as difference between the slopes of Ca^{2+} change after and before EGTA addition (**Fig. 17**). In cells knocked down for Orai2, as compared to control cells, a greater Ca^{2+} influx rate was measured at two minutes after store depletion (**Fig. 21C**,**D**). These findings argue against the possibility of Orai2 being a relevant ER leak channel, a hypothesis that can hardly explain the absence of differences in the ER Ca^{2+} handling upon down-regulation, as well as the increased influx after

store depletion. From down-regulating a leak channel, someone would expect an increased Ca^{2+} content, or, at least, different kinetics in the decrease phase of the cytosolic peak, that in our hands stays unchanged.

Orai2 minimally localizes to the ER

In the search for a better understanding of Orai2 role, we performed confocal imaging on immunofluorescence preparations to unearth its subcellular localization. Looking at the immunohistochemistry of mouse brain sections shown in **Figure 13**, someone can say that there is a diffuse staining of the perinuclear, cytosolic region. Due to the lack of high resolution, typical of the slice preparation, however, it is not trivial to clearly understand the staining pattern. With this in mind we moved to H4-APPswe cells to stain the ER and Orai2 contemporarily and quantify their co-localization. We stained the ER with a rabbit-raised calreticulin antibody, thus hindering the possibility of using an antibody against endogenous Orai2, since no good mouse/rat hosted antibodies exist on the market; we therefore transfected the cells with a Myc-tagged Orai2 construct using an anti-Myc antibody for staining. As shown in **Figure 22A**, a PM-like profile of Orai2 is visible, together with an enrichment in a perinuclear region that can resemble the Golgi apparatus, likely caused by Orai2 overexpression. The Manders' R and Pearson's coefficients, as measured by ImageJ (see M&M), were 0.69 and 0.15, respectively. Studying the localization of a protein upon overexpression, can bring up several issues such as mis-localization, which differently affects Manders' R and Pearson's coefficients. For these reasons, we also stained the endogenous Orai2. To co-stain the ER we tried markers other than calreticulin (SERCA2, not shown) without succeeding, later opting for transfecting an ER-targeted fluorescent protein. As shown in **Figure 22B**, we employed the ER-targeted superfolder GFP (Costantini, et al. 2012) that produced a slightly lower Manders' R, but a higher Pearson's (0.65 and 0.31, respectively), possibly because Orai2 antibody's epitope is near the C-terminus, thus facing the cytosol as for the ER-membrane superfolder GFP. Indeed, moving to an ER-lumen staining, exploiting the turquoise-family fluorescent protein ER-TQ2, gave lower co-localization parameters, with Manders' R standing at 0.50 and Pearson's at 0.23 (**Fig. 22C**). We confirmed the results obtained in H4-APPswe cells also in HEK293T cells employing the same ER-TQ2 fluorescent protein that yielded similar Manders' R and Pearson's coefficients (0.61 and 0.26, respectively; see **Fig. 23A**).

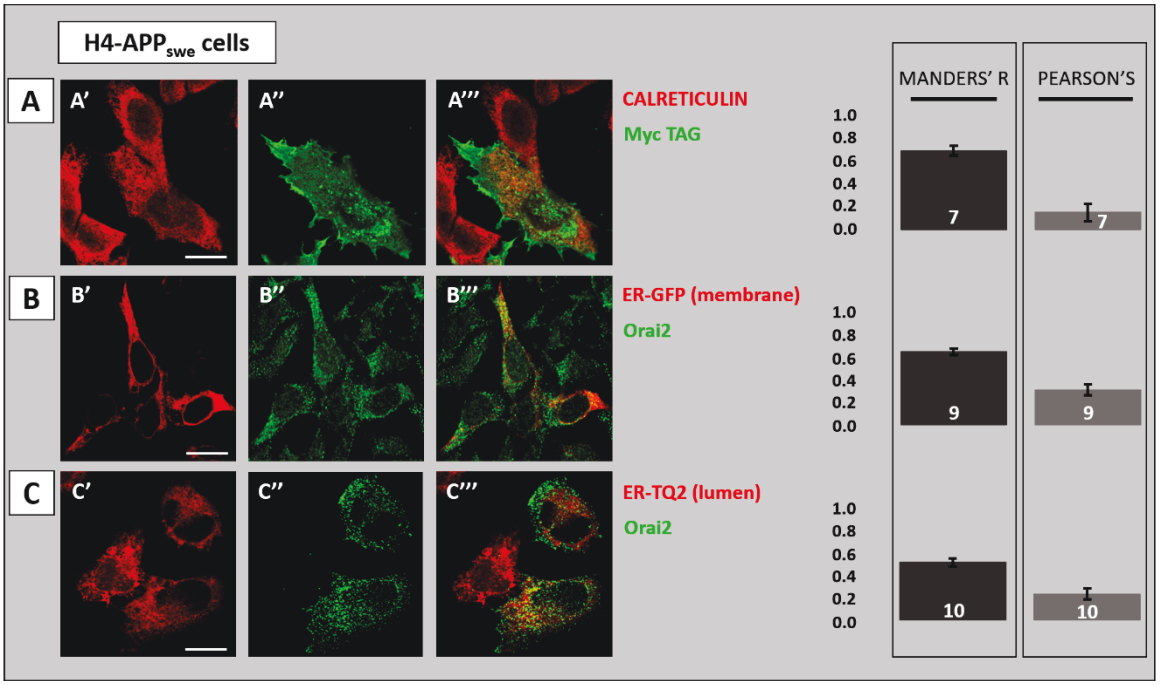

Figure 22: Orai2 partially localizes to the ER. Confocal microscope immunofluorescence analysis of the subcellular localization of endogenous and overexpressed Orai2 in H4-APPswe cells. **A)** H4-APPswe cells were transfected with the cDNA coding for Myc-tagged Orai2. ER red staining with anti-calreticulin (A'), Myc-Orai2 green staining with anti-Myc (A''), merged signals (A'''). Co-localization Manders' R and Pearson's coefficients were calculated giving 0.69 ± 0.04 and 0.15 ± 0.08, respectively. **B)** H4-APPswe cells were transfected with the cDNA coding for a membrane resident, ER-targeted GFP. In B', ER-GFP red staining (B'); anti-Orai2 green staining (B''), merged signals (B'''). Co-localization Manders' R and Pearson's coefficients were calculated giving 0.65 ± 0.03 and 0.31 ± 0.05, respectively. **C)** H4-APPswe cells were transfected with the cDNA coding for ER lumen-targeted Turquoise2 (TQ2). ER-TQ2 red staining (C'), anti-Orai2 green staining (C''), merged signals (C'''). Co-localization Manders' R and Pearson's coefficients were calculated giving 0.50 ± 0.03 and 0.22 ± 0.05, respectively. In all panels the bar size is 10 μm and the graphs show the average coefficients (mean ± SEM, Number of coverslips is shown in the bars). Representative images of at least 3 independent experiments.

Taken together these results suggest that Orai2, if present in the ER, is probably at a rather low level because of its transiting across it to reach the PM. It is however worth noting that with endogenous Orai2, no appreciable PM staining could be observed, either because the protein is not enriched in this compartment, or because of difficulties in maintaining large, intact PM areas upon permeabilization. Unfortunately, the market does not offer an antibody targeted to the extracellular residues of Orai2, thus hindering the possibility of staining the PM without cell permeabilization.

Orai2 localizes to the early endosome compartment

Given the dotted, vesicular-like staining that can be observed for endogenous Orai2, we checked the co-localization with different endosomal markers, namely: early-endosome A1 (EEA1), that is an endosomal tethering molecule whose role is to facilitate the fusion between

smaller early endosomes and form large late endosomes; Rab5, also involved in the maturation from early to late endosomes, and in their recycling to the PM as well; Lysobisphosphatidic acid (LBPA), a particular phospholipid that is present in late endosomes only. As observable in **Figure 23B**,**C**, the co-localization with EEA1 and Rab5 is more relevant (Manders' R of 0.74 and 0.67 and Pearson's of 0.61 and 0.44, for EEA1 and Rab5 respectively). Orai2/LBPA co-staining was lower as quantified by co-localization index (Manders' R = 0.60, Pearson's = 0.28) (**Fig. 23D**), similar to that found with the ER staining. What is appreciable for EEA1 and Rab5 is the higher value of both coefficients, clearly showing better overlapping of Orai2 with the early-endosome compartment. The lower co-localization of Rab5, as compared to EEA1, can be explained by the fact that the latter is a pure early-endosome marker, while Rab5 is involved in the recycling as well as in the recruitment of microtubule-associated motor protein (Guo, et al. 2016), thus diluting the signal.

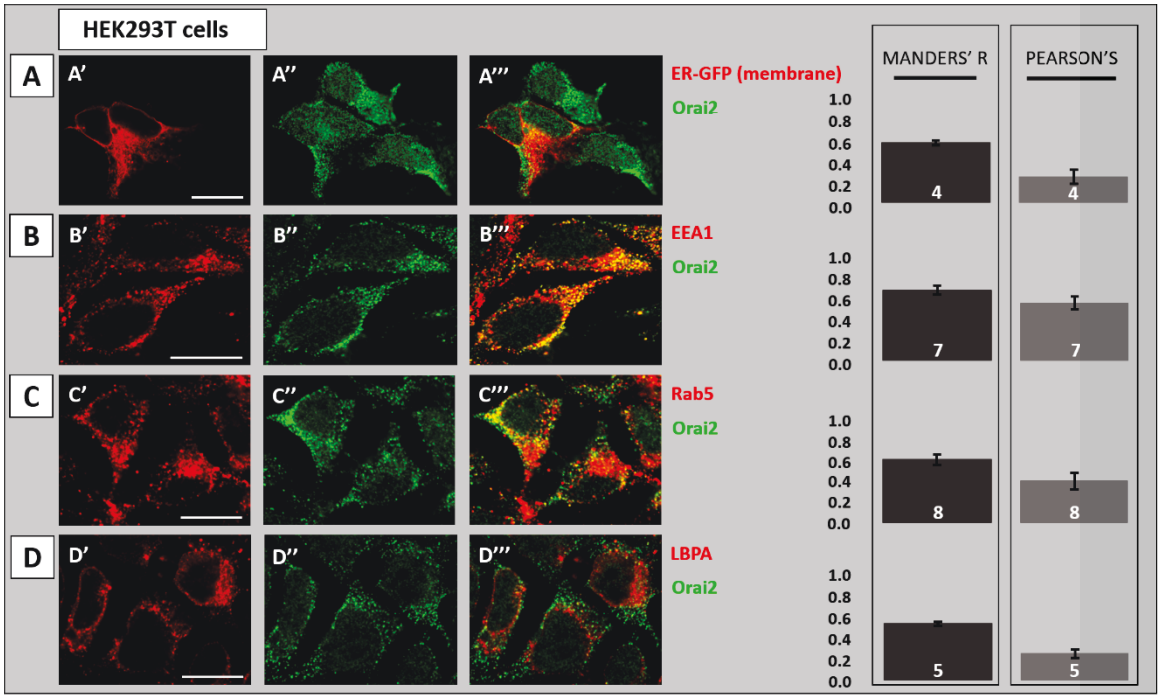

Figure 23: Orai2 localizes to the early endosome compartment. Confocal microscope immunofluorescence analysis of the subcellular localization of endogenous Orai2 in HEK293T cells. **A)** HEK293T cells were transfected with the cDNA coding for a membrane resident, ER-targeted GFP: ER-GFP red staining (A'), anti-Orai2 green staining (A'') and merged signals (A'''). Co-localization Manders' R and Pearson's coefficients were calculated giving 0.61 ± 0.02 and 0.26 ± 0.07, respectively. **B)** HEK293T cells were stained for the early-endosome compartment: anti-EEA1 red staining (B') anti-Orai2 green staining (B'') and merged signals (B'''). Co-localization Manders' R and Pearson's coefficients were calculated giving 0.74 ± 0.04 and 0.61 ± 0.06 respectively. **C)** HEK293T cells were stained for the early- and recycling-endosome compartment: anti-Rab5 red staining (C'), anti-Orai2 green staining (C'') and merged signals (C'''). Co-localization Manders' R and Pearson's coefficients were calculated giving 0.66 ± 0.05 and 0.44 ± 0.09 respectively. **D)** HEK293T cells were stained for the late endosome compartment: anti-LBPA red staining (D'), anti-Orai2 green staining (D'') and merged signals (D'''). Co-localization Manders' R and Pearson's coefficients were calculated giving 0.60 ± 0.02 and 0.28 ± 0.04 respectively. In all panels the bar size is 10 μm and the graphs show the average coefficients (mean ± SEM, Number of coverslips is shown in the bars). Representative images of at least 3 independent experiments.

Orai2 localizes to the early-endosome compartment of wild-type and PS2-N141I cortical neurons

We performed the staining with both Rab5 and EEA1 markers in cortical neurons of WT mice (**Fig. 24A**,**B**), obtaining high Manders' R and Pearson's coefficients (0.63 and 0.35 for Rab5, 0.66 and 0.38 for EEA1, respectively). Orai2 is therefore present at the early endosomal level in cortical neurons as well, albeit the staining with EEA1 was not always clear; despite performing it for most of the following experiments, we decided to display Rab5 staining only, supported by the Pearson's coefficient alone for better clarity. Moving to cortical neurons coming from TG and 2TG mice we noticed that the two TG lines differ not only in comparison to WT but also between them. **Figure 24C** shows how TG neurons display a slightly weaker co-localization of Rab5 with Orai2, while the opposite is true for the 2TG (Pearson's: WT = 0.35, TG = 0.29, 2TG = 0.48). It is worth remembering that both TG and 2TG neurons show similar increased protein levels of Orai2 as assayed by WB, met by strong similarities as far as Ca^{2+} handling is concerned (Kipanyula, et al. 2012a).

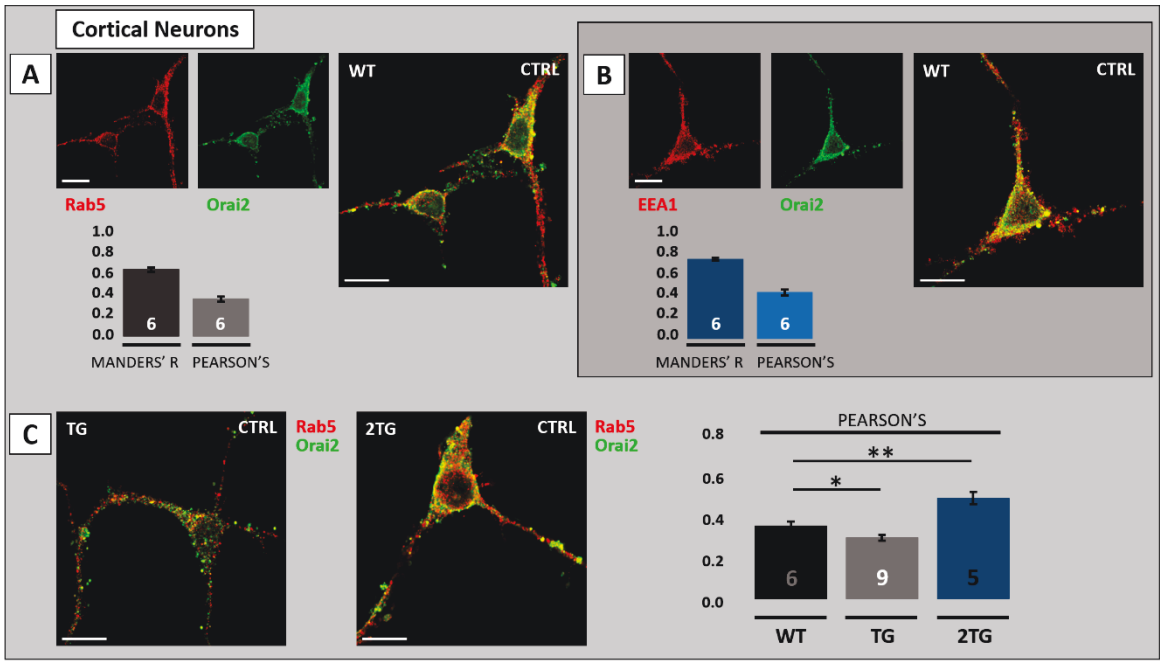

Figure 24: Orai2 localizes to the endosome compartment of cortical neurons from WT and PS2-based AD mice. Confocal microscope immunofluorescence analysis of the subcellular localization of endogenous Orai2 in 12 DIV cortical neurons from WT, TG and 2TG mice (see M&M). **A)** WT neurons were stained for both Rab5 (red) and Orai2 (green). Co-localization Manders' R and Pearson's coefficients were calculated giving 0.63 ± 0.02 and 0.35 ± 0.02, respectively. **B)** WT neurons were stained for both EEA1 (red) and Orai2 (green). Co-localization Manders' R and Pearson's coefficients were calculated giving 0.66 ± 0.01 and 0.38 ± 0.02, respectively. **C)** TG and 2TG neurons were stained for both Rab5 and Orai2. The co-localization Pearson's coefficient was calculated giving 0.29 ± 0.01 and 0.48 ± 0.03, respectively. TG

neurons show a statistically significant decrease as compared to WT (0.29 vs 0.38) while 2TG neurons display a significant increase (0.48 vs 0.38). The Manders' R coefficients (not shown) followed the trend with WT = 0.66 ± 0.01, TG = 0.51 ± 0.01, $p < 0.001$ and 2TG = 0.71 ± 0.02, $p < 0.05$. In all panels the bar size is 10 μm and the graphs show the average coefficients (mean ± SEM, Number of coverslips is shown in the bars, * $p < 0.05$, ** $p < 0.01$, *** $p < 0.001$). Representative images of at least 3 independent experiments.

The striking difference between TG and 2TG neurons can be accounted for by the enlargement of the early-endosomal compartment occurring in sporadic AD. Endosome anomalies, associated with up-regulated expression of Rab5 and other endocytosis-related proteins, are the earliest known disease-specific neuronal response possibly linked to APP dys-metabolism (Cataldo, et al. 2000; Schreij, et al. 2016; Toh and Gleeson 2016). Consistently, 2TG cortical neurons express higher levels of Rab5, when compared to both WT and TG neurons (**Fig. 25**), explaining the greater Orai2-Rab5 co-localization.

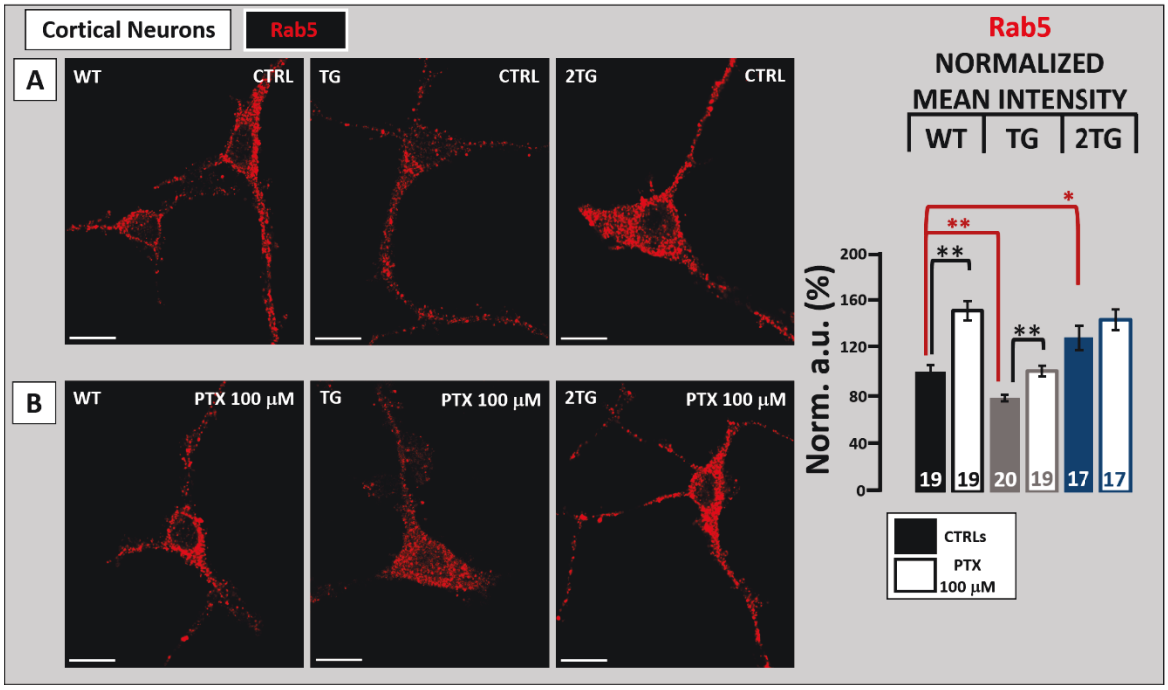

Figure 25: Rab5 staining of cortical neurons changes among genotypes upon cell stimulation. Confocal microscope immunofluorescence analysis of Rab5 staining in WT, TG and 2TG cortical neurons at 12 DIV. **A)** WT, TG and 2TG cortical neurons were treated with mKRB containing different stimuli or the vehicle (CTRL) at 37°C for 5 minutes prior to fixation. They were then stained for Rab5 (red). A region of interest (ROI) was drawn around the perimeter of the cells and the mean intensity of red pixels inside the ROI was quantified. Normalized mean intensity values are shown in the solid (CTRL) bars. WT: 100.0 ± 6.0; TG: 78.3 ± 2.7; 2TG: 128.5 ± 10.1. **B)** WT, TG and 2TG cortical neurons were treated with picrotoxin (PTX 100 μM). Normalized mean intensity values are shown in the hollow (PTX) bars. WT: 150.9 ± 8.1, TG: 100.6 ± 4.5; 2TG: 143.6 ± 8.3. In all panels the bar size is 10 μm and the graphs show the average coefficients (mean ± SEM, Number of coverslips is shown in the bars, * $p < 0.05$, ** $p < 0.01$, *** $p < 0.001$). Representative images of at least 3 independent experiments.

Orai2 and Orai1 localization to early endosomes changes upon cell stimulation

For a long time neuronal CRAC channels and SOCE have been neglected on the common misbelief that neurons, being endowed with VOCCs, do not need any additional Ca^{2+} refilling mechanism. In 2009 *Lalonde et al*, however, demonstrated how at resting membrane potential, SOCE is perennially activated to provide Ca^{2+} entry needed to refill the very leaky neuronal ER (Lalonde, et al. 2014). One year later two articles were published saying that STIM1 can act as switch to activate Orai channels while turning off VOCCs (Park, et al. 2010; Wang, et al. 2010b). With this background in mind we reasoned that increasing neuronal activity will cause massive Ca^{2+} entry through VOCCs, therefore limiting the necessity of SOCE and early endosomes looked like a good place to store CRAC subunits while not needed. Mouse cortical neurons (10-12 DIV) were bathed in standard solution (see M&M for composition) and treated for 5 minutes at 37°C with activity-enhancing compounds, such as KCl (30 mM) to induce a permanent depolarization or picrotoxin (PTX, 100 μM) which, by blocking GABA-mediated neuronal inhibition, induces a Ca^{2+} spiking behaviour (Kipanyula, et al. 2012a). Cells were then fixed to analyse the level of Orai2/Rab5 and Orai1/Rab5 co-localization by immunofluorescence (IF) (**Fig. 26A**). To our surprise KCl was less effective than PTX in inducing early endosome Orai2 localization, with this latter showing only a tendency to increase in WT neurons and no increase at all in 2TG ones upon KCl exposure (KCl, Pearson's: WT = 0.41 [CTRL = 0.35], TG = 0.35 [CTRL = 0.29], 2TG = 0.51 [CTRL = 0.48]). As mentioned above PTX caused a significant larger increase in co-localization between Rab5 and Orai2 for all the three genotypes, with the strongest effect (+ 57%) in WT neurons (PTX, Pearson's: WT = 0.55 [CTRL = 0.35], TG = 0.38 [CTRL = 0.29], 2TG = 0.59 [CTRL = 0.48]) (**Fig. 26B**). These results suggest that, in WT neurons there is a mechanism capable of increasing the endosomal compartmentalisation of Orai2 upon neuronal activation while being more effective during spiking activity. TG neurons follow WT ones, but showing less ample variations in Orai2/Rab5 co-localization, while 2TG neurons appear to have even less room for movement, likely because Orai2 shows a significantly greater endosomal localization when compared to WT neurons (**Fig. 26A**).

As far as Orai1 is concerned, its co-localization with Rab5 varies to a lesser extent as compared to Orai2; Orai1 appears to be similarly distributed across the three genotypes, with absolute Pearson's coefficients that do not display significant differences (Pearson's: WT = 0.48, TG = 0.45, 2TG = 0.41) (see **Fig. 28A**). When stimulated with PTX the dynamics were not overt, being Orai1/Rab5 co-localization almost unchanged in WT neurons and only mildly affected in TG

and 2TG neurons (PTX, Normalized Pearson's to untreated CTRL: WT = 106.4 %, TG = 115.1 %, 2TG = 108.3%) (**Fig. 28B**).

Cells were also challenged with the SERCA pump inhibitor CPA (20 μM) for five minutes in a Ca^{2+}-free EGTA-containing medium (**Fig. 26C**); this treatment should promote the recruitment of Orai2/Orai1 to the PM while preventing its Ca^{2+} inactivation given that, with EGTA outside the cells, the channel opens but there's no Ca^{2+} entry. Strikingly, this treatment had a strong effect, opposite to what expected. Rab5-Orai2 co-localization was enhanced in both WT and TG neurons, and stayed unchanged in 2TG ones (EGTA+CPA Pearson's: WT = 0.44 [CTRL = 0.35], TG = 0.42 [CTRL = 0.29], 2TG = 0.51 [CTRL = 0.48]). Of note, EGTA + CPA treatment was unable to elicit any response from 2TG neurons, further confirming their inability to move the Orai2 pool in and out of endosomes.

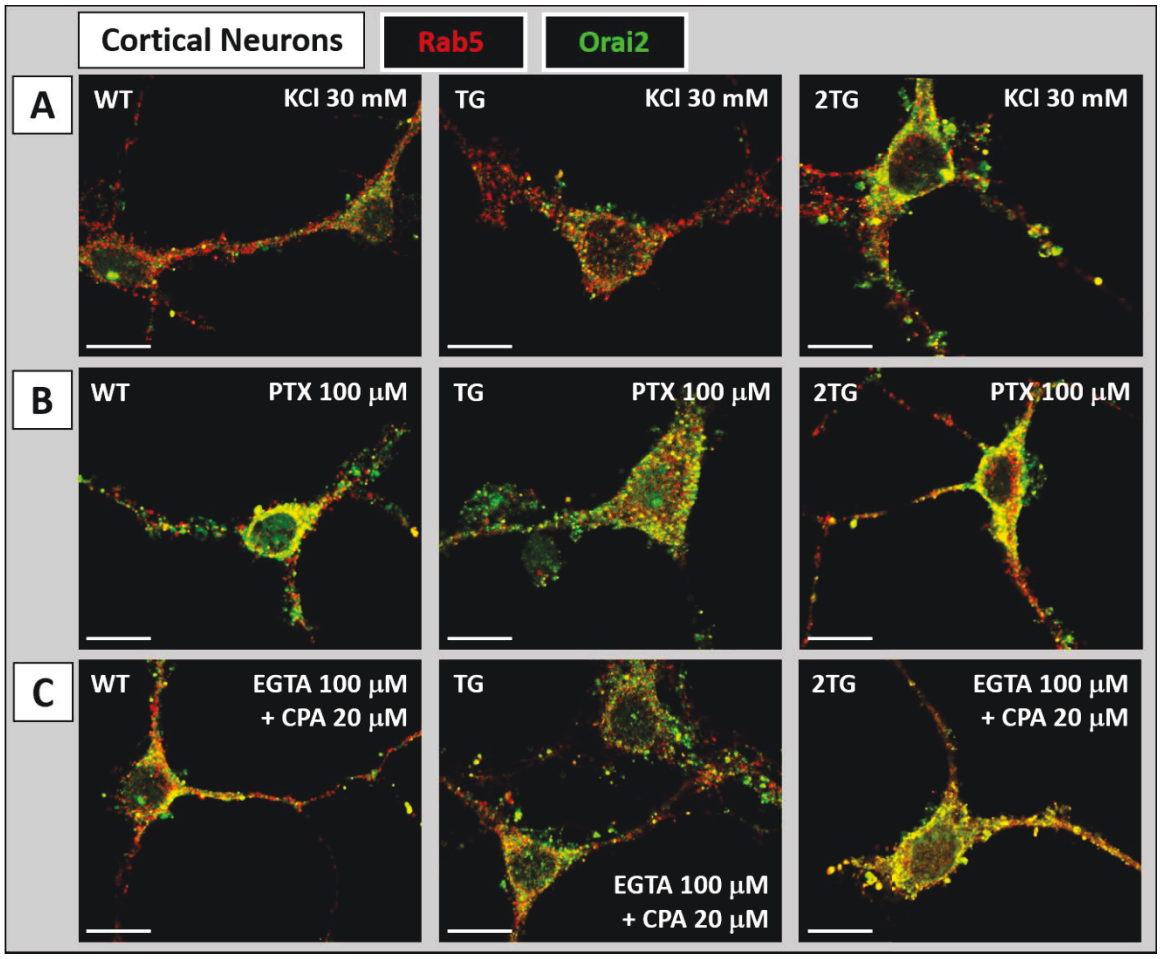

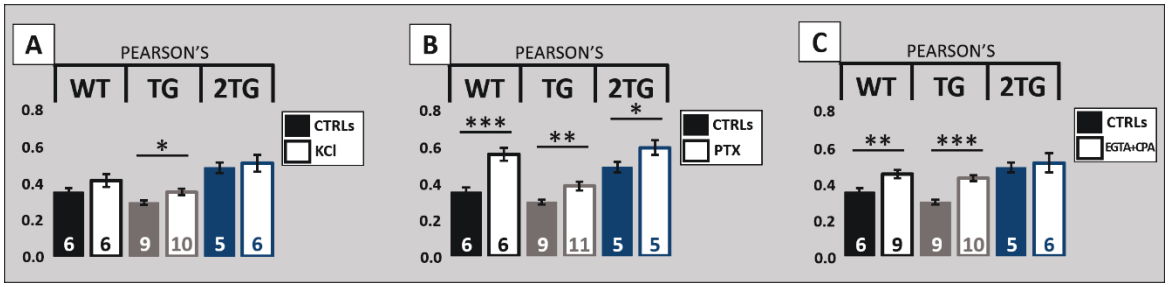

Figure 26: Orai2 localization to endosomes dynamically changes upon neuronal stimulation. Confocal microscope immunofluorescence analysis of the subcellular localization of endogenous Orai2 in 12 DIV cortical neurons from WT and PS2-based AD mice. WT, TG and 2TG cortical neurons were treated at 37ºC for 5 minutes in mKRB in the absence (CTRL) or presence of different stimuli, prior to fixation. They were later stained for both Rab5 and Orai2. Co-localization Manders' R and Pearson's coefficients were calculated and compared to the respective CTRL conditions: Manders' R (CTRL): WT = 0.63 ± 0.02; TG = 0.51 ± 0.01; 2TG = 0.71 ± 0.02. Pearson's (CTRL): WT = 0.35 ± 0.02; TG = 0.29 ± 0.01; 2TG = 0.48 ± 0.03. **A)** KCl (30 mM) treatment: Manders' R (KCl): WT = 0.63 ± 0.02; TG = 0.60 ± 0.02; 2TG = 0.73 ± 0.03. Pearson's (KCl): WT = 0.41 ± 0.03; TG = 0.35 ± 0.02; 2TG = 0.50 ± 0.05. **B)** PTX (100 μM) treatment: Manders' R (PTX): WT = 0.74 ± 0.03; TG = 0.61 ± 0.02; 2TG = 0.77 ± 0.02. Pearson's (PTX): WT = 0.55 ± 0.03; TG = 0.38 ± 0.02; 2TG = 0.59 ± 0.04. **C)** EGTA (100 μM) plus CPA (20 μM) treatment: Manders' R (EGTA+CPA): WT = 0.67 ± 0.02; TG = 0.65 ± 0.02; 2TG = 0.74 ± 0.03. Pearson's (EGTA+CPA): WT = 0.44 ± 0.02; TG = 0.42 ± 0.02; 2TG = 0.50 ± 0.05. In all panels the bar size is 10 μm and the graphs show the average Pearson's coefficients (mean ± SEM, Number of coverslips is shown in the bars, * p <0.05, ** p < 0.01, *** p < 0.001). Representative images of at least 3 independent experiments.

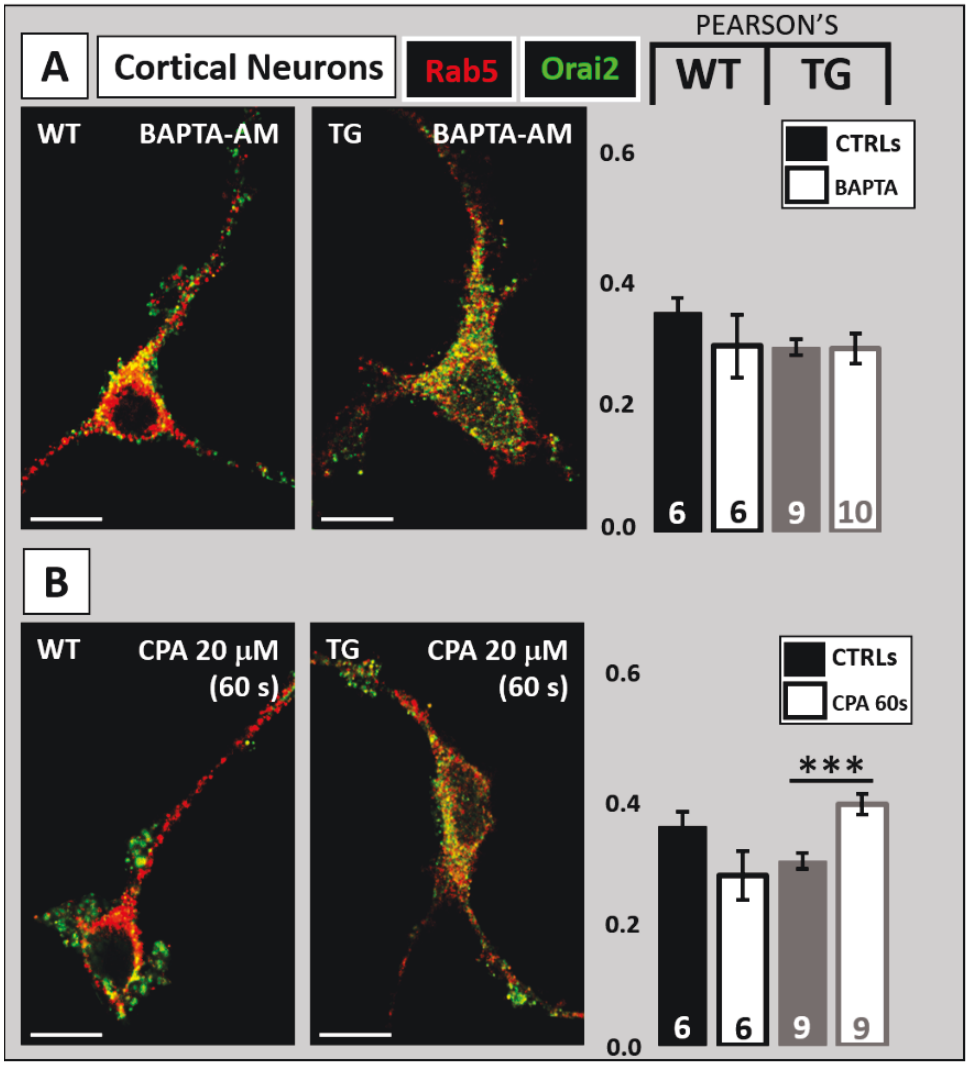

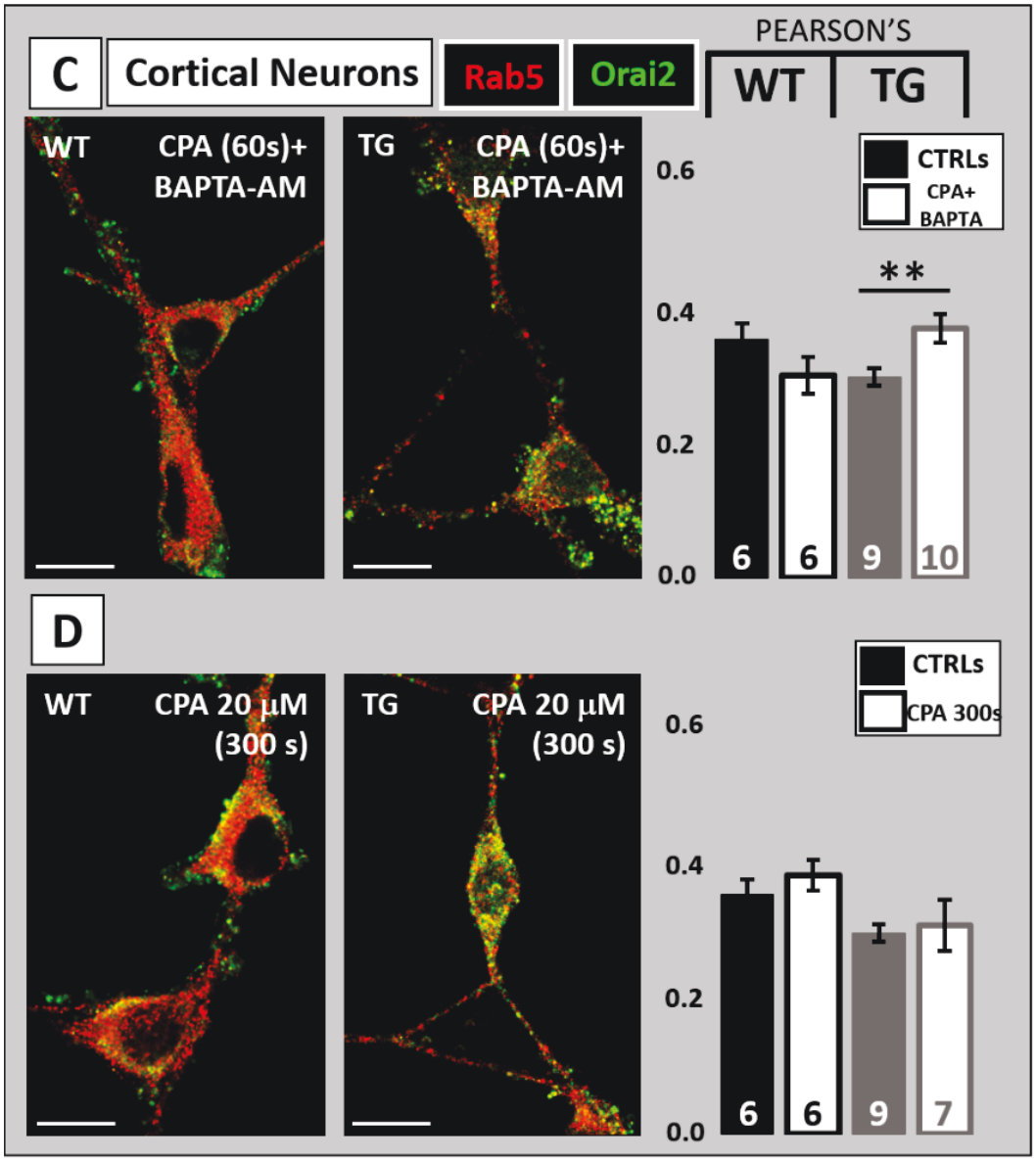

Figure 27: Orai2 localization to endosomes dynamically changes following SOCE manipulation. Confocal microscope immunofluorescence analysis of the subcellular localization of endogenous Orai2 in 12 DIV cortical neurons from WT and TG mice. Ca^{2+} handling was modified in WT and TG cortical neurons bathed in mKRB at 37°C in the absence (CTRL) or presence of different stimuli. They were later fixed and stained for both Rab5 and Orai2. Co-localization Manders' R and Pearson's coefficients were calculated and compared to CTRL conditions. **A)** Neurons were incubated for 30 minutes with BAPTA-AM (5 μM) in mKRB at 37°C. Manders' R (CTRL): WT = 0.63 ± 0.02; TG = 0.51 ± 0.01. Pearson's (CTRL): WT = 0.35 ± 0.02; TG = 0.29 ± 0.01. Manders' R (BAPTA-AM): WT = 0.56 ± 0.05; TG = 0.54 ± 0.02. Pearson's (BAPTA-AM): WT = 0.29 ± 0.05; TG = 0.29 ± 0.02. **B)** Neurons were treated with CPA (20 μM) for 60 seconds in mKRB at 37°C. Manders' R CPA-60s): WT = 0.49 ± 0.02; TG = 0.61 ± 0.03. Pearson's (CPA-60s): WT = 0.27 ± 0.04; TG = 0.38 ± 0.02. **C)** WT and TG cortical neurons were incubated for 30 minutes with BAPTA-AM (5 μM) in mKRB at 37°C and then treated with CPA (20 μM) for 60 seconds in mKRB at 37°C. Manders' R (CPA-60s + BAPTA-AM): WT = 0.57 ± 0.04; TG = 0.81 ± 0.02. Pearson's (CPA-60s + BAPTA-AM): WT = 0.29 ± 0.03; TG = 0.48 ± 0.02. **D)** Neurons were treated for 300 seconds with CPA (20 μM) in mKRB at 37°C. Manders' R (CPA-300s): WT = 0.65 ± 0.02; TG = 0.54 ± 0.02. Pearson's(CPA-300s): WT = 0.37 ± 0.02; TG = 0.30 ± 0.04. In all panels the bar size is 10 μm and the graphs show the average Pearson's coefficients (mean ± SEM, Number of coverslips is shown in the bars, ** $p < 0.01$, *** $p < 0.001$). Representative images of at least 3 independent experiments.

As shown in **Figures 27** and **28**, I also addressed the timing issue of Orai2 and Orai1 localization, by reducing the CPA treatment to 1 minute and leaving a physiological concentration of extracellular $CaCl_2$ (1 mM). Such a treatment decreased, albeit not significantly, the endosomal localization of Orai2 in WT neurons, while significantly increasing it in TG neurons (**Fig. 27B**) (CPA/60 seconds, Pearson's: WT = 0.27 [CTRL = 0.35], TG = 0.38 [CTRL = 0.29]). This phenomenon held true for Orai1 as well, only in TG neurons there is an accumulation of Orai1 at the endosomal level after a brief SOCE induction (CPA/60 seconds, Normalized Pearson's: WT = 98.3 %, TG = 114.6%, 2TG = 109.8%) (**Fig. 28C**). We posited that whether Orai2 motion in and out of endosomes was dependent on transient Ca^{2+} rises, an intracellular fast Ca^{2+} chelating agent, such as BAPTA, would nullify it, or at least decrease Oria2/Rab5 co-localization. When cells were pre-treated with BAPTA-AM (5 μM) for 30 minutes in culture medium, the treatment *per se* did not significantly alter Orai2 localization (BAPTA-AM Pearson's: WT = 0.29 [CTRL = 0.35], TG = 0.29 [CTRL = 0.29]) (**Fig. 27A**). However, in BAPTA-loaded cells, a 1-minute-CPA treatment in Ca^{2+} produced an Orai2 localization comparable to that obtained with CPA alone (**Fig. 27B,C**) (CPA 60 seconds + BAPTA-AM Pearson's: WT = 0.29 [CTRL = 0.35], TG = 0.36 [CTRL = 0.29]). Finally, as shown in **Figure 27D**, a 5-minute-CPA treatment in the presence of extracellular Ca^{2+} - at variance with the same treatment in the absence of Ca^{2+} (**Fig. 26C)** - yielded no significant difference (CPA/300 seconds, Pearson's: WT = 0.37 [CTRL = 0.35], TG = 0.30 [CTRL = 0.29]).

As far as Orai1 is concerned, I should note firstly that, at variance with Orai2, no difference was observed in Ora1/Rab5 co-localization among genotypes (**Fig. 28A**) and secondly that, in the presence of extracellular Ca^{2+}, the CPA treatment caused significant, albeit small, shifts in Orai1 co-localization only in the transgenic mouse lines (**Fig. 28C**). In particular, in TG neurons endosomal Orai1 localization increased with both short and long CPA treatments in the presence of extracellular Ca^{2+}, while in 2TG neurons, it was unchanged by a 60-second-CPA treatment and reduced by the longer one (**Fig. 28C,D**). Note that in WT neurons no change was observed with both the treatments (CPA/300 seconds, Normalized Pearson's: WT = 94.4 %, TG = 122.6 %, 2TG = 80.8 %). Similar results were obtained when Mander's R coefficients were used for comparison (data not shown).

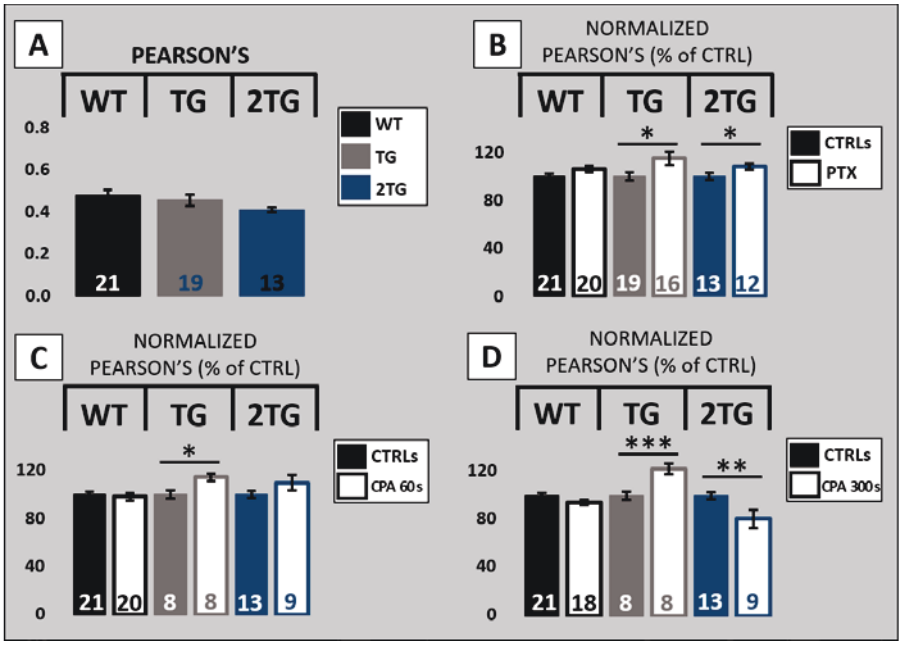
A
PEARSON'S
WT
TG
2TG
0.8
0.6
0.4
0.2
0.0
21
19
13
WT
TG
2TG
B
NORMALIZED
PEARSON'S (% of CTRL)
WT
TG
2TG
120
80
40
0
21
20
19
16
13
12
*
*
CTRLs
PTX
C
NORMALIZED
PEARSON'S (% of CTRL)
WT
TG
2TG
120
80
40
0
21
20
8
8
13
9
*
CTRLs
CPA 60s
D
NORMALIZED
PEARSON'S (% of CTRL)
WT
TG
2TG
120
80
40
0
21
18
8
8
13
9
***
**
CTRLs
CPA 300s

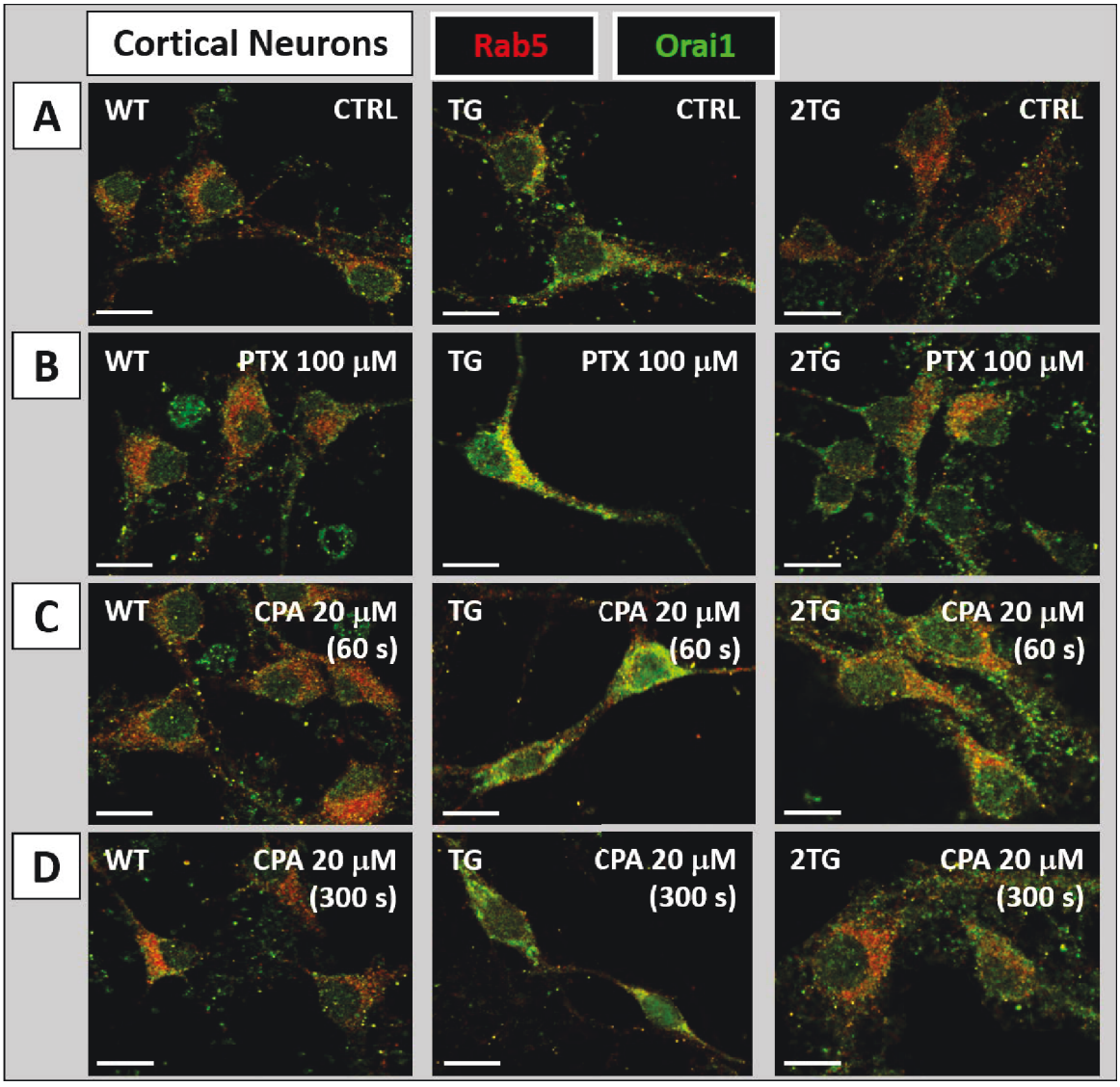
Cortical Neurons
Rab5
Orai1
A
WT
CTRL
TG
CTRL
2TG
CTRL
B
WT
PTX 100 µM
TG
PTX 100 µM
2TG
PTX 100 µM
C
WT
CPA 20 µM
(60 s)
TG
CPA 20 µM
(60 s)
2TG
CPA 20 µM
(60 s)
D
WT
CPA 20 µM
(300 s)
TG
CPA 20 µM
(300 s)
2TG
CPA 20 µM
(300 s)

Figure 28: Orai1 localization to endosomes dynamically changes upon neuronal stimulation and SOCE manipulation. Confocal microscope immunofluorescence analysis of the subcellular localization of endogenous Orai1 in 12 DIV cortical neurons from WT and PS2-based AD mice. WT, TG and 2TG cortical neurons were treated at 37ºC for 5 minutes in mKRB in the absence (CTRL) or presence of different stimuli, prior to fixation. They were later stained for both Rab5 and Orai1. **A)** Co-localization Manders' R and Pearson's coefficients were calculated and compared to the respective CTRL conditions: Manders' R (CTRL): WT = 0.75 ± 0.01; TG = 0.72 ± 0.02; 2TG = 0.73 ± 0.01. Pearson's (CTRL): WT = 0.48 ± 0.02; TG = 0.45 ± 0.03; 2TG = 0.41 ± 0.01. **B)** PTX (100 μM) treatment: Normalized Manders' R (PTX): WT = 103.9 ± 1.0; TG = 104.2 ± 2.1; 2TG = 103.5 ± 0.8. Pearson's (PTX): WT = 106.4 ± 2.7; TG = 115.1 ± 5.5; 2TG = 108.3 ± 2.7. **C)** 60 second-treatment with CPA (20 μM): Manders' R (CPA 60 s): WT = 101.7 ± 0.8; TG = 107.4 ± 1.6; 2TG = 105.2 ± 1.5. Pearson's (CPA 60 s): WT = 98.3 ± 3.1; TG = 114.6 ± 3.1; 2TG = 109.8 ± 6.4. **D)** 300 second-treatment with CPA (20 μM): Manders' R (CPA 300 s): WT = 100.2 ± 1.0; TG = 110.3 ± 1.9; 2TG = 93.2 ± 2.5. Pearson's (CPA 300 s): WT = 94.4 ± 2.4; TG = 122.6 ± 4.6; 2TG = 80.8 ± 7.5. In all panels the bar size is 10 μm and the graphs show the average Normalized Pearson's coefficients (mean ± SEM, Number of coverslips is shown in the bars, * $p < 0.05$, ** $p < 0.01$, *** $p < 0.001$). Representative images of at least 3 independent experiments.

DISCUSSION

It might stem from my professional bias, but it is easy to realize the importance of Ca^{2+} when it comes to CNS function and dysfunction. A harder task would be to tackle one by one every single subtle or harsh imbalance, to come up with a comprehensive hypothesis that can set the ground for tomorrow's research. It is not indeed an easy task even to enumerate and summarize the long list of findings for what concerns Ca^{2+} dysregulations in AD. The years of the "ER Ca^{2+} overload" hypothesis (Tu, et al. 2006) appear to be long gone even in their promoters' mind, leaving the rest of us, researchers with a thing for Ca^{2+} signalling, in a much greater confusion than just few years ago. The "ER Ca^{2+} overload" hypothesis stated that PSs, on top of being the γ-secretase catalytic core, are also part of what's known as ER leak channel, that is a molecularly unknown entity that constantly allows a Ca^{2+} leakage across the ER membrane. FAD-associated PS mutations disrupt this pleiotropic role, reducing or even abolishing the leak, thus leading to Ca^{2+} overload (Supnet and Bezprozvanny 2010; Supnet and Bezprozvanny 2011; Tu, et al. 2006). How this overload would hamper the cell fate in ageing soon became a hot-topic, with a focus on the exaggerated activation of both the ryanodine and IP3 receptors (Chakroborty, et al. 2009; Cheung, et al. 2008; Green and LaFerla 2008; Stutzmann, et al. 2006) and their likely rebound on mitochondria toxicity and cell death. As for November 2016, only the Foskett's group provided a sequel to their story of IP3R hyperexcitability (Shilling, et al. 2014), and they did that after putting a stone over the long-lasting dispute on PSs' ER leak role (Shilling, et al. 2012).

This brief introduction to bring the reader through the same path we followed to come up with this study. When looking at mutant PS2-based AD mouse models (Kipanyula, et al. 2012b), cell lines or human FAD fibroblasts (Brunello, et al. 2009; Giacomello, et al. 2005; Zampese, et al. 2011b; Zatti, et al. 2006; Zatti, et al. 2004) one will not find any degree of ER Ca^{2+} overload, on the contrary PS2-based models always display a substantial reduction of ER Ca^{2+} content and release. This decreased Ca^{2+} content is accounted for by SERCA2 pump inhibition (Brunello, et al. 2009) as well as a diminished Ca^{2+} entry upon store depletion, that is found in cell lines overexpressing PS2 mutants (Giacomello, et al. 2005; Zatti, et al. 2004), transgenic cortical neurons expressing either mutant PS2 (Yoo, et al. 2000) or PS1 (Leissring, et al. 2000), as well as FAD patient-derived fibroblasts and immune cells (Giacomello, et al. 2005; Jaworska, et al. 2013; Zatti, et al. 2004). Being SOCE a feature that is altered in both PS1- and PS2-based models, it gained much attention lately, from those who were former proponents of the overload hypothesis. This is good news; it serves both the purposes of bringing back together the researchers in AD field toward a common

objective, and allowing the still scarce knowledge of SOCE in neurons to be deepened. Bezprozvanny's group proposed STIM2 as the essential SOCE component responsible for the degeneration of neuronal spines; a degeneration that is driven by a defect in spine SOCE, which they attribute to a specific neuronal SOC (nSOC) channel, the cause being either mutant PS1 or APP expression or the concomitant Aβ accumulation (Sun, et al. 2014; Zhang, et al. 2015a). It was, however, another paper that caught our attention: Meyer's group was suggesting, through a thorough siRNA-based screening, that both PS2 and the CRAC channel subunit Orai2 were responsible for the maintenance of the physiological ER Ca^{2+} content (Bandara, et al. 2013). In their hands, the down-regulation of both the proteins caused a significant Ca^{2+} overload, whereas their overexpression reduces the store Ca^{2+} content; they went further, aided by a mathematical model, in saying that both proteins act as ER Ca^{2+} leak channels (Bandara, et al. 2013). This brought up again the possibility of mutant PSs being underperforming leak channels, thus leading to overload. While this role cannot be completely excluded for endogenous PSs, a lot of data have established the FAD-linked mutant PSs do not behave as defective ER leak channels (Shilling, et al. 2012; Zampese, et al. 2011a). Nonetheless leaving this controversy behind, the Orai2 finding was a good starting ground to investigate the interplay between decreased ER Ca^{2+} content, reduced SOCE and Aβ production/release.

Phenomenology tells us that an imbalance in SOCE is met by an imbalance in Aβ production/release: initial studies carried out in CHO-APP cells demonstrated that SOCE inhibition increases Aβ42 release (Yoo, et al. 2000) whereas in neurons and SH-SY5Y cells an increased CCE also increases Aβ42 release (Al-Mousa and Michelangeli 2012; Pierrot, et al. 2004). Consistently with first data, Zeiger and colleagues reported decreased Aβ production following SOCE potentiation by overexpressing STIM1 and Orai1 in HEK-APPswe cells (Zeiger, et al. 2013). We pursued the issue by setting up a model that mimicked the ER Ca^{2+} depletion observed in mutant PS2 expressing cells, without altering SOCE and γ-secretase alongside, employing specific inhibitors rather than heterologous protein expression. Upon a 24-hour-treatment with CPA, at a low concentration, a partial (about 40%) ER depletion is obtained without elevating cytosolic Ca^{2+}. Under this condition, the Aβ42 level in the extracellular medium is increased by about 50%. Combining reduction of store Ca^{2+} content to SOCE inhibition with BTP-2 causes an additional 40% increase in the Aβ42 level. Of note, the SOCE inhibitor's effect is not simply due to further store depletion, since SOCE inhibition alone - in the absence of store depletion - accounted for a significant increase (about 16%) in Aβ42 detection in the conditioned media. These results underlie the existence of at least two different, Ca^{2+}-dependent mechanisms that control Aβ42 production/secretion, based on the store Ca^{2+} content and the SOCE level, respectively.

SOCE takes place thanks to many players, among which the ER-resident Ca^{2+} sensor STIM1 and the PM channel subunit Orai1, with the additional components STIM2 and Orai2/Orai3 playing an ancillary, modulatory role (Hoth and Niemeyer 2013), but see (Zhang, et al. 2016) for the primary role exerted by Orai2 in neuronal SOC. We thoroughly characterized our mutant PS2-based mouse models at 3-6 months of age, screening for proteins involved in spine maintenance (PSD95, NMDAR2B) and Ca^{2+} homeostasis (STIM/Orai). The most consistent change was in Orai2 level, showing a trend to be increased in cortices from both TG (PS2.30H line) and 2TG (B6.152H line) mice, possibly underlying a PS2-dependent mechanism (E. Scremin, unpublished data). Indeed, neurons from these mouse lines share similar defects in Ca^{2+} stores and ER/mitochondria coupling, notwithstanding the APP overexpression, PS2 cDNA insertion sites and the slightly different background (L. Ozmen, personal communication). Thus far we have evidence that Orai2 levels are untouched in PS2KO mice (unpublished data), suggesting a very specific and selective mechanism, likely due to a gain-of-function brought about by the mutant PS2. Silencing of human mutant PS2 will be carried out at the neuronal level, in adult mice *in vivo,* to see whether its down-regulation can rescue defects in Ca^{2+} homeostasis and Orai2 expression together with brain hyper-excitability, the latter was recently described by our group in PS2-based TG mice (Fontana, et al. 2017). What we know so far is that the majority of Orai2 is expressed at the neuronal, rather than the glial level; 80 % pure neuronal cultures show a greater degree of overexpression compared to the tissue, and immunohistochemical staining in sagittal slices highlights a rather selective neuronal distribution. To better address this issue, cultures of primary astrocytes will be checked for Orai2 expression levels by Western blot; while specific markers for astrocytes, microglia and oligodendrocytes will be used *in situ*.

Indeed, if compared to glial cells, a high Orai2 expression level was partly expected in neurons on the basis of previously reported mRNA levels (Berna-Erro, et al. 2009; Zhang, et al. 2016). Although our data in neuronal cultures indicate that Orai1 is regularly expressed, Orai1 immunostaining in brain slices is mandatory. At the *in situ* level and with high magnification, few neurons can be found without any Orai2 staining throughout the cortex and in the hippocampal hilus, thus reinforcing the idea of cell-specific expression, whether or not it is modulated by mutant PS2 has to be confirmed yet.

Playing with Orai2 expression levels in cell lines, I confirmed Bandara and colleagues' findings showing that Orai2 overexpression reduces the ER Ca^{2+} content (Bandara, et al. 2013). In addition I also showed that this reduction results in functional defects of ER Ca^{2+} handling since it impairs the IP3-induced Ca^{2+} release as well. Orai1 was not identified as a player of ER Ca^{2+} homeostasis by Bandara and co-workers, but curiously enough, in our hands, its overexpression also partially

reduced the IP3-induced Ca^{2+} release in the same cell model. Albeit lower in amplitude than that caused by Orai2, it was statistically significant and points in the direction of a SOCE defect as the prime cause of ER Ca^{2+} content decrease. It is fairly known, indeed, that overexpressing a CRAC channel alone, without matching the expression of its STIM counterpart, leads to a general loss of SOCE efficiency (Zeiger, et al. 2013). This to say that in addition to being a putative ER leak channel, Orai2, if overexpressed, hampers the normal SOCE efficiency, in a stronger fashion than Orai1, thus leading to a reduced Ca^{2+} supply for the ER. In other words, we cannot rule out the fact that Orai2 might be an ER leak channel, but we provide evidence that it is a less efficient SOCE mediator, possibly affecting the store Ca^{2+} content only indirectly [see also (Hoth and Niemeyer 2013)]. In fact, whether expressed alone or in combination with STIM1, Orai2 dampens SOCE, as compared to the endogenous machinery or to STIM1 and Orai1 co-expression, respectively. On the same line Orai2 down-regulation altered the IP3-induced Ca^{2+} release neither in H4-APPswe cells nor in HEK293T cells, whereas its effect on SOCE was rather controversial. In fact, when the classical protocol of "Ca^{2+} add-back" is employed in HEK293T cells to measure SOCE (following a challenge with a SERCA pump inhibitor in the absence of extracellular Ca^{2+}), the Orai2 knocked-down cells displayed no difference as compared to control cells. In contrast, when SOCE was elicited by challenging H4-APPswe cells with IP3-generating agonists or SERCA blockers, in the presence of extracellular Ca^{2+}, Orai2 knock-down had the effect of potentiating the Ca^{2+} entry after store depletion. While these discrepancies could be explained by the fact that two different cell lines were employed for the two type of experiments, these results might also disclose an intriguing Ca^{2+} dependency of Orai2 trafficking to the PM, a suggestion also derived by IF experiments (see below). Notwithstanding, further exploring this issue is mandatory.

In order to be an ER Ca^{2+} leak channel, Orai2 has to localize to the ER; and this is the case in both H4-APPswe and HEK293T cells. The Manders' overlap coefficient R changed little going from endogenous to overexpressed Orai2, reflecting the fact that the vast majority of overexpressed Orai2 does not get stuck in the ER, but rather accumulates in what looks like Golgi apparatus and PM. We surely have to investigate this thoroughly, but the lack of increase in Manders' R coefficient, upon overexpression, argues against a primary ER localization for Orai2, consistently with Ca^{2+} results that show a SOCE impairment. We expected that Orai2 overexpression would have caused its accumulation in the ER, which could explain, positing a leak function, the reduction in store content in this condition. Strikingly, the co-localization Pearson's coefficient increased upon switching from overexpressed to endogenous Orai2, particularly when a membrane-bound, instead of a luminal, ER marker was employed. These results allow us to state that Orai2 surely localizes, at least partially, to the ER; however, tuning upwards its expression does not alter the

localization to this organelle, making hard to believe that the effect seen on Ca^{2+} content could be attributed to an increased leakage. We were already puzzled by the *in situ* staining of Orai2, that can be defined everything but PM-like, and we confirmed this finding in cell lines, either. Endogenous Orai2 staining in fixed cells comes with a dotted texture, spread throughout the cytoplasm around the nucleus, reaching areas not covered by the ER staining; this pattern looked vesicular, and hence we stained for endosomal proteins obtaining very high levels of co-localization. This is specifically true for the early endosomes' marker EEA1 and for Rab5, that binds to both early and recycling endosomes (Murray, et al. 2016; Villasenor, et al. 2016; Wandinger-Ness and Zerial 2014). A lower level was found for the late endosomal compartment, comparable to that of the ER; this could mean that Orai2 passes through the ER for its maturation and goes to late endosomes/lysosomes for degradation, while standing between early and recycling endosomes for its function. Fixing the cells after SOCE induction, together with co-localization analysis with recycling endosome markers (Rab4/Rab11) as well as PM markers could help in solving this interesting issue.

We also addressed the possibility of having a dynamic pool of Orai2 in cultured cortical neurons. In these latter, Orai2 displays the same staining pattern as in cell lines and the co-localization with EEA1 and Rab5 shows an enrichment of the protein in the early and recycling endosomal compartment, as well. Neurons, however, are endowed with many Ca^{2+} channels, ranging from the ligand-activated, such as NMDAR, to the voltage-gated L-, T-, R- and P/Q- type. This allowed us to differentially stimulate neurons, either increasing their activity employing depolarizing protocols, or evoking ER Ca^{2+} release. In the basal condition of unstimulated neurons, the co-localization of Orai2 with endosomal markers comes in three different fashions, depending on the genotype. TG neurons show a smaller endosomal enrichment than WT, whereas 2TG neurons show a marked increase, despite both showing similar increased expression levels when it comes to Western blot. The difference is to be attributed to the presence of mutant APP in 2TG neurons: the increased co-localization of Orai2 to endosomes does not come alone, on the contrary, it is perfectly met by a similar increase of Rab5. Endosomal anomalies are, in fact, a key feature of AD, in its familial form as well as in the sporadic disease (Cataldo, et al. 2000; Schreij, et al. 2016; Toh and Gleeson 2016). This separation between PS2-only and PS2APP neurons is kept along the various treatments administered: inducing depolarization, with either KCl (30 mM) or the GABA-A inhibitor PTX, promotes Orai2 dynamics in TG, but not in 2TG neurons. If we compare TG neurons with the WT counterpart we can say that the similarities are more than the differences: both react to stimulation by increasing the amount of Orai2 found in endosomes, with the TG neurons being less effective in moving Orai2 inside. This relocation of Orai2 does not happen in

2TG neurons, they already have a much higher endosomal enrichment of Orai2 with its level being close to saturation: whereas PTX caused a huge increase of endosomal Orai2 compartmentalization in WT neurons, it only gave a very modest increase in 2TG neurons. If compared to WT neurons, they sit on the opposite side with respect to TG, with the latter following WT at a reduced pace, while 2TG seem unflappable. These findings might be explained by the higher Ca^{2+} spiking activity expected in transgenic neurons, if compared to WT, upon PTX treatment (Kipanyula, et al. 2012b). This condition could better approximate the KCl condition with Orai2 becoming much less mobile.

The same holds true when it comes to inducing SOCE with the blockage of SERCA pumps in the absence of Ca^{2+}: 2TG neurons are insensitive to this treatment. This peculiarity possibly accounts for the different effect of the two mutant transgenes, whereas PS2 seems less dramatic in changing the fate of Orai2, retaining the direction while decreasing the intensity, APP appears to be stronger: it counteracts the PS2-dependent effect of reduced endosomal Orai2 enrichment, without allowing further changing. Whether this effect could derive from APP itself or one of its numerous cleavage products has to be investigated yet [see (Lee, et al. 2015; Lee, et al. 2010)].

Strikingly enough, a 5-minute-long store depletion did not cause a movement of Orai2 in and out of endosomes in 2TG, in contrast both WT and TG neurons seem to accumulate Orai2 in endosomes even in this situation. The presence of extracellular Ca^{2+} during store depletion actually neutralizes this accumulation: 5 minutes of SERCA inhibition, leaving Ca^{2+} entry to occur, produces no changes in Orai2 localization. To clarify this issue, we tried to deplete the store for a shorter time period prior to fixation, allowing us to fix the cells when they are experiencing a maximal SOCE. However, this treatment did not cause any change in Orai2 localization in WT neurons, while again increasing endosomal accumulation in TG neurons. This phenomenon was also independent of the presence of intracellular Ca^{2+} hot-spots, generated on the ER surface or in the sub-PM area, since chelation of intracellular Ca^{2+}, by loading the cells with BAPTA-AM was unable to prevent it. We cannot, however, exclude a different kind of Ca^{2+} dependency, which relies on a more global Ca^{2+} elevation rather than on spatially restricted Ca^{2+} rises. BAPTA, indeed, prevents the generation of Ca^{2+} microdomains, but it can only partially buffer the bulk cytosolic Ca^{2+} increase generated upon SOCE activation. The interpretation of this results is everything but trivial: TG neurons differ a lot from WT when it comes to Ca^{2+} homeostasis, with approximately half the ER Ca^{2+} content (Kipanyula, et al. 2012a) and a reduced SOCE (Yoo, et al. 2000).

Moving to Orai1, we first noticed a similar co-localization with Rab5 across the three genotypes; this is in accordance with the Western blot analysis that did not highlight any difference as far as

Orai1 expression levels. The difference between Orai1 and Orai2 are retained during stimulation as well: while PTX caused endosomal accumulation of Orai2 in all neuronal types, albeit with different intensities, upon PTX treatment, Orai1 appears to be much less dynamic. Specifically, WT neurons are insensitive to PTX stimulus, whereas TG and 2TG were concordant in retrieving Orai1 into endosomes, albeit to a smaller degree when compared to Orai2. Activation of SOCE elicited by CPA brought about a behaviour similar to that of Orai2 when the stimulus was applied for 1 minute. Indeed, in WT neurons Orai1/Rab5 co-localization remained stable upon store depletion, possibly because Orai1 was already in place with no need for dynamic changes; conversely TG and 2TG neurons showed a tendency toward internalization, statistically significant only for TG neurons. Switching to a 5-minute-treatment with CPA, the immobility of Orai1 in WT neurons was confirmed, the endosomal enrichment in TG neurons was further pursued, while a reverse effect, with a pronounced reduction of Orai1/Rab5 co-localization, was found in 2TG neurons.

Modelling this complicated picture is not an easy task; however, some points are rather clear, such as Orai2 being more mobile than Orai1. In the presence of extracellular Ca^{2+}, upon store depletion TG, but not WT, neurons internalize both the Orai subunits, especially of the Orai2 subtype. In WT neurons a similar behaviour was observed only in the absence of extracellular Ca^{2+}, possibly highlighting in TG neurons an imbalance in constitutive endo-exocytosis. Moreover, in WT neurons, and to a lesser extent also in TG, Orai2 shows an endosomal accumulation when activity-enhancing compounds, such as PTX, are employed. Of note, store depletion elicits diverse behaviour for the two Orai proteins: WT neurons appear to be much less sensitive, if any at all, to CPA treatments, whether short or prolonged. In TG neurons both Orai1 and Orai2 are internalized upon 1 minute CPA application, with Orai1 further enriched in endosomes after 5 minutes, while Orai2 goes back to the pre-treatment distribution. Unfortunately, Orai2 dynamics in 2TG neurons were not assayed, and we can only infer that the difference observed in Orai1 localization upon a 5-minute-treatment with CPA has to be ascribed to the presence of mutant APP transgene. The road is still long and pieces of precious information are still missing, however a novel and unexpected dynamic localization of Orai2 was discovered, a thorough characterization of its properties concerning Ca^{2+} homeostasis are presented, and a link between this still mysterious protein and AD is provided.

MATERIALS AND METHODS

Cell culture and transfection

H4-APPswe and HEK293T cell lines were grown in DMEM containing 10% FCS, supplemented with L-glutamine (2 mM), penicillin (100 U/mL) and streptomycin (100 μg/mL), in humidified atmosphere containing 5% CO_2. Transfection was performed at 60% confluence using TransIT LT1 Transfection Reagent (Mirus) for overexpression, using a ratio of 4:1 for the cDNA coding for the protein/s of interest (or the void-vector) and the cDNA coding for the Ca^{2+} probe. The transfection mix was maintained for 5 hours before removal and substitution with the standard culture medium, or with a medium with reduced FCS (2%) for ELISA. For RNAi experiments cells were transfected using Lipofectamine RNAiMAX transfection reagent (Life Technologies). siRNAs (human Orai2 MISSION esiRNA EHU060251, human Orai1 MISSION esiRNA EHU120081, Universal Negative Control #1 MISSION siRNA SIC001) were added at the transfection mix to a final concentration of 25 nM, without removal. Aequorin and Fura-2 experiments were performed 24 and 48 hours after transfection, for overexpression and downregulation, respectively.

Cytosolic Ca^{2+} measurements with aequorin

H4-APPswe, HEK293T or HeLa cells (3-5x10^5) were plated on coverslips (13 mm diameter), after 24 hours they were transfected with the cDNA of interest and used for Ca^{2+} experiments the day after transfection (or 2 days after transfection for siRNA experiments). The day of experiment cells were incubated at 37°C with coelenterazine (5 μM) for 1 hour in a modified Krebs-Ringer buffer [mKRB, in mM: 140 NaCl, 2.8 KCl, 2 $MgCl_2$, 10 4-[2-hydroxyethyl]-1-piperazineethanesulfonic acid (HEPES), 11 glucose, pH 7.4] containing $CaCl_2$ (1 mM) unless otherwise stated, and then transferred to the perfusion chamber. All the luminescence measurements were carried out in mKRB at 37°C. The experiments were terminated by cell permeabilization with digitonin (100 μM) in a hypotonic Ca^{2+}-rich solution (10 mM $CaCl_2$ in H_2O) to discharge the remaining unused aequorin pool. The light signal was collected as previously described (Brini, et al. 1995).

Cytosolic Ca^{2+} imaging with Fura-2

H4-APPswe cells were incubated with Fura-2/AM (1 μM), pluronic F-127 (0.02%), and sulfinpyrazone (200 μM) for 40 minutes at 37 °C in mKRB and then left 20 minutes at room temperature (RT) in the same solution. Upon washing, Fura-2–loaded cells were visualized by a 20X ultraviolet-permeable objective (Olympus Biosystems GmbH, Planegg, Germany) on an inverted microscope (Zeiss Axiovert 100, Jena, Germany), were then processed for Ca^{2+}imaging. Alternating excitation wavelengths of 340 and 380 nm were obtained by a monochromator (polychrome V, TILL-Photonics) controlled by Roboscope software (developed by C. Ciubotaru, VIMM, Padua, Italy). A neutral density filter, UVND 0.6 (Chroma, USA), was used in the excitation pathway. The emitted fluorescence was measured at 500–530 nm. Images were acquired every 5 seconds, with 200-ms exposure time at each wavelength, by a PCO SensiCam QE (Kelheim, Germany) camera controlled by the same software. Regions of interest, corresponding to the entire soma, were selected for Ca^{2+} imaging. Coverslips were mounted in custom made chamber (1 mL) and bathed in mKRB. Cells were challenged at RT with the different stimuli by quick mixing. The ratio of the emitted fluorescence intensities (F340/F380) was averaged offline and normalized to the value measured before agonist addition. Traces are averages of 20–40 cells and are representative of 5–15 independent experiments.

ER Ca^{2+} imaging with G-CEPIA1er

To monitor ER Ca^{2+} levels, HeLa cells were transfected using TransIT LT1 (Mirus) with the complementary DNA coding for the probe G-CEPIA1er. Cells were analyzed after 24 hours by using an inverted microscope (Zeiss Axiovert 100) with a 40X oil objective (Fluar, NA 1.30). Excitation light at 480 nm was produced by a monochromator (polychrome V; TILL Photonics) and passed through a dichroic mirror (505 DRLP ext XF73). The emitted fluorescence was measured at 500–530 nm. Images were acquired using a cooled CCD camera (SensiCam QE PCO, Kelheim, Germany). All filters and dichroics were from Chroma Technologies (Bellow Falls, VT, USA). Images were collected at 1 Hz with 200-ms exposure time. Traces are from single cells and are representative of 20–40 cells coming from 3-4 independent cell batches.

Animals

The transgenic mouse lines PS2.30H (TG) and B6.152H (2TG) were kindly donated by Dr. L. Ozmen (F. Hoffmann-La Roche Ltd, Basel, Switzerland) (Ozmen, et al. 2009; Rhein, et al. 2009; Richards, et al. 2003). Both lines have the background strain of C57BL/6 mice, which were used as wt

controls and purchased from Charles River (Lecco, Italy). All procedures were carried out in strict adherence to the Italian regulations on animal protection and care and with the explicit approval of the local veterinary authority (CEASA Nr 56880). Mouse line features:

(1) The PS2.30H is a homozygous single transgenic line expressing the FAD-linked mutant human PS2-N141I under the mouse prion protein promoter. These mice display 2-3-fold increase of PS2 levels, both in cortices and hippocampi, as compared to WT.

(2) The B6.152H is a homozygous double transgenic line, also named PS2APP, which expresses the PS2-N141I FAD mutant under the mouse prion protein promoter together with the FAD-linked *Swedish* human mutant APP-K670M/N671L; the latter under the Thy1 promoter, thus expressed only at the neuronal level. As for the PS2.30H line, these animals present 2-3-fold increase in PS2, met by a similar increase in APP levels.

(3) The C57BL/6J WT mice share the prevalent (> 90%) genetic background of the other lines.

All the here used adult animals were age-matched female mice, given that in the 2TG line females anticipate the pathology, as likely occurring in humans (Ozmen, et al. 2009).

Primary neuronal cultures

Mouse primary neuronal cultures were obtained from cortices dissected from 0 to 1 day new-born mice as previously described (Kipanyula, et al. 2012a). Cells were seeded on poly-L-lysine (100 µg mL^{-1}) coated coverslips at a density of $3x10^5$ cells cm^{-2} in MEM Gibco containing glucose (20 mm), L-glutamine (0.5 mm), N2 supplement (1%), B27 supplement (0.5%), biotin (3.6 µm), pyruvic acid (1 mm), penicillin (25 µg mL^{-1}), streptomycin (25 µg mL^{-1}), neomycin (50 µg mL^{-1}) and horse serum (10%). After 24 h plating, the complete MEM was replaced with serum- and antibiotic-free Neurobasal medium containing B27 (2%) and L-glutamine (2 mm), unless otherwise stated. Fresh medium was added (1/5 of total volume) every 4th day.

Experiments were carried out between 10-12 days in vitro (DIV).

Immunohistochemistry

Dissection was performed as follow: brains were put in PFA 4% solution immediately after removal from skull and left 48 hours at 4°C for fixation. They were later washed in PBS (in mM: 137 NaCl, 2.7 KCl, 10 Na_2HPO_4, 1.8 KH_2PO_4, pH 7.4) three times, 30 minutes each washing. Slicing was

performed on a Leica VT1000S vibroslicer at 4°C, producing 50 μm thick slices that were stored in TBS (in mM: 150 NaCl, 50 Tris, pH 7.4) at 4°C until usage. For staining, floating sagittal slices were incubated one hour in blocking solution (5% Goat serum, 0.2% Triton X-100 in TBS) at RT. Antibodies were incubated in blocking solution overnight at 4°C and slices were washed three times (5 minutes each). Secondary Alexa-conjugated antibody was incubated in blocking solution for 1 hour at RT. Slices were mounted on a microscope slide with Mowiol and stored at 4°C until usage. Antibodies and markers were: anti-Orai2 (Sigma-Aldrich PRS4111), anti-neuronal nuclei NeuN (Clone A60, Millipore), NucRed Dead 647 Ready Probes (Invitrogen).

Immunofluorescence

H4-APPswe cells, HEK293T cells or cultured cortical neurons, seeded on 13 mm coverlips as above, were treated as specified in the figures: drugs were dissolved in mKRB (or DMSO) and the treatment was carried out at 37°C. Cells were fixed with a PFA (4%) plus sucrose (20%) solution for 10 minutes at RT. They were washed three times with PBS (5 minutes each) and incubated with blocking solution (10% Goat serum, 0.2% gelatine, 2% BSA in PBS) for 30 minutes. Primary antibodies were incubated in blocking solution for 1 hour at RT and coverslips were then washed three times. Secondary Alexa-conjugated antibodies were incubated for 45 minutes at RT and coverslips were washed prior to mounting. They were mounted on microscope slides with Mowiol and kept at 4°C until usage. Antibodies and markers: anti-Orai2 (Sigma-Aldrich PRS4111), anti-Myc (Millipore), anti-CRT (Abcam ab2907); anti-EEA1 (BD Bioscience), anti-Rab5 (Synaptic Systems), anti-LBPA (kindly donated by D. A. Tehran, C. Montecucco).

Confocal analysis

H4-APPswe, HEK293T or cultured cortical neurons expressing Myc-tagged Orai2 or stained with the specific antibody, were analysed with a Leica SP5 confocal system (DM IRE2) using the WILL white laser line. Co-localization analysis for Orai2 and either CRT, ER-GFP, ER-TQ2, EEA1, Rab5 or LBPA was performed on z-stacks acquired with 0.5 μm steps. For co-localization analyses, green and red channel images were acquired independently, and photomultiplier gain for each channel was adjusted to minimize background noise and saturated pixels and maintained among different set of experiments. Once acquired, images were not modified further. Analyses were carried out on single-plane images using ImageJ plug-ins. Particularly a background ROI was selected, identical for the two channels, and the corresponding backgrounds were subtracted through ImageJ ROI

plug-in. Subsequently, ROIs were designed corresponding to the cell profiles, as defined by the external perimeter of the investigated marker (CRT, ER-GFP, ER-TQ2, EEA1, Rab5, LBPA), and applied as such to the Orai2 channel. The overlap Manders' R and Pearson's coefficients were calculated applying the ImageJ co-localization analysis plug-in.

Preparation of protein extracts and Western blot analysis

H4-APPswe cells, cultured cortical neurons or tissue (cortices and hippocampi) were harvested and treated as follow: cells or tissues were homogenized and solubilized in RIPA buffer (50 mM Tris, 150 mM NaCl, 1% Triton X-100, 0.5% deoxycholic acid, 0.1% SDS, protease inhibitor cocktail, phosphatase inhibitor cocktail, pH 7.5) and incubated on ice for 30 minutes. Un-solubilized material was spun down at 70000 g for 30 minutes at 4°C. Supernatant was collected and protein concentration quantified using a BCA assay kit (EuroClone). Proteins (30-50 μg) for primary cultures; 50-70 μg for brain homogenates) were loaded onto custom made polyacrylamide gels (10 or 12%) and immunoblotted.

WB analyses were carried out with anti-Orai1 (Sigma-Aldrich O8264), anti-Orai2 (Alomone ACC-061), anti-actin (Sigma-Aldrich), anti-alpha-tubulin (Santa Cruz Biotechnology). Immuno-bands were visualized by the chemiluminescence reagent ECL (Amersham, GE Healthcare, UK Ltd) or LiteAblot TURBO (EuroClone) on a Uvitec Mini HD9 (Eppendorf) instrument. Band intensities were analysed by using ImageJ.

Quantitative reverse-transcription polymerase chain reaction (qPCR)

H4-APPswe cells, seeded in 12-well culture plates were transfected with siRNAs. After 48 hours they were washed twice with PBS and total RNA was extracted using the NucleoSpin RNA purification kit (Macherey-Nagel) and then quantified with NanoDrop 2000 (Thermo Scientific). For each sample, 1 μg of total RNA was reverse-transcribed into cDNA using the SuperScript II Reverse Transcriptase (Invitrogen) following the manufacturer's instructions. PCR amplification was performed in an iQ5 Thermal Cycler (BioRad), using SYBR Green Supermix (BioRad) as reagent. For each cDNA, the efficiency of the reaction was estimated with a standard curve by using the cDNA reverse transcript from non-transfected H4-APPswe cells. The transcript of GAPDH, cypA and B2M were used as internal control. The following primers (Invitrogen) were employed:

cypA: 5’-TTCATCTGCACTGCCAAGA-3’ and 5’-TCGAGTTGTCCACAGTCAGC-3’; B2M: 5’-TATCCAGCGTACTCCAAAGA-3’ and 5’-GACAAGTCTGAATGCTCCAC-3’; GAPDH: 5’-CACCATCTTCCAGGAGCGAG-3’ and 5’-TTCACACCCATGACGAACAT-3’; Orai1: 5’-AGTTACTCCGAGGTGATGAGC-3’ and 5’-TAGTCGTGGTCAGCGTCCAG-3’; Orai2 “primer A”: 5’-TGAGCAACATCCACAACCTGA-3’ and 5’- GGGAGGAACTTGATCCAGCAG-3’; Orai2 “primer B”: 5’-GATGGAGAGCCTGAGTTGGC-3’ and 5’- GGTCGATAGGCACGTTAAGC-3’. Data are expressed as percentage ratio change relative to the HPRT1 transcript (mean ± SEM, n = number of wells).

ELISA

Conditioned media from either H4-APPswe or CHO-7PA2 cells were collected and mixed with a 10X solution of phosphatase and protease inhibitors (cOmplete, Mini, protease inhibitor cocktail, Roche; PhosSTOP phosphatase inhibitor cocktail, Roche, in RIPA buffer). Once thoroughly vortexed they were spun at >13000 g for 15 minutes at 4°C to eliminate cell debris; supernatants were collected and stored at -80°C until use. After the removal of the conditioned media, cells were harvested and lysed in RIPA buffer to quantify proteins concentration for loading control. At the moment of performing the ELISA assay, the conditioned media were thawed and loaded into the plate as such. The Wako 290-62601 and the Anaspec #55552 assays were employed where indicated.

Materials

Histamine, ATP, EGTA, PTX, KCl, $CaCl_2$ and digitonin were purchased from Sigma-Aldrich, while CPA and ionomycin from Calbiochem. All other materials were analytical of the highest available grade.

Data analysis

Data were analysed using Origin 8.0 SR6 (OriginLab Corporation, Northampton, MA, USA) and Microsoft Excel 2010 (Microsoft Corporation, Redmond, WA, USA). Values are expressed as

mean ± SEM (*n* = number of independent experiments). Statistical significance was evaluated by unpaired two-tailed Student's *t*-test, **P* < 0.05, ***P* < 0.01, ****P* < 0.001.

REFERENCES

Adunsky, A., et al. 1991 Increased cytosolic free calcium in lymphocytes of Alzheimer patients. Journal of Neuroimmunology 33(2):167-72.

Agostini, M., and C. Fasolato 2016 When, where and how? Focus on neuronal calcium dysfunctions in Alzheimer's Disease. Cell Calcium.

Al-Mousa, F., and F. Michelangeli 2012 Some Commonly Used Brominated Flame Retardants Cause Ca2+-ATPase Inhibition, Beta-Amyloid Peptide Release and Apoptosis in SH-SY5Y Neuronal Cells. Plos One 7(4).

Alberdi, E., et al. 2010 Amyloid beta oligomers induce Ca2+ dysregulation and neuronal death through activation of ionotropic glutamate receptors. Cell Calcium 47(3):264-72.

Alberdi, E., et al. 2013 Ca^{2+}-dependent endoplasmic reticulum stress correlates with astrogliosis in oligomeric amyloid β-treated astrocytes and in a model of Alzheimer's disease. Aging Cell 12(2):292-302.

Albrecht, T., et al. 2015 Fluorescent biosensors illuminate calcium levels whithin defined beta-cell endosome subpopulations. Cell Calcium 57(4):263-74

Albuquerque, E. X., et al. 2009 Mammalian nicotinic acetylcholine receptors: from structure to function. Physiological Reviews 89(1):73-120.

Allen, D. G., J. R. Blinks, and F. G. Prendergast 1977 Aequorin luminescence:relation of light emission to calcium concentration - a calcium-independent component. Science 195:996-998.

Amcheslavsky, A., et al. 2015 Molecular biophysics of Orai store-operated Ca2+ channels. Biophys J 108(2):237-46.

Anderson, S., et al. 1981 Sequence and organization of the human mitochondrial genome. Nature 290(9 April 1981):457-465.

Arispe, N., J. C. Diaz, and O. Simakova 2007 Aβ ion channels. Prospects for treating Alzheimer's disease with Aβ channel blockers. Biochimica et Biophysica Acta 1768(8):1952-65.

Arispe, N., et al. 2010 Polyhistidine peptide inhibitor of the Aβ calcium channel potently blocks the Aβ-induced calcium response in cells. Theoretical modeling suggests a cooperative binding process. Biochemistry 49(36):7847-53.

Baba, Y., et al. 2006 Coupling of STIM1 to store-operated Ca2+ entry through its constitutive and inducible movement in the endoplasmic reticulum. Proc Natl Acad Sci U S A 103(45):16704-9.

Baird, G. S., D. A. Zacharias, and R. Y. Tsien 1999 Circular permutation and receptor insertion within green fluorescent proteins. Proceedings of the National Academy of Sciences of the United States of America 96(20):11241-6.

Bajar, B. T., et al. 2016 A Guide to Fluorescent Protein FRET Pairs. Sensors (Basel) 16(9).

Bandara, S., S. Malmersjo, and T. Meyer 2013 Regulators of calcium homeostasis identified by inference of kinetic model parameters from live single cells perturbed by siRNA. Sci Signal 6(283):ra56.

Bathori, G., et al. 2006 Ca2+-dependent control of the permeability properties of the mitochondrial outer membrane and voltage-dependent anion-selective channel (VDAC). J Biol Chem 281(25):17347-58.

Benfenati, V., et al. 2011 An aquaporin-4/transient receptor potential vanilloid 4 (AQP4/TRPV4) complex is essential for cell-volume control in astrocytes. Proc Natl Acad Sci U S A 108(6):2563-8.

Berna-Erro, A., et al. 2009 STIM2 regulates capacitive Ca2+ entry in neurons and plays a key role in hypoxic neuronal cell death. Sci Signal 2(93):ra67.

Bernardi, P., et al. 1984 Pathway for uncoupler-induced calcium efflux in rat liver mitochondria: inhibition by ruthenium red. Biochemistry 23(8):1645-51.

Berridge, M. J. 1998 Neuronal calcium signaling. Neuron 21(1):13-26.

— 2010 Calcium hypothesis of Alzheimer's disease. Pflügers Archiv 459(3):441-9.

— 2014 Calcium regulation of neural rhythms, memory and Alzheimer's disease. The Journal of physiology 592(Pt 2):281-93.

Berridge, M. J., M. D. Bootman, and H. L. Roderick 2003 Calcium signalling: dynamics, homeostasis and remodelling. Nature Reviews. Molecular Cell Biology 4(7):517-529.

Berridge, M. J., P. Lipp, and M. D. Bootman 2000 The versatility and universality of calcium signalling. Nature Reviews. Molecular Cell Biology 1(1):11-21.

Birnbaum, J. H., et al. 2015 Calcium flux-independent NMDA receptor activity is required for Aβ oligomer-induced synaptic loss. Cell Death & Disease 6.

Bojarski, L., et al. 2009 Presenilin-dependent expression of STIM proteins and dysregulation of capacitative Ca^{2+} entry in familial Alzheimer's disease. Biochimica et Biophysica Acta 1793(6):1050-7.

Bonora, M., et al. 2013 Subcellular calcium measurements in mammalian cells using jellyfish photoprotein aequorin-based probes. Nat Protoc 8(11):2105-18.

Bragadin, M., T. Pozzan, and G. F. Azzone 1979 Kinetics of Ca^{2+} carrier in rat liver mitochondria. Biochemistry 18(26):5972-5978.

Brandman, O., et al. 2007 STIM2 is a feedback regulator that stabilizes basal cytosolic and endoplasmic reticulum Ca^{2+} levels. Cell 131(7):1327-39.

Brini, M. 2008 Calcium-sensitive photoproteins. Methods 46(3):160-6.

Brini, M., and E. Carafoli 2009 Calcium pumps in health and disease. Physiological Reviews 89(4):1341-78.

Brini, M., et al. 1995 Transfected aequorin in the measurement of cytosolic Ca^{2+} concentration ($[Ca^{2+}]_c$): a critical evaluation. The Journal of Biological Chemistry 270:9896-9903.

Brunello, L., et al. 2009 Presenilin-2 dampens intracellular Ca^{2+} stores by increasing Ca^{2+} leakage and reducing Ca^{2+} uptake. Journal of Cellular and Molecular Medicine 13:3358-69.

Brunkan, A. L., and A. M. Goate 2005 Presenilin function and gamma-secretase activity. Journal of Neurochemistry 93(4):769-92.

Caballero, E., et al. 2016 A new procedure for amyloid β oligomers preparation enables the unambiguous testing of their effects on cytosolic and mitochondrial Ca^{2+} entry and cell death in primary neurons. Neuroscience Letters 612:66-73.

Cahalan, M. D. 2009 STIMulating store-operated Ca^{2+} entry. Nature Cell Biology 11(6):669-77.

Calcraft, P. J., et al. 2009 NAADP mobilizes calcium from acidic organelles through two-pore channels. Nature 459(7246):596-600.

Cataldo, A. M., et al. 2000 Endocytic pathway abnormalities precede amyloid beta deposition in sporadic Alzheimer's disease and Down syndrome: differential effects of APOE genotype and presenilin mutations. Am J Pathol 157(1):277-86.

Catterall, W.A. 2000 Structure and regulation of voltage-gated Ca^{2+} channels. Annual Review of Cell and Developmental Biology 16:521-555.

Ceglia, I., et al. 2015 APP intracellular domain-WAVE1 pathway reduces amyloid-beta production. Nat Med 21(9):1054-9.

Chakroborty, S., et al. 2012 Stabilizing ER Ca^{2+} channel function as an early preventative strategy for Alzheimer's disease. PloS One 7(12):e52056.

Chakroborty, S., et al. 2009 Deviant ryanodine receptor-mediated calcium release resets synaptic homeostasis in presymptomatic 3xTg-AD mice. The Journal of Neuroscience 29(30):9458-70.

Chandra, S., et al. 1991 Calcium sequestration in the Golgi apparatus of cultured mammalian cells revealed by laser scanning confocal microscopy and ion microscopy. Journal of Cell Science 100 (Pt 4):747-52.

Chen, T. W., et al. 2013 Ultrasensitive fluorescent proteins for imaging neuronal activity. Nature 499(7458):295-300.

Chen, Y. R., and C. G. Glabe 2006 Distinct early folding and aggregation properties of Alzheimer amyloid-beta peptides A beta 40 and A beta 42 - Stable trimer or tetramer formation by A beta 42. Journal of Biological Chemistry 281(34):24414-24422.

Cheung, K. H., et al. 2010 Gain-of-function enhancement of IP3 receptor modal gating by familial Alzheimer's disease-linked presenilin mutants in human cells and mouse neurons. Science Signaling 3(114):ra22.

Cheung, K. H., et al. 2008 Mechanism of Ca^{2+} disruption in Alzheimer's disease by presenilin regulation of $InsP_3$ receptor channel gating. Neuron 58(6):871-83.

Chyung, J. H., D. M. Raper, and D. J. Selkoe 2005 gamma-secretase exists on the plasma membrane as an intact complex that accepts substrates and effects intramembrane cleavage. Journal of Biological Chemistry 280(6):4383-4392.

Citron, M., et al. 1997 Mutant presenilins of Alzheimer's disease increase production of 42-residue amyloid beta-protein in both transfected cells and transgenic mice. Nature Medicine 3(1):67-72.

Clapham, D. E. 2007 Calcium signaling. Cell 131(6):1047-58.

Coen, K., et al. 2012 Lysosomal calcium homeostasis defects, not proton pump defects, cause endo-lysosomal dysfunction in PSEN-deficient cells. Journal of Cell Biology 198(1):23-35.

Coon, A. L., et al. 1999 L-type calcium channels in the hippocampus and cerebellum of Alzheimer's disease brain tissue. Neurobiology of Aging 20(6):597-603.

Costantini, L. M., et al. 2012 Assessing the tendency of fluorescent proteins to oligomerize under physiologic conditions. Traffic 13(5):643-9.

Crouch, P. J., et al. 2005 Copper-dependent inhibition of human cytochrome c oxidase by a dimeric conformer of amyloid-β_{1-42}. Journal of Neuroscience 25(3):672-9.

Csala, M., G. Banhegyi, and A. Benedetti 2006 Endoplasmic reticulum: a metabolic compartment. FEBS Lett 580(9):2160-5.

De Felice, F. G., et al. 2007 Abeta oligomers induce neuronal oxidative stress through an N-methyl-D-aspartate receptor-dependent mechanism that is blocked by the Alzheimer drug memantine. The Journal of Biological Chemistry 282(15):11590-601.

de la Fuente, S., et al. 2013 Ca2+ homeostasis in the endoplasmic reticulum measured with a new low-Ca2+-affinity targeted aequorin. Cell Calcium 54(1):37-45.

De Mario, A., et al. 2015 The prion protein constitutively controls neuronal store-operated Ca^{2+} entry through Fyn kinase. Frontiers in Cellular Neuroscience 9:416.

De Stefani, D., M. Patron, and R. Rizzuto 2015 Structure and function of the mitochondrial calcium uniporter complex. Biochimica et Biophysica Acta 1853(9):2006-11.

De Stefani, D., et al. 2011 A forty-kilodalton protein of the inner membrane is the mitochondrial calcium uniporter. Nature.

De Strooper, B. 2007 Loss-of-function presenilin mutations in Alzheimer disease. Talking Point on the role of presenilin mutations in Alzheimer disease. EMBO Report 8(2):141-6.

De Strooper, B., and W. Annaert 2010 Novel Research Horizons for Presenilins and gamma-Secretases in Cell Biology and Disease. Annual Review of Cell and Developmental Biology, Vol 26 26:235-260.

De Strooper, B., T. Iwatsubo, and M. S. Wolfe 2012 Presenilins and gamma-Secretase: Structure, Function, and Role in Alzheimer Disease. Cold Spring Harbor Perspectives in Medicine 2(1).

De Strooper, B., and E. Karran 2016 The Cellular Phase of Alzheimer's Disease. Cell 164(4):603-15.

Decker, H., et al. 2010 Amyloid-β peptide oligomers disrupt axonal transport through an NMDA receptor-dependent mechanism that is mediated by glycogen synthase kinase 3β in primary cultured hippocampal neurons. Journal of Neuroscience 30(27):9166-71.

Del Prete, D., F. Checler, and M. Chami 2014 Ryanodine receptors: physiological function and deregulation in Alzheimer disease. Molecular Neurodegeneration 9:21.

Demuro, A., et al. 2005 Calcium dysregulation and membrane disruption as a ubiquitous neurotoxic mechanism of soluble amyloid oligomers. The Journal of Biological Chemistry 280(17):17294-300.

Demuro, A., and I. Parker 2013 Cytotoxicity of intracellular aβ42 amyloid oligomers involves Ca^{2+} release from the endoplasmic reticulum by stimulated production of inositol trisphosphate. The Journal of Neuroscience 33(9):3824-33.

Di Virgilio, F., C. Fasolato, and T. H. Steinberg 1988 Inhibitors of membrane transport system for organic anions block fura-2 excretion from PC12 and N2A cells. Biochem J 256(3):959-63.

Drago, I., et al. 2008 Calcium dynamics in the peroxisomal lumen of living cells. The Journal of Biological Chemistry 283(21):14384-90.

Dziewczapolski, G., et al. 2009 Deletion of the alpha7 nicotinic acetylcholine receptor gene improves cognitive deficits and synaptic pathology in a mouse model of Alzheimer's disease. Journal of Neuroscience 29(27):8805-15.

Edmonds, E. C., et al. 2015 Subtle Cognitive Decline and Biomarker Staging in Preclinical Alzheimer's Disease. Journal of Alzheimers Disease 47(1):231-242.

Ertekin-Taner, N. 2007 Genetics of Alzheimer's disease: a centennial review. Neurologic Clinics 25(3):611-67, v.

Espana, J., et al. 2010 β-Amyloid Disrupts Activity-Dependent Gene Transcription Required for Memory through the CREB Coactivator CRTC1. Journal of Neuroscience 30(28):9402-9410.

Facchinetti, F., et al. 2006 Nimodipine selectively stimulates β-amyloid 1-42 secretion by a mechanism independent of calcium influx blockage. Neurobiology of Aging 27(2):218-227.

Fasolato, C., B. Innocenti, and T. Pozzan 1994 Receptor-activated Ca^{2+} influx: how many mechanisms for how many channels? Trends in Pharmacological Sciences 15:77-83.

Fedrizzi, L., et al. 2008 Interplay of the Ca2+-binding protein dream with presenilin in neuronal Ca2+ signaling. The Journal of Biological Chemistry.

Feng, X., et al. 2014 Drosophila TRPML forms PI(3,5)P2-activated cation channels in both endolysosomes and plasma membrane. J Biol Chem 289(7):4262-72.

Ferreiro, E., et al. 2006 An endoplasmic-reticulum-specific apoptotic pathway is involved in prion and amyloid-β peptides neurotoxicity. Neurobiology of Disease 23(3):669-78.

Feske, S., et al. 2006 A mutation in Orai1 causes immune deficiency by abrogating CRAC channel function. Nature 441(7090):179-85.

Filadi, R., et al. 2015 Mitofusin 2 ablation increases endoplasmic reticulum-mitochondria coupling. Proceedings of the National Academy of Sciences of the United States of America 112(17):E2174-81.

— 2016 Presenilin 2 Modulates Endoplasmic Reticulum-Mitochondria Coupling by Tuning the Antagonistic Effect of Mitofusin 2. Cell reports 15(10):2226-38.

Florean, C., et al. 2008 High content analysis of gamma-secretase activity reveals variable dominance of presenilin mutations linked to familial Alzheimer's disease. Biochimica et Biophysica Acta 1783(8):1551-60.

Fontana, R., et al. 2017 Early hippocampal hyperexcitability in PS2APP mice: role of mutant PS2 and APP. Neurobiol Aging 50:64-76.

Forette, F., et al. 2002 The prevention of dementia with antihypertensive treatment. Archives of Internal Medicine 162(18):2046-2052.

Forstl, H., and A. Kurz 1999 Clinical features of Alzheimer's disease. European Archives of Psychiatry and Clinical Neuroscience 249(6):288-290.

Foskett, J. K., et al. 2007 Inositol trisphosphate receptor Ca^{2+} release channels. Physiological Reviews 87(2):593-658.

Fukumori, A., et al. 2010 Three-amino acid spacing of presenilin endoproteolysis suggests a general stepwise cleavage of gamma-secretase-mediated intramembrane proteolysis. J Neurosci 30(23):7853-62.

Gan, K. J., and M. A. Silverman 2015 Dendritic and axonal mechanisms of Ca2+ elevation impair BDNF transport in Abeta oligomer-treated hippocampal neurons. Molecular Biology of the Cell 26(6):1058-71.

Gant, J. C., et al. 2006 Early and simultaneous emergence of multiple hippocampal biomarkers of aging is mediated by Ca^{2+}-induced Ca^{2+} release. Journal of Neuroscience 26(13):3482-90.

Giacomello, M., et al. 2005 Reduction of Ca^{2+} stores and capacitative Ca^{2+} entry is associated with the familial Alzheimer's disease presenilin-2 T122R mutation and anticipates the onset of dementia. Neurobiology of Disease 18(3):638-648.

Goedert, M., and M. G. Spillantini 2006 A century of Alzheimer's disease. Science 314(5800):777-81.

Green, K. N., and F. M. LaFerla 2008 Linking calcium to Abeta and Alzheimer's disease. Neuron 59(2):190-4.

Greotti, E., et al. 2016 Characterization of the ER-Targeted Low Affinity Ca(2+) Probe D4ER. Sensors (Basel) 16(9).

Griesbeck, Oliver, et al. 2001 Reducing the environmental sensitivity of yellow fluorescent protein. Mechanism and applications. The Journal of Biological Chemistry 276(31):29188–29194.

Grigoriev, I., et al. 2008 STIM1 is a MT-plus-end-tracking protein involved in remodeling of the ER. Curr Biol 18(3):177-82.

Grynkiewicz, G., M. Poenie, and R. Y. Tsien 1985 A new generation of Ca^{2+} indicators with greatly improved fluorescence properties. The Journal of Biological Chemistry 260:3440-3450.

Guo, X., et al. 2016 Rab5 and its effector FHF contribute to neuronal polarity through dynein-dependent retrieval of somatodendritic proteins from the axon. Proc Natl Acad Sci U S A 113(36):E5318-27.

Haas, L. T., et al. 2016 Metabotropic glutamate receptor 5 couples cellular prion protein to intracellular signalling in Alzheimer's disease. Brain 139(Pt 2):526-46.

Haass, C., and D. J. Selkoe 2007 Soluble protein oligomers in neurodegeneration: lessons from the Alzheimer's amyloid β-peptide. Nature Reviews. Molecular Cell Biology 8(2):101-12.

Hanson, J. E., et al. 2015 Altered GluN2B NMDA receptor function and synaptic plasticity during early pathology in the PS2APP mouse model of Alzheimer's disease. Neurobiology of Disease 74:254-62.

Hansson, C. A., et al. 2004 Nicastrin, presenilin, APH-1, and PEN-2 form active γ-secretase complexes in mitochondria. The Journal of Biological Chemistry 279(49):51654-51660.

Hansson Petersen, C. A., et al. 2008 The amyloid beta-peptide is imported into mitochondria via the TOM import machinery and localized to mitochondrial cristae. Proc Natl Acad Sci U S A 105(35):13145-50.

Hardy, J., and D. Allsop 1991 Amyloid deposition as the central event in the aetiology of Alzheimer's disease. Trends in Pharmacological Sciences 12(10):383-8.

Hardy, J., and D. J. Selkoe 2002 The amyloid hypothesis of Alzheimer's disease: progress and problems on the road to therapeutics. Science 297(5580):353-356.

Harraz, O. F., and C. Altier 2014 STIM1-mediated bidirectional regulation of Ca(2+) entry through voltage-gated calcium channels (VGCC) and calcium-release activated channels (CRAC). Front Cell Neurosci 8:43.

Hedskog, L., et al. 2013 Modulation of the endoplasmic reticulum-mitochondria interface in Alzheimer's disease and related models. Proceedings of the National Academy of Sciences of the United States of America 110(19):7916-21.

Henze, K., and W. Martin 2003 Evolutionary biology: essence of mitochondria. Nature 426(6963):127-8.

Hernandez, C. M., et al. 2010 Loss of α_7 nicotinic receptors enhances β-amyloid oligomer accumulation, exacerbating early-stage cognitive decline and septohippocampal pathology in a mouse model of Alzheimer's disease. Journal of Neuroscience 30(7):2442-53.

Herreman, A., et al. 2000 Total inactivation of γ-secretase activity in presenilin-deficient embryonic stem cells. Nature Cell Biology 2(7):461-462.

Honarnejad, K., and J. Herms 2012 Presenilins: role in calcium homeostasis. International Journal of Biochemistry & Cell Biology 44(11):1983-6.

Hooper, R., B. S. Rothberg, and J. Soboloff 2014 Neuronal STIMulation at rest. Science Signaling 7(335):pe18.

Horikawa, K., et al. 2010 Spontaneous network activity visualized by ultrasensitive Ca(2+) indicators, yellow Cameleon-Nano. Nat Methods 7(9):729-32.

Hoth, M., and B. A. Niemeyer 2013 The neglected CRAC proteins: Orai2, Orai3, and STIM2. Curr Top Membr 71:237-71.

Hou, X., et al. 2012 Crystal structure of the calcium release-activated calcium channel Orai. Science 338(6112):1308-13.

Inayama, M., et al. 2015 Orai1-Orai2 complex is involved in store-operated calcium entry in chondrocyte cell lines. Cell Calcium 57(5-6):337-47.

Inouye, S., et al. 1985 Cloning and sequence analysis of cDNA for the luminescent protein aequorin. Proceedings of the National Academy of Sciences of the United States of America 82(10):3154-3158.

Jaworska, A., et al. 2013 Analysis of calcium homeostasis in fresh lymphocytes from patients with sporadic Alzheimer's disease or mild cognitive impairment. Biochim Biophys Acta 1833(7):1692-9.

Jayadev, S., et al. 2010 Alzheimer's disease phenotypes and genotypes associated with mutations in presenilin 2. Brain 133:1143-1154.

Joseph, S. K., et al. 1997 Membrane insertion, glycosylation, and oligomerization of inositol trisphosphate receptors in a cell-free translation system. J Biol Chem 272(3):1579-88.

Jurgensen, S., et al. 2011 Activation of D1/D5 dopamine receptors protects neurons from synapse dysfunction induced by amyloid-β oligomers. The Journal of Biological Chemistry 286(5):3270-6.

Kaether, C., et al. 2006 Amyloid precursor protein and Notch intracellular domains are generated after transport of their precursors to the cell surface. Traffic 7(4):408-15.

Kapur, A., et al. 1998 L-Type calcium channels are required for one form of hippocampal mossy fiber LTP. Journal of Neurophysiology 79(4):2181-90.

Kar, P., et al. 2012 Different agonists recruit different stromal interaction molecule proteins to support cytoplasmic Ca2+ oscillations and gene expression. Proc Natl Acad Sci U S A 109(18):6969-74.

Karran, E., M. Mercken, and B. De Strooper 2011 The amyloid cascade hypothesis for Alzheimer's disease: an appraisal for the development of therapeutics. Nature Reviews Drug Discovery 10(9):698-U1600.

Khosravani, H., et al. 2008 Prion protein attenuates excitotoxicity by inhibiting NMDA receptors. Journal of Cell Biology 181(3):551-565.

Kim, J., et al. 2007 Biogenesis of gamma-secretase early in the secretory pathway. Journal of Cell Biology 179(5):951-963.

Kim, J., et al. 2014 Beta-amyloid oligomers activate apoptotic BAK pore for cytochrome *c* release. Biophysical Journal 107(7):1601-8.

Kimberly, W. T., et al. 2000 The transmembrane aspartates in presenilin 1 and 2 are obligatory for gamma-secretase activity and amyloid beta-protein generation. Journal of Biological Chemistry 275(5):3173-3178.

Kipanyula, M. J., et al. 2012a Ca^{2+} dysregulation in neurons from transgenic mice expressing mutant presenilin 2. Aging Cell 11(5):885-893.

Kito, H., et al. 2015 Regulation of store-operated Ca2+ entry activity by cell cycle dependent up-regulation of Orai2 in brain capillary endothelial cells. Biochem Biophys Res Commun 459(3):457-62.

Kraft, R. 2015 STIM and ORAI proteins in the nervous system. Channels:235-243.

Krieger-Brauer, H. I., and M. Gratzl 1983 Effects of monovalent and divalent cations on Ca2+ fluxes across chromaffin secretory membrane vesicles. J Neurochem 41(5):1269-76.

Kurup, P., et al. 2010 Aβ-mediated NMDA receptor endocytosis in Alzheimer's disease involves ubiquitination of the tyrosine phosphatase STEP61. Journal of Neuroscience 30(17):5948-57.

Lacruz, R. S., and S. Feske 2015 Diseases caused by mutations in ORAI1 and STIM1. Ann N Y Acad Sci 1356:45-79.

LaFerla, F. M. 2010 Pathways linking A beta and tau pathologies. Biochemical Society Transactions 38:993-995.

LaFerla, F. M., K. N. Green, and S. Oddo 2007 Intracellular amyloid-beta in Alzheimer's disease. Nature Reviews Neuroscience 8(7):499-509.

Lalonde, J., G. Saia, and G. Gill 2014 Store-operated calcium entry promotes the degradation of the transcription factor Sp4 in resting neurons. Science Signaling 7(328):ra51.

Lambert, M. P., et al. 1998 Diffusible, nonfibrillar ligands derived from Abeta1-42 are potent central nervous system neurotoxins. Proceedings of the National Academy of Sciences of the United States of America 95(11):6448-53.

Landfield, P. W. 1994 Increased hippocampal Ca^{2+} channel activity in brain aging and dementia. Hormonal and pharmacologic modulation. Annals of the New York Academy of Sciences 747:351-64.

Lauren, J., et al. 2009 Cellular prion protein mediates impairment of synaptic plasticity by amyloid-β oligomers. Nature 457(7233):1128-U84.

Lazzari, C., et al. 2015 Aβ42 oligomers selectively disrupt neuronal calcium release. Neurobiology of Aging 36(2):877-885.

Leal, N. S., et al. 2016 Mitofusin-2 knockdown increases ER-mitochondria contact and decreases amyloid beta-peptide production. Journal of Cellular and Molecular Medicine.

Lee, J. H., et al. 2015 Presenilin 1 Maintains Lysosomal Ca^{2+} Homeostasis via TRPML1 by Regulating vATPase-Mediated Lysosome Acidification. Cell Reports 12(9):1430-44.

Lee, J. H., et al. 2010 Lysosomal proteolysis and autophagy require presenilin 1 and are disrupted by Alzheimer-related PS1 mutations. Cell 141(7):1146-58.

Lee, L., P. Kosuri, and O. Arancio 2014 Picomolar amyloid-β peptides enhance spontaneous astrocyte calcium transients. Journal of Alzheimer's Disease 38(1):49-62.

Leissring, M.A., et al. 2000 Capacitative calcium entry deficits and elevated luminal calcium content in mutant presenilin-1 knockin mice. Journal of Cell Biology 149(4):793-798.

Lesne, S. E. 2014 Toxic oligomer species of amyloid-beta in Alzheimer's disease, a timing issue. Swiss medical weekly 144:w14021.

Lesne, S. E., et al. 2013 Brain amyloid-β oligomers in ageing and Alzheimer's disease. Brain 136(Pt 5):1383-98.

Lesne, S., et al. 2006 A specific amyloid-beta protein assembly in the brain impairs memory. Nature 440(7082):352-7.

Lewis, R. S. 2007 The molecular choreography of a store-operated calcium channel. Nature 446(7133):284-7.

Li, Z., et al. 2007 Mapping the interacting domains of STIM1 and Orai1 in Ca2+ release-activated Ca2+ channel activation. J Biol Chem 282(40):29448-56.

Lim, D., et al. 2016 Calcium signalling toolkits in astrocytes and spatio-temporal progression of Alzheimer's disease. Current Alzheimer Research 13(4):359-69.

Liou, J., et al. 2007 Live-cell imaging reveals sequential oligomerization and local plasma membrane targeting of stromal interaction molecule 1 after Ca^{2+} store depletion. Proceedings of the National Academy of Sciences of the United States of America 104(22):9301-6.

Liou, J., et al. 2005 STIM is a Ca^{2+} sensor essential for Ca^{2+}-store-depletion-triggered Ca^{2+} influx. Current Biology 15(13):1235-41.

Lissandron, V., et al. 2010 Unique characteristics of Ca^{2+} homeostasis of the trans-Golgi compartment. Proceedings of the National Academy of Sciences of the United States of America 107(20):9198-203.

Liu, Y. T., et al. 2007 NMDA receptor subunits have differential roles in mediating excitotoxic neuronal death both in vitro and in vivo. Journal of Neuroscience 27(11):2846-2857.

Llinas, R., J. R. Blinks, and C. Nicholson 1972 Calcium transient in presynaptic terminal of squid giant synapse: detection with aequorin. Science 176(4039):1127-9.

Lombardo, S., and U. Maskos 2015 Role of the nicotinic acetylcholine receptor in Alzheimer's disease pathology and treatment. Neuropharmacology 96(Pt B):255-62.

Ma, Q. H., et al. 2008 A TAG1-APP signalling pathway through Fe65 negatively modulates neurogenesis. Nature Cell Biology 10(3):283-U29.

Mahapatra, N. R., et al. 2004 A dynamic pool of calcium in catecholamine storage vesicles. Exploration in living cells by a novel vesicle-targeted chromogranin A-aequorin chimeric photoprotein. The Journal of Biological Chemistry 279(49):51107-21.

Manczak, M., et al. 2006 Mitochondria are a direct site of Aβ accumulation in Alzheimer's disease neurons: implications for free radical generation and oxidative damage in disease progression. Human Molecular Genetics 15(9):1437-49.

Mank, M., et al. 2008 A genetically encoded calcium indicator for chronic in vivo two-photon imaging. Nature Methods 5(9):805-11.

Marciani, D. J. 2016 A retrospective analysis of the Alzheimer's disease vaccine progress - The critical need for new development strategies. Journal of Neurochemistry 137(5):687-700.

Martell, J. D., et al. 2012 Engineered ascorbate peroxidase as a genetically encoded reporter for electron microscopy. Nat Biotechnol 30(11):1143-8.

McCarthy, J. V., C. Twomey, and P. Wujek 2009 Presenilin-dependent regulated intramembrane proteolysis and gamma-secretase activity. Cellular and Molecular Life Sciences 66(9):1534-1555.

McLarnon, J. G., et al. 2005 Perturbations in calcium-mediated signal transduction in microglia from Alzheimer's disease patients. Journal of Neuroscience Research 81(3):426-35.

Meckler, X., and F. Checler 2016 Presenilin 1 and Presenilin 2 Target gamma-Secretase Complexes to Distinct Cellular Compartments. J Biol Chem 291(24):12821-37.

Meldolesi, J., and T. Pozzan 1998 The endoplasmic reticulum Ca^{2+} store: a view from the lumen. Trends in Biochemical Sciences 23:10-14.

Mercer, J. C., et al. 2006 Large store-operated calcium selective currents due to co-expression of Orai1 or Orai2 with the intracellular calcium sensor, Stim1. J Biol Chem 281(34):24979-90.

Michikawa, T., et al. 1999 Calmodulin mediates calcium-dependent inactivation of the cerebellar type 1 inositol 1,4,5-trisphosphate receptor. Neuron 23(4):799-808.

Minano-Molina, A. J., et al. 2011 Soluble oligomers of amyloid-β peptide disrupt membrane trafficking of α-amino-3-hydroxy-5-methylisoxazole-4-propionic acid receptor contributing to early synapse dysfunction. The Journal of Biological Chemistry 286(31):27311-21.

Minta, A., J. P. Kao, and R. Y. Tsien 1989 Fluorescent indicators for cytosolic calcium based on rhodamine and fluorescein chromophores. The Journal of Biological Chemistry 264(14):8171-8.

Mitchell, K. J., et al. 2001 Dense core secretory vesicles revealed as a dynamic Ca^{2+} store in neuroendocrine cells with a vesicle-associated membrane protein aequorin chimaera. The Journal of Cell Biology 155(1):41-51.

Miyawaki, A., et al. 1999 Dynamic and quantitative Ca^{2+} measurements using improved cameleons. Proceedings of the National Academy of Sciences of the United States of America 96:2135-2140.

Miyawaki, A., et al. 1997 Fluorescent indicators for Ca^{2+} based on green fluorescent proteins and calmodulin. Nature 388:882-887.

Moccia, F., et al. 2015 Stim and Orai proteins in neuronal Ca^{2+} signaling and excitability. Frontiers in Cellular Neuroscience 9:153.

Muik, M., et al. 2012 Ca(2+) release-activated Ca(2+) (CRAC) current, structure, and function. Cell Mol Life Sci 69(24):4163-76.

Murray, D. H., et al. 2016 An endosomal tether undergoes an entropic collapse to bring vesicles together. Nature 537(7618):107-111.

Nagai, T., et al. 2001 Circularly permuted green fluorescent proteins engineered to sense Ca^{2+}. Proceedings of the National Academy of Sciences of the United States of America 98(6):3197-3202.

Nagai, T., et al. 2004 Expanded dynamic range of fluorescent indicators for Ca^{2+} by circularly permuted yellow fluorescent proteins. Proceedings of the National Academy of Sciences of the United States of America 101(29):10554-10559.

Nakai, J., M. Ohkura, and K. Imoto 2001 A high signal-to-noise Ca^{2+} probe composed of a single green fluorescent protein. Nature Biotechnology 19(2):137-141.

Nguyen, N., et al. 2013 STIM1 participates in the contractile rhythmicity of HL-1 cells by moderating T-type Ca(2+) channel activity. Biochim Biophys Acta 1833(6):1294-303.

Nimmrich, V., et al. 2008 Amyloid beta oligomers (A beta(1-42) globulomer) suppress spontaneous synaptic activity by inhibition of P/Q-type calcium currents. The Journal of Neuroscience 28(4):788-97.

Oules, B., et al. 2012 Ryanodine receptor blockade reduces amyloid-β load and memory impairments in Tg2576 mouse model of Alzheimer disease. The Journal of Neuroscience 32(34):11820-34.

Ozmen, L., et al. 2009 Expression of transgenic APP mRNA is the key determinant for beta-amyloid deposition in PS2APP transgenic mice. Neuro-degenerative Diseases 6(1-2):29-36.

Palmer, A. E., and R. Y. Tsien 2006 Measuring calcium signaling using genetically targetable fluorescent indicators. Nature Protocols 1(3):1057-65.

Parihar, M. S., and T. Hemnani 2004 Alzheimer's disease pathogenesis and therapeutic interventions. Journal of Clinical Neuroscience 11(5):456-467.

Park, C. Y., A. Shcheglovitov, and R. Dolmetsch 2010 The CRAC channel activator STIM1 binds and inhibits L-type voltage-gated calcium channels. Science 330(6000):101-5.

Patel, S., and R. Docampo 2010 Acidic calcium stores open for business: expanding the potential for intracellular Ca^{2+} signaling. Trends in Cell Biology 20(5):277-86.

Patel, S., S.K. Joseph, and A.P. Thomas 1999 Molecular properties of inositol 1,4,5-trisphosphate receptors. Cell Calcium 25(3):247-264.

Patron, M., et al. 2014 MICU1 and MICU2 finely tune the mitochondrial Ca^{2+} uniporter by exerting opposite effects on MCU activity. Molecular Cell 53(5):726-37.

Paula-Lima, A. C., J. Brito-Moreira, and S. T. Ferreira 2013 Deregulation of excitatory neurotransmission underlying synapse failure in Alzheimer's disease. Journal of Neurochemistry 126(2):191-202.

Pavlov, P. F., et al. 2011 Mitochondrial γ-secretase participates in the metabolism of mitochondria-associated amyloid precursor protein. Faseb Journal 25(1):78-88.

Perl, D. P. 2010 Neuropathology of Alzheimer's Disease. Mount Sinai Journal of Medicine 77(1):32-42.

Perrin, R. J., A. M. Fagan, and D. M. Holtzman 2009 Multimodal techniques for diagnosis and prognosis of Alzheimer's disease. Nature 461(7266):916-922.

Persechini, A., J. A. Lynch, and V. A. Romoser 1997 Novel fluorescent indicator proteins for monitoring free intracellular Ca^{2+}. Cell Calcium 22:209-216.

Pierrot, N., et al. 2004 Intraneuronal amyloid-beta1-42 production triggered by sustained increase of cytosolic calcium concentration induces neuronal death. J Neurochem 88(5):1140-50.

Pietrobon, D., F. Di Virgilio, and T. Pozzan 1990 Structural and functional aspects of calcium homeostasis in eukaryotic cells. European Journal of Biochemistry 193:599-622.

Pirttimaki, T. M., et al. 2013 α7 Nicotinic receptor-mediated astrocytic gliotransmitter release: Aβ effects in a preclinical Alzheimer's mouse model. PloS One 8(11):e81828.

Pizzo, P., et al. 2001 Role of capacitative calcium entry on glutamate-induced calcium influx in type-I rat cortical astrocytes. Journal of Neurochemistry 79(1):98-109.

Pizzo, P., et al. 2012 Mitochondrial Ca^{2+} homeostasis: mechanism, role, and tissue specificities. Pflugers Archiv : European journal of physiology 464(1):3-17.

Pizzo, P., et al. 2011 Ca^{2+} signalling in the Golgi apparatus. Cell calcium 50(2):184-92.

Podor, B., et al. 2015 Comparison of genetically encoded calcium indicators for monitoring action potentials in mammalian brain by two-photon excitation fluorescence microscopy. Neurophotonics 2(2):021014.

Pozzan, T., et al. 1994 Molecular and cellular physiology of intracellular calcium stores. Physiological Reviews 74(3):595-636.

Putney, J.W., Jr., and C.M. Ribeiro 2000 Signaling pathways between the plasma membrane and endoplasmic reticulum calcium stores. Cellular and Molecular Life Sciences 57(8-9):1272-1286.

Puzzo, D., et al. 2015 The Keystone of Alzheimer Pathogenesis Might Be Sought in Aβ Physiology. Neuroscience 307:26-36.

Raffaello, A., et al. 2013 The mitochondrial calcium uniporter is a multimer that can include a dominant-negative pore-forming subunit. EMBO J 32(17):2362-76.

Rapizzi, E., et al. 2002 Recombinant expression of the voltage-dependent anion channel enhances the transfer of Ca^{2+} microdomains to mitochondria. Journal of Cell Biology 159(4):613-624.

Raychaudhury, B., et al. 2006 Peroxisome is a reservoir of intracellular calcium. Biochimica et Biophysica Acta 1760(7):989-92.

Reese, L. C., and G. Taglialatela 2011 A role for calcineurin in Alzheimer's disease. Current Neuropharmacology 9(4):685-92.

Resende, R., et al. 2008 Neurotoxic effect of oligomeric and fibrillar species of amyloid-beta peptide 1-42: involvement of endoplasmic reticulum calcium release in oligomer-induced cell death. Neuroscience 155(3):725-37.

Rhein, V., et al. 2009 Amyloid-beta and tau synergistically impair the oxidative phosphorylation system in triple transgenic Alzheimer's disease mice. Proceedings of the National Academy of Sciences of the United States of America 106(47):20057-62.

Richards, J. G., et al. 2003 PS2APP transgenic mice, coexpressing hPS2mut and hAPPswe, show age-related cognitive deficits associated with discrete brain amyloid deposition and inflammation. The Journal of Neuroscience 23(26):8989-9003.

Rizzuto, R., et al. 1993 Microdomains with high Ca^{2+} close to IP_3-sensitive channels that are sensed by neighboring mitochondria. Science 262(5134):744-747.

Rizzuto, R., W. Carrington, and R. A. Tuft 1998 Digital imaging microscopy of living cells. Trends in Cell Biology 8:288-292.

Rizzuto, R., and T. Pozzan 2006 Microdomains of intracellular Ca^{2+}: molecular determinants and functional consequences. Physiological Reviews 86(1):369-408.

Rizzuto, R., et al. 1992 Rapid changes of mitochondrial Ca^{2+} revealed by specifically targeted recombinant aequorin. Nature 358(6384):325-327.

Roderick, H. L., and M. D. Bootman 2003 Bi-directional signalling from the InsP3 receptor: regulation by calcium and accessory factors. Biochem Soc Trans 31(Pt 5):950-3.

Rodriguez-Garcia, A., et al. 2014 GAP, an aequorin-based fluorescent indicator for imaging Ca2+ in organelles. Proc Natl Acad Sci U S A 111(7):2584-9.

Ronicke, R., et al. 2011 Early neuronal dysfunction by amyloid β oligomers depends on activation of NR2B-containing NMDA receptors. Neurobiology of Aging 32(12):2219-2228.

Roos, J., et al. 2005 STIM1, an essential and conserved component of store-operated Ca^{2+} channel function. Journal of Cell Biology 169(3):435-45.

Rudolf, R., et al. 2003 Looking forward to seeing calcium. Nature Reviews. Molecular Cell Biology 4(7):579-586.

Rush, T., and A. Buisson 2014 Reciprocal disruption of neuronal signaling and Abeta production mediated by extrasynaptic NMDA receptors: a downward spiral. Cell and Tissue Research 356(2):279-86.

Rutter, G.A., C. Fasolato, and R. Rizzuto 1998 Calcium and organelles: a two-sided story. Biochemical and Biophysical Research Communications 253(3):549-557.

Sabbioni, S., et al. 1997 GOK: a gene at 11p15 involved in rhabdomyosarcoma and rhabdoid tumor development. Cancer Res 57(20):4493-7.

Saftig, P., and J. Klumperman 2009 Lysosome biogenesis and lysosomal membrane proteins: trafficking meets function. Nature Reviews. Molecular Cell Biology 10(9):623-635.

Sannerud, R., et al. 2016 Restricted Location of PSEN2/gamma-Secretase Determines Substrate Specificity and Generates an Intracellular Abeta Pool. Cell 166(1):193-208.

Scheenen, W. J. J. M., et al. 1998 Ca^{2+} depletion from granules inhibits exocytosis - A study with insulin-secreting cells. Journal of Biological Chemistry 273(30):19002-19008.

Scheuner, D., et al. 1996 Secreted amyloid beta-protein similar to that in the senile plaques of Alzheimer's disease is increased in vivo by the presenilin 1 and 2 and APP mutations linked to familial Alzheimer's disease. Nature Medicine 2(8):864-70.

Schreij, A. M., E. A. Fon, and P. S. McPherson 2016 Endocytic membrane trafficking and neurodegenerative disease. Cell Mol Life Sci 73(8):1529-45.

Scott, H. L., et al. 2002 Aberrant expression of the glutamate transporter excitatory amino acid transporter 1 (EAAT1) in Alzheimer's disease. Journal of Neuroscience 22(3).

Seidler, N. W., et al. 1989 Cyclopiazonic acid is a specific inhibitor of the Ca2+-ATPase of sarcoplasmic reticulum. J Biol Chem 264(30):17816-23.

Selkoe, D. J., and J. Hardy 2016 The amyloid hypothesis of Alzheimer's disease at 25years. Embo Molecular Medicine 8(6):595-608.

Sevigny, J., et al. 2016 Amyloid PET Screening for Enrichment of Early-Stage Alzheimer Disease Clinical Trials Experience in a Phase 1b Clinical Trial. Alzheimer Disease & Associated Disorders 30(1):1-7.

Shaner, N. C., P. A. Steinbach, and R. Y. Tsien 2005 A guide to choosing fluorescent proteins. Nat Methods 2(12):905-9.

Shen, J. 2014 Function and Dysfunction of Presenilin. Neurodegenerative Diseases 13(2-3):61-63.

Shen, J., and J. Wu 2015 Nicotinic Cholinergic Mechanisms in Alzheimer's Disease. International Review of Neurobiology 124:275-92.

Shilling, D., et al. 2012 Lack of evidence for presenilins as endoplasmic reticulum Ca^{2+} leak channels. The Journal of Biological Chemistry.

Shilling, D., et al. 2014 Suppression of $InsP_3$ receptor-mediated Ca^{2+} signaling alleviates mutant presenilin-linked familial Alzheimer's disease pathogenesis. Journal of Neuroscience 34(20):6910-23.

Shim, A. H., L. Tirado-Lee, and M. Prakriya 2015 Structural and functional mechanisms of CRAC channel regulation. J Mol Biol 427(1):77-93.

Shimojo, M., et al. 2007 Decreased A beta secretion by cells expressing familial Alzheimer's disease-linked mutant presenilin 1. Neuroscience Research 57(3):446-453.

Shmigol, A., et al. 1994 Different properties of caffeine-sensitive Ca^{2+} stores in peripheral and central mammalian neurones. Pflügers Archiv 426(1-2):174-176.

Shuttleworth, T. J. 2012 STIM and Orai proteins and the non-capacitative ARC channels. Front Biosci (Landmark Ed) 17:847-60.

Simakova, O., and N. J. Arispe 2006 Early and late cytotoxic effects of external application of the Alzheimer's Abeta result from the initial formation and function of Abeta ion channels. Biochemistry 45(18):5907-15.

Smith, I. F., et al. 2002 Ca^{2+} stores and capacitative Ca^{2+} entry in human neuroblastoma (SH- SY5Y) cells expressing a familial Alzheimer's disease presenilin-1 mutation. Brain Research 949(1-2):105-11.

Sokolov, Y., et al. 2006 Soluble amyloid oligomers increase bilayer conductance by altering dielectric structure. The Journal of General Physiology 128(6):637-47.

Stathopulos, P. B., and M. Ikura 2010 Partial unfolding and oligomerization of stromal interaction molecules as an initiation mechanism of store operated calcium entry. Biochem Cell Biol 88(2):175-83.

Stathopulos, P. B., L. Zheng, and M. Ikura 2009 Stromal interaction molecule (STIM) 1 and STIM2 calcium sensing regions exhibit distinct unfolding and oligomerization kinetics. J Biol Chem 284(2):728-32.

Stathopulos, P. B., et al. 2008 Structural and mechanistic insights into STIM1-mediated initiation of store-operated calcium entry. Cell 135(1):110-22.

Stieren, E., et al. 2010 FAD mutations in amyloid precursor protein do not directly perturb intracellular calcium homeostasis. PLoS One 5(8):e11992.

Stutzmann, G. E., et al. 2006 Enhanced ryanodine receptor recruitment contributes to Ca^{2+} disruptions in young, adult, and aged Alzheimer's disease mice. The Journal of Neuroscience 26(19):5180-9.

Sun, L., et al. 2015 Structural basis of human gamma-secretase assembly. Proc Natl Acad Sci U S A 112(19):6003-8.

Sun, S. Y., et al. 2014 Reduced Synaptic STIM2 Expression and Impaired Store-Operated Calcium Entry Cause Destabilization of Mature Spines in Mutant Presenilin Mice. Neuron 82(1):79-93.

Supnet, C., and I. Bezprozvanny 2010 Neuronal calcium signaling, mitochondrial dysfunction, and Alzheimer's disease. Journal of Alzheimer's Disease 20 Suppl 2:S487-98.

— 2011 Presenilins function in ER calcium leak and Alzheimer's disease pathogenesis. Cell Calcium 50(3):303-9.

Supnet, C., et al. 2010 Up-regulation of the type 3 ryanodine receptor is neuroprotective in the TgCRND8 mouse model of Alzheimer's disease. Journal of Neurochemistry 112(2):356-65.

Suzuki, J., et al. 2014 Imaging intraorganellar Ca2+ at subcellular resolution using CEPIA. Nat Commun 5:4153.

Thastrup, O., et al. 1990 Thapsigargin, a tumor promoter, discharges intracellular Ca^{2+} stores by specific inhibition of the endoplasmic reticulum Ca^{2+}-ATPase. Proceedings of the National Academy of Sciences of the United States of America 87:2466-2470.

Thestrup, T., et al. 2014 Optimized ratiometric calcium sensors for functional in vivo imaging of neurons and T lymphocytes. Nat Methods 11(2):175-82.

Thibault, O., J. C. Gant, and P. W. Landfield 2007 Expansion of the calcium hypothesis of brain aging and Alzheimer's disease: minding the store. Aging Cell 6(3):307-17.

Thibault, O., R. Hadley, and P. W. Landfield 2001 Elevated postsynaptic $[Ca^{2+}]_i$ and L-type calcium channel activity in aged hippocampal neurons: relationship to impaired synaptic plasticity. Journal of Neuroscience 21(24):9744-56.

Thinakaran, G., and E. H. Koo 2008 Amyloid precursor protein trafficking, processing, and function. The Journal of Biological Chemistry 283(44):29615-9.

Toh, W. H., and P. A. Gleeson 2016 Dysregulation of intracellular trafficking and endosomal sorting in Alzheimer's disease: controversies and unanswered questions. Biochem J 473(14):1977-93.

Tolia, A., and B. De Strooper 2009 Structure and function of gamma-secretase. Seminars in Cell & Developmental Biology 20(2):211-218.

Tong, B. C., et al. 2016 Familial Alzheimer's disease-associated presenilin 1 mutants promote gamma-secretase cleavage of STIM1 to impair store-operated Ca2+ entry. Sci Signal 9(444):ra89.

Tsien, R. Y. 1980 New calcium indicators and buffers with high selectivity against magnesium and protons: design, synthesis, and properties of prototype structures. Biochemistry 19(11):2396-404.

— 1998 The green fluorescent protein. Annual Review of Biochemistry 67:509-544.

Tsien, R. Y., T. Pozzan, and T. J. Rink 1982 Calcium homeostasis in intact lymphocytes: cytoplasmic free calcium monitored with a new, intracellularly trapped fluorescent indicator. Journal of Cell Biology 94:325-334.

Tsien, R. Y., and D. Prasher 1998 Molecular biology and mutation of GFP. Methods in Cell Biology in press.

Tu, H., et al. 2006 Presenilins form ER Ca^{2+} leak channels, a function disrupted by familial Alzheimer's disease-linked mutations. Cell 126(5):981-93.

Um, J. W., et al. 2013a Metabotropic glutamate receptor 5 is a coreceptor for Alzheimer aβ oligomer bound to cellular prion protein. Neuron 79(5):887-902.

— 2013b Metabotropic glutamate receptor 5 is a coreceptor for Alzheimer abeta oligomer bound to cellular prion protein. Neuron 79(5):887-902.

Um, J. W., et al. 2012 Alzheimer amyloid-beta oligomer bound to postsynaptic prion protein activates Fyn to impair neurons. Nature neuroscience 15(9):1227-35.

Vais, H., et al. 2016 EMRE Is a Matrix Ca(2+) Sensor that Governs Gatekeeping of the Mitochondrial Ca(2+) Uniporter. Cell Rep 14(3):403-10.

Veng, L. M., M. H. Mesches, and M. D. Browning 2003 Age-related working memory impairment is correlated with increases in the L-type calcium channel protein α_{1D} ($Ca_v1.3$) in area CA1 of the hippocampus and both are ameliorated by chronic nimodipine treatment. Brain Research. Molecular Brain Research 110(2):193-202.

Verkhratsky, A., et al. 2016 Astroglia dynamics in ageing and Alzheimer's disease. Current Opinion in Pharmacology 26:74-79.

Vig, M., et al. 2006 CRACM1 multimers form the ion-selective pore of the CRAC channel. Current Biology 16(20):2073-9.

Villasenor, R., Y. Kalaidzidis, and M. Zerial 2016 Signal processing by the endosomal system. Curr Opin Cell Biol 39:53-60.

Walker, E. S., et al. 2005 Presenilin 2 familial Alzheimer's disease mutations result in partial loss of function and dramatic changes in Abeta 42/40 ratios. Journal of Neurochemistry 92(2):294-301.

Walsh, D. M., et al. 2002a Naturally secreted oligomers of amyloid beta protein potently inhibit hippocampal long-term potentiation in vivo. Nature 416(6880):535-9.

Walsh, D. M., et al. 2002b Amyloid-β oligomers: their production, toxicity and therapeutic inhibition. Biochemical Society Transactions 30(4):552-557.

Wandinger-Ness, A., and M. Zerial 2014 Rab proteins and the compartmentalization of the endosomal system. Cold Spring Harb Perspect Biol 6(11):a022616.

Wang, H. Y., et al. 2000 β-Amyloid$_{1-42}$ binds to α_7 nicotinic acetylcholine receptor with high affinity. Implications for Alzheimer's disease pathology. The Journal of Biological Chemistry 275(8):5626-32.

Wang, Y., X. Deng, and D. L. Gill 2010a Calcium signaling by STIM and Orai: intimate coupling details revealed. Science Signaling 3(148):pe42.

Wang, Y., et al. 2010b The calcium store sensor, STIM1, reciprocally controls Orai and CaV1.2 channels. Science 330(6000):105-9.

Williams, R. T., et al. 2001 Identification and characterization of the STIM (stromal interaction molecule) gene family: coding for a novel class of transmembrane proteins. Biochem J 357(Pt 3):673-85.

Wissenbach, U., et al. 2007 Primary structure, chromosomal localization and expression in immune cells of the murine ORAI and STIM genes. Cell Calcium 42(4-5):439-46.

Wojda, U., E. Salinska, and J. Kuznicki 2008 Calcium ions in neuronal degeneration. IUBMB Life 60(9):575-90.

Wolfe, M. S. 2007 When loss is gain: reduced presenilin proteolytic function leads to increased Abeta42/Abeta40. Talking Point on the role of presenilin mutations in Alzheimer disease. EMBO Report 8(2):136-40.

Wong, A. K., et al. 2013 Heterogeneity of Ca2+ handling among and within Golgi compartments. J Mol Cell Biol 5(4):266-76.

Wu, J., et al. 2016 Heteromeric alpha7beta2 Nicotinic Acetylcholine Receptors in the Brain. Trends in pharmacological sciences 37(7):562-74.

Wuytack, F., L. Raeymaekers, and L. Missiaen 2002 Molecular physiology of the SERCA and SPCA pumps. Cell Calcium 32(5-6):279-305.

Yoo, A.S., et al. 2000 Presenilin-mediated modulation of capacitative calcium entry. Neuron 27(3):561-572.

You, H. T., et al. 2012 Aβ neurotoxicity depends on interactions between copper ions, prion protein, and N-methyl-D-aspartate receptors. Proceedings of the National Academy of Sciences of the United States of America 109(5):1737-1742.

Zahs, K. R., and K. H. Ashe 2010 'Too much good news' - are Alzheimer mouse models trying to tell us how to prevent, not cure, Alzheimer's disease? Trends Neurosci 33(8):381-9.

Zalk, R., et al. 2015 Structure of a mammalian ryanodine receptor. Nature 517(7532):44-9.

Zampese, E., et al. 2009 Ca^{2+} dysregulation mediated by presenilins in Familial Alzheimer's Disease: causing or modulating factor? Current Trends in Neurology 3:1-14.

Zampese, E., et al. 2011a Presenilin-2 modulation of ER-mitochondria interactions. Communicative & Integrative Biology 4(3):357-360.

Zampese, E., et al. 2011b Presenilin 2 modulates endoplasmic reticulum (ER)-mitochondria interactions and Ca^{2+} cross-talk. Proceedings of the National Academy of Sciences of the United States of America 108(7):2777-82.

Zampese, E., and P. Pizzo 2012 Intracellular organelles in the saga of Ca2+ homeostasis: different molecules for different purposes? Cellular and molecular life sciences : CMLS 69(7):1077-104.

Zatti, G., et al. 2006 Presenilin mutations linked to familial Alzheimer's disease reduce endoplasmic reticulum and Golgi apparatus calcium levels. Cell Calcium 39(6):539-50.

Zatti, G., et al. 2004 The presenilin 2 M239I mutation associated with familial Alzheimer's disease reduces Ca^{2+} release from intracellular stores. Neurobiology of Disease 15(2):269-278.

Zeiger, W., et al. 2013 Ca^{2+} Influx through Store-operated Ca^{2+} Channels Reduces Alzheimer Disease β-Amyloid Peptide Secretion. Journal of Biological Chemistry 288(37):26955-26966.

Zempel, H., et al. 2010 Aβ oligomers cause localized Ca^{2+} elevation, missorting of endogenous Tau into dendrites, Tau phosphorylation, and destruction of microtubules and spines. The Journal of Neuroscience 30(36):11938-50.

Zhang, H., et al. 2016 Store-Operated Calcium Channel Complex in Postsynaptic Spines: A New Therapeutic Target for Alzheimer's Disease Treatment. J Neurosci 36(47):11837-11850.

Zhang, H., et al. 2015a Neuronal Store-Operated Calcium Entry and Mushroom Spine Loss in Amyloid Precursor Protein Knock-In Mouse Model of Alzheimer's Disease. Journal of Neuroscience 35(39):13275-86.

Zhang, S. L., et al. 2006 Genome-wide RNAi screen of Ca^{2+} influx identifies genes that regulate Ca^{2+} release-activated Ca^{2+} channel activity. Proceedings of the National Academy of Sciences of the United States of America 103(24):9357-62.

Zhang, X., C. J. Yu, and S. S. Sisodia 2015b The topology of pen-2, a gamma-secretase subunit, revisited: evidence for a reentrant loop and a single pass transmembrane domain. Mol Neurodegener 10:39.

Zheng, H., and E. H. Koo 2006 The amyloid precursor protein: beyond amyloid. Molecular Neurodegeneration 1.

Zheng, L., et al. 2008 Biophysical characterization of the EF-hand and SAM domain containing Ca2+ sensory region of STIM1 and STIM2. Biochem Biophys Res Commun 369(1):240-6.

Zhou, Y., et al. 2010 STIM1 gates the store-operated calcium channel ORAI1 in vitro. Nat Struct Mol Biol 17(1):112-6.

Zhou, Y., et al. 2013 Initial activation of STIM1, the regulator of store-operated calcium entry. Nat Struct Mol Biol 20(8):973-81.

Zhu, M. X., et al. 2010a Calcium signaling via two-pore channels: local or global, that is the question. American Journal of Physiology. Cell Physiology 298(3):C430-41.

Zhu, M. X., et al. 2010b TPCs: Endolysosomal channels for Ca^{2+} mobilization from acidic organelles triggered by NAADP. FEBS Letters 584(10):1966-74.

Zitt, C., et al. 2004 Potent inhibition of Ca2+ release-activated Ca2+ channels and T-lymphocyte activation by the pyrazole derivative BTP2. J Biol Chem 279(13):12427-37.